OXIDATION AND DECARBURIZATION KINETICS

OF

IRON - CARBON ALLOYS

IN

CARBON DIOXIDE - CARBON MONOXIDE ATMOSPHERES

OXIDATION AND DECARBURIZATION KINETICS OF IRON - CARBON ALLOYS IN CARBON DIOXIDE - CARBON MONOXIDE ATMOSPHERES

By

GARY JOHN BILLINGS, B. A. (CHEMISTRY)

A Thesis

Submitted to the Faculty of Graduate Studies

in Partial Fulfilment of the Requirements

for the Degree

Master of Science

McMaster University

Hamilton, Ontario, Canada

April 1966

MASTER OF SCIENCE (Metallurgy) 1966 McMASTER UNIVERSITY

Hamilton, Ontario.

TITLE: Oxidation and Decarburization Kinetics of Iron-Carbon Alloys in Carbon dioxide - Carbon Monoxide Atmospheres

AUTHOR: Gary John Billings, B. A. (McMaster University)

SUPERVISOR: Professor W. W. Smeltzer

NUMBER OF PAGES: 120

Abstract

In this thesis, the results of oxidation and decarburization experiments with pure iron-carbon alloys over the temperature range 800 - 950°C, and in atmospheres of varying carbon monoxide - carbon dioxide ratio are reported. Most of the experimental work is concerned with a 1.065 weight percent carbon alloy at temperatures where austenite is the stable phase. Complex kinetic behaviour was observed for this alloy in the range 10 - 100 volume percent carbon dioxide. An analysis is given which in turn associates the kinetics with a pure diffusion controlled decarburization model and a pure surface controlled decarburization model. The latter best represents the interaction of the decarburization mechanism with the scaling process on γ - iron. Metallographic evidence is provided where possible in support of the results of the afore-mentioned analysis. Mathematical relations are introduced which attempt to describe qualitatively the kinetics of the carbon alloys in all the atmospheres employed. A statement is made as to the applicability of the model to carbon steels in general at temperatures where austenite is the stable phase and where the atmospheres employed are of various carbon monoxide - carbon dioxide ratio.

Acknowledgements

The author is indebted to Dr. W. W. Smeltzer whose guidance and interest in every stage of the study was greatly appreciated.

The author is also indebted to Dr. J. S. Kirkaldy, whose patient supervision while Dr. Smeltzer was on sabbatical leave during the terminal stages of the study, was especially appreciated.

The author is also indebted to Dr. L. A. Morris who designed and built the kinetic apparatus, and to Dr. G. R. Purdy who supplied the alloys used in this study.

A grateful acknowledgement to Dr. R. G. Ward, whose helpful guidance at the very outset of the author's entrance into the graduate studies program, is also extended.

The chemical analysis of the alloys used in this study were obtained through the good offices of Mr. B. Fox and Mr. J. Kelley, The Steel Co. of Canada Ltd., and Mr. H. Neumeyer and Mr. M. Van Osten, the department of Metallurgy & Metallurgical Engineering, McMaster University.

This project was supported by grants from the American Iron and Steel Institute to Dr. W. W. Smeltzer and an Ontario Graduate Fellowship awarded to the author in 1965.

TABLE OF CONTENTS

LIST OF ILLUSTRATIONS

LIST OF TABLES

CHAPTER 1

INTRODUCTION

Consumer demand for steels conforming to increasingly rigorous specifications of strength, composition, and durability has encouraged the investigation of the behaviour of steels under simulated manufacturing conditions. Of particular interest are the effects of gaseous environment on the composition of steels during various stages of heat treatment. Commercial steel, being a multicomponent alloy, necessarily has a more complex oxidation behaviour than that of pure iron in a given gaseous environment. The behaviour of such steels is not easily amenable to scientific analysis so field testing of specific commercial steels is still the most expedient means of determining environmental effects. Our study will therefore be restricted to binary alloys of iron and carbon. Few attempts have been made to describe mathematically the mechanisms of oxidation of alloys for which the alloying component forms a volatile oxide and the base metal oxidizes concurrently, for the problem in most cases is extremely complex. For one thing, the oxidation products of one of the components, tends to interfere with the oxidation kinetics of the other. Furthermore, scale morphology and resistance of the metal to diffusion of the alloying component add to the complexity.

In consideration of Fe-C alloys, it was decided to use carbon monoxide - carbon dioxide atmospheres which leads to the formation of a single stable oxide phase, wüstite. By changing the composition of the gas atmosphere it is possible on the one hand to suppress completely the oxidation of the base metal, iron, and observe the isothermal kinetics

under conditions of simultaneous oxidation of carbon and iron. Furthermore, a temperature range can be selected whereby oxidation rates are slow enough to be monitored accurately, and where scales are adherent and do not show a tendency to spall.

In the following chapters, the results of these kinetic experiments are set forth along with some metallographic evidence. We commence with a review of pertinent oxidation theory, and publications relevant to the problem.

CHAPTER 2

LITERATURE REVIEW

2.1 Introduction

The following sections summarize pertinent metal and alloy oxidation principles along with the publications which bear on this study.

2.2.1 Oxidation of Single Metals

Most oxides are semi-conductors and have electrical conductivities many orders of magnitude less than a metal. Their conductivity is therefore mainly electronic, as distinguished from ionic, and may be derived from the movement of electron holes (p-type semi-conductors) or electrons (n-type semi-conductors). The n-type semi-conductors are characterized by either excess ions present in interstitial positions in the oxide lattice, such as ZnO, or, by anion vacancies in lattice positions as occurs in Fe_2O_3 and TiO_2. Such semi-conductors are classified as metal excess oxides. The p-type semi-conductors are characterized by cation vacancies in lattice positions and are classified as metal deficit oxides examples of which are Cu_2O, NiO, and FeO. The type of lattice defect structure which occurs for a given metal, largely determines the oxidation rate of the metal. Accordingly, as the tendency for an oxide lattice toward a perfect stoichiometric ionic structure devoid of defects increases, diffusion rates in the oxide decrease since little or no concentration gradient can exist across the width of the scale. However, this limiting case is rarely observed since most oxides are able to establish a con-

centration gradient by solution of small amounts of oxygen or excess metal. At temperatures conducive to the operation of diffusion transport mechanisms, metal ions move toward the oxide-gas interface and anions move inward, toward the metal. Diffusion of one of the species, anion or cation, usually predominates so that scales are found to form either at the metal-oxide interface, or oxide-gas interface (anion and cation diffusion, respectively.) Electrical neutrality in the oxide is realized by movement of electrons in the appropriate direction.

2.2.2 Oxidation Kinetics of Pure Metals (Thick Films)

Oxidation according to a parabolic law is common, wherein diffusion of cations or anions is rate controlling and a relatively compact oxide is produced. However, other rate laws are evident if processes other than simple diffusion occur. As a rule where a number of processes occur simultaneously, the process which operates at the slower rate will determine the overall rate. The observed rate law therefore yields information concerning the mechanism of this controlling process.

Kinetic data obtained during experiments entailing metal-gas reactions are most conveniently recorded in the form of weight loss or gain per unit area ($\Delta m/A$), as a function of time "t". In the case of a parabolic law, the rate of increase in oxide thickness is proportional to the reciprocal of the film thickness

$$\text{ie.} \quad \frac{dx}{dt} = \frac{K}{x} \tag{1}$$

which yields upon integration $x^2 = 2Kt + C$ (2)

Since the thickness of an oxide is proportional to the amount of oxygen it contains, we can write:

$$(\Delta m/A)^2 = Kpt \qquad (3)$$

where C, the integration constant is equal to zero if this law applies from time zero.

Other rate laws are observed if the rate controlling process is other than simple diffusion. A linear rate law is commonly observed.

$$\Delta m/A = K_L t \qquad (4)$$

In this case the rate of increase in weight per unit area is a constant. This behaviour is often observed in porous films where the gas can contact metal directly. Such cases are associated with interface control since the transfer of atoms to the growing film is controlled at the metal-gas interface.

For the case of a thick oxide layer, which also contains growing voids, Evans [2] has found that a logarithmic law fits the data and accounts for the reduction in area of the diffusion interface as a function of time. This law is written as follows:

$$\Delta m/A = K_E \log (at + b) \qquad (5)$$

where K_E; a; and b are constants.

2.2.3 Effect of Temperature and Pressure

In the formation of very stable oxides, for low pressure of gaseous oxygen (>1mm.), effects of variation in pressure of oxygen are not large. However, in the case where the gaseous oxygen can adsorb on the oxide at the oxide gas interface, migration of metal to the adsorbed oxygen from the metal-oxide interface can occur since the adsorbed oxygen creates vacant cation sites. Thus, a small pressure dependence of oxidation rate will be expected. This pressure dependence was predicted by Wagner[3] for the classical example:

$$Cu \xrightarrow{O_2} Cu_2O \qquad (6)$$

Wagner discovered that the lattice defect structure of Cu_2O was affected by oxygen pressure in such a way as to increase the concentration gradient of the diffusing species. In the same system at temperatures where there is a layer of CuO on top of the Cu_2O, the concentration gradient is fixed on either side of the Cu_2O layer and hence no pressure dependence is observed. If a metal on the other hand, is subject to low oxygen pressures, a problem arises as to the availability of oxygen at the reaction interface, so it is the degree of availability of the gas at the reaction interface that controls the rate of oxidation.

The effect of temperature on oxidation kinetics is that common to chemical reactions, and rate parameters generally obey the Arrhenius equation:

$$K_i = K_o\, e^{-Q/RT} \qquad (7)$$

where K_i is any rate parameter, K_o is a constant, and Q is the heat of activation. One ascertains the activation energy for an oxidation reaction by plotting the logarithm of the rate parameter found experimentally, versus the reciprocal of the absolute temperature. The slope of the resulting curve yields a value of Q/R where R is the gas constant. A non-linear plot usually gives a hint that more than a single process is involved.

2.2.4 Rate Laws Applied to Experimental Observations

Seybolt [1] has enumerated some of the variables which complicate the application of simple rate laws to experimental data. These variables are 1) Porosity in the growing oxide; 2) Cracking off or spalling of the oxide; 3) Oxide sintering; 4) Solution of oxygen in the metal; 5) Multiple

oxide layers partially separated during oxidation; 6) Change of physical dimensions of test specimens; 7) Formation of volatile oxides; 8) Oxidation to higher gaseous oxides; 9) Oxide plasticity versus oxide brittleness; 10) Interaction between oxides. In view of this large number of possible artifacts it is surprising that any of the simple kinetic laws stated previously are realized.

As often happens, when an oxide layer has built up to a certain critical thickness, it cracks or spalls allowing oxidizing gas to contact the metal directly. Pilling and Bedworth [4] explained the spalling of oxides in terms of forces in the oxides. The forces were supposed to depend on the ratio of the relative molecular volume of oxide to the atomic volume of metal. If this ratio exceeds unity, the oxide is under compression and hence should be stable and protective. Conversely, if the ratio is less than unity, the oxide should be porous, loosely coherent, and hence non-protective. This criterion has been questioned by several investigators. Vermilyea [5] has raised the point that if an oxide grows by diffusion of cations through the oxide layer, each new layer is formed at the oxide-gas interface. Since each new layer is only required to fit the preceding layer, there is no opportunity for stresses to build up within the layer.

If oxide continuously spalls, melts, vaporizes or is quickly removed from the metal, the resulting increase in the rate of attack is termed as catastrophic oxidation. This is distinguished from break-away oxidation which entails a sudden change of mechanism leading to increased oxidation rates not necessarily accompanied by spalling.

The remaining factor which limits application of simple rate laws to experimental observation occurs with reactive metals where the diffusive

character of the oxide changes with time. Examples of the type are exhibited by metals like titanium and niobium. In these cases an initially defective oxide changes with time to more dense oxide and the kinetics change from linear to approximately parabolic.

2.2.5 Combination of Rate Laws

When the kinetics of a particular metal-gas system exhibit a transition from one rate law to another, the cause may be changes in oxide morphology or change in the mode of growth of the oxide. Such kinetics must then be described by rate law combinations. An example of such rate law combination is afforded by the work of Smeltzer [6] et al, who found that Ti, Zr, and Hf in the range 300 - 600°C. oxidized too rapidly for the process to be explained by a normal diffusion process. Consequently, two parallel reactions were postulated as occurring. One reaction involved standard lattice diffusion of oxygen via anion vacancies; the other reaction involved diffusion of oxygen along short circuiting paths (grain boundaries in the oxide, or dislocation pipes). This model coupled with the assumption that the density of short-circuiting oxygen sites decrease exponentially with time, led to a theoretical rate law which satisfactorily fit the observed data.

Pettit and Wagner[54] made a diffusion analysis for the transition from a linear to parabolic rate law during the oxidation of iron to wüstite in CO - CO_2 mixtures. It was found that over the temperature range 700 - 1100°C, the rate of oxidation is linear and controlled by the dissociation of CO_2 at the iron surface, the iron acting as catalyst for oxide thickness of the order of 4×10^{-4} to 1×10^{-2} CM. For larger

oxide thicknesses, the authors, using the method of Rickert and Wagner[55], derived equations describing the transition in kinetics from linear to parabolic. The theory presented was experimentally verified by the authors.

2.2.6 Prediction of Oxidation Rates and The Theory of Parabolic Oxidation

Wagner[7, 9] has offered a general theory for the rate of growth of a compact oxide film and has succeeded in deriving the experimentally observed rate constants for the case of parabolic oxidation of Cu. The original form of the derived expression was in terms of electrical conductivity and transference numbers of ions and electrons. The most popular form of the relation makes use of more easily determined ion mobilities. Wagner writes the following expression for the rational rate constant Kr:

$$Kr = Ceq \int_{a_o}^{a_1} \left[\left(\frac{Z_1}{Z_2}\right) D_1 + D_2\right] d\ln a \qquad (8)$$

Kr = equivalents / cm^2/sec. (for a reaction product 1 cm. thick)

a_o = activity of oxygen at metal-oxide interface

a_i = activity of oxygen at oxide-gas interface

Z_1 = valence of oxygen

Z_2 = valence of metal

D_1 = anion diffusivity

D_2 = cation diffusivity

C eq = oxygen concentration (equivalents /$(cm.)^3$

From the equation it is apparent that in general the corrosion rate depends upon the difference in activity of oxygen between the outside and inside layer, and that large diffusivities mean increased rate of attack of the

metal. It may be noted that the theory of parabolic oxidation has been shown to be valid for copper, iron, cobalt and nickel.

2.3 Alloy Oxidation

2.3.1 Introduction

Analysis of the results of oxidation experiments employing alloys is complicated because in binary alloys there is the possibility of one or more three-component oxides. Moreover, precipitation of subscale is a frequent occurrance. Diffusion in the alloy substrate is a further complication.

2.3.2 Effect of Minor Additions of Alloying Constituent

It has been found by Wagner and Zimens[9] and Gensch and Hauffe[10] that addition of higher valence impurities to p-type oxides increase the oxidation rate, while addition of lower valence impurities decreases the rate. In the case of the n-type scales, just the reverse is true. On the average, additions of 0.1 to 1 atom percent of the impurity change the rate by a factor of approximately ten. An exception to this is addition of 0.1 - 1 atom percent aluminum to zinc, which decreases the oxidation rate of zinc by a factor of 300!

2.3.3 Selective Oxidation of Alloys

The term selective oxidation, refers to the oxidation of only the active component of a binary alloy. The three important considerations which enhance the occurence of selective oxidation are: 1) a large difference in the oxide stability of the two components 2) a very low

oxygen partial pressure 3) a high percentage of active component.

Selective oxidation is also observed in comparatively dilute alloys if the oxygen partial pressure is too low to allow the more noble oxide to form. The minimum oxygen pressure required for oxidation of the most stable oxide may be computed from thermodynamic data, if the activity of the less noble element is known. For specific examples of selective oxidation the reader is referred to the standard works[11, 12, 13, 14] on this subject.

2.3.4 Internal Oxidation

Internal oxidation occurs only in alloys where a more reactive component preferentially oxidizes within the alloy. The mechanism involves diffusion of oxygen through the solid alloy. Wagner[15] stated that internal oxidation will be observed when one component present in amount of less than 10 atom percent, forms a more stable oxide than the more concentrated, more noble, component. Moreover, if the concentration of the less noble constituent is sufficiently high, the volume of the precipitated oxide becomes so large, that further oxygen diffusion into the alloy is inhibited. Hence for sufficient concentrations of the less noble alloy constituent only one scale is predicted. Wagner[15] described the conditions for the critical composition mathematically and the reader is urged to consult the reference as the treatment is not relevant to the present study.

2.3.5 Metal Diffusion in and Oxidation Behaviour of Alloys

With most alloys, more than one oxide commonly forms. Oxide

solid solutions also occur in some cases and often have a pronounced effect on both the oxidation mechanism and oxidation rate. As a result, no theory of alloy oxidation has succeeded in predicting exactly the course of oxidation of a randomly chosen alloy. Wagner [16, 17, 18] has had some success in predicting results in a system which constitutes a limiting case. Indeed, the system Ni-Pt is such a limiting case in that Pt does not oxidize in the usual sense. In this case, the only oxide which forms is that of the major constituent and both the lattice defect structure of NiO and the oxidation properties of pure nickel are well known. Wagner[18] went on to calculate the oxidation rate of the Ni-Pt alloy and found it agreed reasonably well with experiment. Unfortunately, similar calculations applied to other alloy systems are not realizable because of inadequate information about the pertinent parameters.

2.3.6 The Status of Alloy Oxidation

From the brief description of alloy oxidation given in the preceding sections it is apparent that the theoretical descriptions are generally qualitative. Most experimenters are of the opinion that more careful work involving the structural nature and composition of the scales on different alloy phases is needed. The effects of variables such as metallurgical structure, temperature, oxygen pressure and contact time, must be more critically examined.

The understanding of the details of oxidation behaviour of multi-component systems, such as high alloy steels and superalloys, can only be rather superficial in view of the high degree of complexity of

the systems. The technological situation is further complicated by the complex and ill-defined environmental conditions. The considerations of temperature cycling and changing relative stability of oxides are further sources of complications. For such materials and conditions, it is still expedient to employ field tests for information which has bearing on actual problems. However, in the near future, we may expect the accumulation of basic results to serve us increasingly in materials selection.

2.4 Principles of Oxidation Involving the System Fe-C-O

2.4.1 Introduction

In this section we shall consider the following sub-sections in order of increasing complexity; (a) the oxidation of pure iron, (b) the oxidation of pure carbon, (c) equilibrium in the Fe-C-O system, (d) selective oxidation of carbon in Fe-C alloys, and finally (e) concurrent oxidation of iron and carbon in Fe-C alloys.

2.4.2 Oxidation of Pure Iron

It is well known that iron exposed to an environment of dry gaseous oxygen at temperatures above 570°C will react to form three stable oxides. These oxides in order of appearance in a typical[19] specimen cross section are, wüstite (FeO) immediately adjacent to the metal, then magnetite (Fe_3O_4) and then hematite (Fe_2O_3). Below 570°C the wüstite phase is unstable, hence only magnetite and hematite will be observed. The lowest oxide of iron (FeO) is [20] a p-type semi-conductor which is metal deficient and has a high percentage of lattice defects in the form of cation

vacancies and positive holes (Fe^{3+} ions). The oxide grows almost entirely by cation diffusion as proven by inert marker and radioactive tracer studies, and the conductivity is derived from movement of the positive holes.

In air or oxygen in the temperature range 0 - 200°C, a logarithmic oxidation rate[21] law is obeyed for pure iron. Above 200°C parabolic kinetics are observed[20, 22]. As mentioned previously in section 2.2.6, and on the basis of experiments of Himmel[56] et al, the Wagner theory of parabolic oxidation is applicable above 570°C and accounts for the temperature dependence of the parabolic scaling rate[26] in the temperature range 510 - 1000°C.

Scales showing good properties of adherence and compactness can be grown on iron at linear rates in atmospheres of low oxidation potentials. In particular, the oxygen potentials in carbon dioxide atmospheres are sufficiently low to permit linear growth of compact scales. Hauffe and Pfeiffer[23] demonstrated this by oxidizing iron in carbon dioxide - carbon monoxide atmospheres over the temperature range 900 - 1000°C. They found that wüstite was the only scale formed and that uptake of oxygen was directly proportional to time suggesting that a phase boundary reaction was rate controlling. Moreover, it was found that the linear reaction rate was directly proportional to a fractional positive power of the ratio of component gas partial pressures. This observed dependence was:

$$K_L \propto (PCO_2/PCO)^{0.71} \qquad (9)$$

On this basis the authors suggested that the overall rate determining reaction was the dissociation of gaseous carbon dioxide at

the wüstite surface producing adsorbed oxygen ions according to;

$$CO_2 = O^-_{ads.} + CO + Fe^{++\oplus} \quad (10)$$

where $Fe^{++\oplus}$ denotes a positive hole. The chemisorbed oxygen is then taken up by the wüstite according to;

$$O^-ads = FeO + \square + Fe^{++\oplus} \quad (11)$$

where $\square$ denotes an iron cation vacancy. The work of other experimentalists [24, 25] essentially confirms this result for iron in carbon dioxide-carbon monoxide atmospheres. Pettit Yinger and Wagner [25], using the assumption of rate controlling chemisorption went on to define the rate of formation of oxide in terms of the partial pressures of the two components of the gaseous atmosphere. They obtained the relation

$$\dot{n} = K^1 PCO_2 - K^{11} PCO \quad (12)$$

where $\dot{n}$ = the number of equivalents of oxide formed per unit area per unit time and K^1 and K^{11} are the specific reaction rate constants for the forward and reverse reactions respectively, as given by equation (10) of this section. Since the chemisorption reaction is assumed to be rate controlling, the concentration of lattice defects in wüstite will be given by the equilibrium between iron and wüstite in accordance with the fact that the rate of dissociation of carbon dioxide is [26] a function of electronic defects in the oxide. Therefore no specific term need be employed in the kinetic equation for defect concentration. For the equilibrium defined by:

$$Fe + CO_2 = CO + Fe\ O \quad (13)$$

the equilibrium constant

$$K = PCO_2/PCO \quad (14)$$

Also, at equilibrium,

$$\dot{n} = 0 \qquad \text{from (12)}$$

from hence

$$k^{11}/k^{1} = PCO_2/PCO \qquad (15)$$

or, by combination of (14) and (15),

$$K = PCO_2/PCO = k^{11}/k^{1} \qquad (16)$$

at equilibrium (16). Substituting (16) into (12) and writing PCO_2 in terms of the total pressure gives:

$$K_L = K^{1} P (1 + K) (NCO_2 - NCO_2\ eq) \qquad (17)$$

where NCO_2 = molefraction of CO_2 in the atmosphere as obtained from consideration of equation (13).

Nearly simultaneously, Smeltzer[26] employing the same assumption that the chemisorption reaction determined the kinetics, also assumed that the adsorption reaction was irreversible and postulated the following sequence of steps for the oxidation reaction:

$$CO_2\ (g) \xrightarrow{K_2} O^{=}_{ads.} + 2\oplus_{o/g} + CO\ (g) \qquad (18)$$

$$O^{=}_{ads.} \xrightarrow{K_3} FeO + \square_{o/g} \qquad (19)$$

$$\square_{o/g} + 2\oplus_{o/g} \rightleftarrows \square_{M/O} + 2\oplus_{M/O} \qquad (20)$$

$$Fe_{M/O} + \square_{M/O} + 2\oplus_{M/O} \rightleftarrows Nil \qquad (21)$$

$$O^{=}_{ads.} + 2\oplus_{o/g} \xrightarrow{K_6} 1/2O_2\ (g) \qquad (22)$$

g - refers to gaseous phase

o/g - refers to oxide-gas interface

M/O - refers to metal-oxide interface

Nil - refers to annulment of lattice defects by solution of iron into the oxide

He further reasoned that if the concentration of vacancies and positive holes equalled their equilibrium values, a parabolic dependance would be obtained. Since the rates observed were in fact linear, it was then assumed that equations (18) and (19), were the rate controlling processes. From these considerations he derived an expression for the surface coverage, "θ", considering that it remained constant during oxidation, and that the lattice defects in the oxide are equilibrated with the metal phase. The expression obtained for the surface coverage was

$$\theta = (K_2/K_3K_6K)(PCO_2 - PCO_2\ eq.)/\frac{1+ K\ (PCO_2-PCO_2eq.)}{K_3K_6K} \qquad (23)$$

where K_2, K_3 and K_6 are the rate constants for oxygen chemisorption, wüstite formation and oxygen desorption, respectively. K and PCO_2 eq. are defined as for equations (14) and (17). Two cases were considered with respect to equation (23). The first being that the surface coverage, θ, approaches zero and reaction (18) becomes rate determining, and secondly, that the rate of incorporation as given by (19), is rate controlling. This gave for the first case:

$$K_L = K_2\ (PCO_2 - PCO_2\ eq.) \qquad 0 < \theta < 1 \qquad (24)$$

and, for the second case:

$$K_L = \frac{K_3K_2}{K_3+K_6K}\ (PCO_2 - PCO_2\ eq.) \qquad (K_2 << K_3 + K_6K) \qquad (25)$$

Linear relations were found for plots of K_L versus the partial pressures of carbon dioxide above the equilibrium value, in support of the theory. More recently Turkdogan[27] has derived an expression for linear oxidation kinetics in carbon dioxide - carbon monoxide systems by applying Eyring's[28] theory of absolute reaction rates. The expression

is in terms of oxygen activities at the oxide-gas interface in equilibrium with the gas phase. Good agreement is demonstrated between the theory and experiment. Thus the analysis carried out for oxidation of pure iron in CO - CO_2 atmospheres all lead to identical expressions for the dependency of oxidation rates on CO_2 partial pressure.

2.5 Oxidation of Carbon

Hedden[29] et al have proposed the following mechanism, applicable to the oxidation of pure amorphous carbon with CO_2 over the temperature range 800 - 1050°C.

$$CO_2 \rightleftarrows CO_2, \text{ ads.} \tag{26}$$

$$CO_2\text{ads} + [C] \rightarrow CO\text{ads} + CO \tag{27}$$

$$CO \rightarrow CO\text{ads or } CO\text{ads} \rightarrow CO \tag{28}$$

Reaction(27) is proposed as rate determining and an electronic "reciprocal" effect between the carbon lattice and chemisorbed species is described. Accordingly, an adsorbed CO_2 molecule dissociates into a chemisorbed $^{+}(C = O)$ group and a $(C = O)^{-}$ group. The $(C = O)^{-}$ groups bound on the surface of the carbon form an "oxide" layer. This type of dissociation is thought to be due to the electronegativity of the oxygen atom of the CO group. Suhrmann[30], has proposed this mechanism in the case of oxidation of Bi, which has a similar structure to amorphous carbon. The proposal, stated previously by Hedden, that CO chemisorbed on carbon is most likely to be positively polarized ($^{+}(C = O)$ ads) also follows from Suhrmann's work. Hedden further proposed that since the speed of dissociation of adsorbed CO_2 is dependent on flow of electrons to the surface sites occupied by CO_2 ads., hence dissociation might initially

be facilitated by formation of $(C = O)^-$ ads. electron donors. As the dissociation continues, however, other adjacent CO ads. groups compete for lattice electrons due to the electronegative character of the oxygen atom, and become negatively polarized to form effectively, an oxide film. The depletion of lattice electrons to form the film should cause the dissociation rate of CO_2 to decrease in the long run and this is in fact observed experimentally, since, by introducing small amounts of various electron donors and acceptors, Hedden et al finds in confirmation, that electron donors do in fact increase the dissociation rate of CO_2. The reverse effect is noted for additions of electron acceptors. The actual vaporization of carbon then involves interaction of the surface film of $(C = O)^-$ with electron acceptors such as $^+(C = O)$. The authors also note that the same mechanism may be applicable for the system

$$C + H_2O \rightarrow CO + H_2 \qquad (29)$$

where donor interactions of adsorbed H atoms might be analagous.

2.6 Equilibrium In The System Fe-C-O

Dunwald and Wagner[34] and later Smith[35] studied the equilibrium of Fe-carbon alloys with CO - CO_2 mixtures. In particular, Smith made an extensive study, over the temperature range 750°C to 1200°C. The range of alloy composition was from .0008% to 1.5% carbon and the range of gas composition was from 0.3 to 27% CO_2 in the CO - CO_2 mixture. The equilibrium involved in the case of iron-carbon alloys in CO - CO_2 mixtures was represented as:

$$CO_2 + C\ (\text{dissolved in } \gamma\text{-Fe}) \rightleftarrows 2CO \qquad (30)$$

whence $$P^2CO/PCO_2\ A_c = K_2 \quad (31)$$

where P is measured in atmospheres and K_2 is the equilibrium constant. From a knowledge of the phases present over the temperature range, in relation to the carburizing power of a given gas atmosphere, it was found that for the equilibrium of Fe-carbon alloys in CO - CO_2 mixtures, the reaction under consideration was:

$$CO_2 + C \text{ graphite} \rightleftarrows 2CO \quad (32)$$

whence $$P^2CO/PCO_2 = r_2' = K_4 \quad (33)$$

This case is similar for all temperatures between 738° and 910°C except that as the temperature increases, the range of stability of ferrite decreases at the expense of an increase in the range of stability of the austenite. For the temperatures 1000° and 1200°C for the carbon range 0 to 1.5%, the only solid phases encountered are austenite and graphite at equilibrium.

If graphite is chosen as the standard state for carbon, it is apparent that K_2 in equation (31) is identical with K_4 of equation (33). Equation (31) may then be written

$$A_c = P^2CO/PCO_2\ K_4 = r_2/K_4 \quad (34)$$

Where A_c is the activity of carbon in iron relative to graphite, and r_2 is the ratio P^2CO/PCO_2 for equilibrium with carbon dissolved in Fe at a concentration corresponding to A_c.

The author went on to measure r_2 experimentally, along with the corresponding carbon content and was able to calculate the activity of carbon and various other thermodynamic quantities pertaining to these systems.

2.7 Selective Oxidation of Carbon In Metal-Carbon Alloys

Doehlemann[31] oxidized Ni, Co, and Fe - carbon alloy foils in CO - CO_2 atmospheres over the temperature range 920° - 970°C. For the chosen experimental conditions, he asserted that diffusion processes in the alloy foil or gas phase, could not be rate determining, except possibly in the case of very high reaction rates. In this model, (the mathematical derivation of which will be rephrased in the theoretical section of this thesis) the reaction scheme suggested is described as follows:

The surface of the foil is considered to be divided into active and inactive sites. Two parallel reactions occur via these sites. In the first reaction an Oads. on an inactive site obtained from the dissociation of CO_2 at the surface of the foil cannot react with carbon and will be in equilibrium with CO and CO_2. The surface diffusion of Oads. from inactive sites to active sites where reaction with dissolved carbon can occur is therefore rate determining. The pertinent reactions summarily are:

$$CO_2 \underset{K_1'}{\overset{K_1}{\rightleftarrows}} CO + \text{Oads. (inactive)} \tag{35}$$

$$\text{Oads inactive} \xrightarrow[K_2]{\text{surface diffusion}} \text{Oads active} \tag{36}$$

$$\text{C in metal} + \text{Oads active} \rightleftarrows CO \tag{37}$$

As stated previously, the rate determining partial reaction is (36) while reaction (35) is in equilibrium. The second reaction sequence

$$CO_2 \rightleftarrows \text{Oads. active} + CO\uparrow \tag{38}$$

is controlling and is again completed by the equilibrium step described by (37). The final expression for the rate of decarburization as obtained by Doehlemann contains two corresponding terms, viz.,

$$-\frac{dc}{dt} = \left(K_1 PCO_2 + K_2 \frac{PCO_2}{PCO}\right)\left(1 - \frac{Ce}{C}\right) \qquad (39)$$

K_1 and K_2 are defined by reactions (35) and (36) respectively Ce is the equilibrium concentration of carbon in the alloy for fixed PCO_2/PCO ratio in the atmosphere and C is the concentration of carbon in the alloy at any time. Doehlemann's experiments with metal-carbon alloys in atmospheres of fixed PCO_2/PCO and variable PCO_2 has confirmed the linear relation for the initial loss of carbon from an Fe-C foil as given by (39) above.

Recently, Grabke[44] has studied the kinetics of the exchange of oxygen between CO_2 and CO over the temperature range 800° to 1000°C at iron foil as catalyst. Radiocarbon was employed to follow the course of the reaction. It was found that the decarburization and carburization of iron in CO - CO_2 mixtures proceeded by the following mechanism:

$$CO_2 \underset{K_1'}{\overset{K_1}{\rightleftarrows}} CO + Oads \qquad (40)$$

and

$$Oads + C_{\gamma\text{-}Fe} \underset{K_2}{\overset{K_2}{\rightleftarrows}} CO \qquad (41)$$

and that reaction (40) is rate determining with the important consideration that thin foils are used. From this it was shown that the rate of dissociation of CO_2 was equal to the decarburization rate of thin Fe-carbon foils.

A mathematical relation expressing change in carbon content as a function of time is derived. It is assumed as in the Doehlemann work[31] that for the phase boundary reaction in the decarburization and carburization of iron a mechanism described by equations (40) and (41) is valid.

For these two steps the overall reaction is:

$$CO_2 + \underset{\gamma\text{-Fe}}{C} = 2CO \tag{42}$$

The rate equations are written as follows:

$$-\frac{\dot{n}\ CO_2}{A} = k_1\ PCO_2 - k_1'\ PCO\ \theta_O \tag{43}$$

$$-\frac{\dot{n}C}{A} = k_2\ \theta_O\ [C] - k_2'\ PCO \tag{44}$$

$\dot{n}$ = number of equivalents

A = total specimen area

θ_O = coverage of surface with oxygen

k_1, k_1', k_2 and k_2' are rate constants as shown in (40) and (41)

[C] = concentration of carbon in the austenite

The surface coverage θ_O is calculated under assumed steady state conditions

ie. $-\dot{n}\ CO_2 = -\dot{n}C$

hence
$$\theta_O = \frac{k_1\ PCO_2 + k_2'\ PCO}{k_2\ [C] + k_1'\ PCO} \tag{45}$$

Substituting (45) in (43) the expression

$$\frac{-\dot{n}\ CO_2}{A} = \frac{-\dot{n}c}{A} = \frac{k_1\ k_2\ PCO_2\ [C] - k_1'\ k_2'\ PCO^2}{k_2\ [C] + k_1'\ PCO} \tag{46}$$

is obtained. The next assumption made is that reaction (40) is rate controlling if decarburization or carburization is measured at thin foils. The equilibrium for step (41) is considered as always adjusted since the diffusion of the dissolved carbon to the surface of iron and its reaction with Oads. should be very fast ie. it is assumed that

$$k_1'\ PCO << k_2\ [C] \tag{47}$$

Equation (46) thus becomes:

$$\frac{-\dot{n}c}{A} = \frac{k_1\ PCO_2\ [1 - k_1'\ k_2'\ PCO^2\ ]}{k_1\ k_2\ PCO_2\ [C]} \tag{48}$$

From the equilibrium conditions for (43) and (44) equation

$$\frac{PCO^2\ k_1'\ k_2'}{PCO_2\ k_1\ k_2} = [C]_{eq} = K\ \frac{PCO^2}{PCO_2} \tag{49}$$

K being the equilibrium constant for the overall reaction. By combination of (48) and (49) the final equation is

$$-\frac{\dot{n}\ C}{A} = (k_1\ PCO_2)\ (1 - \frac{Ceq}{[C]}) \tag{50}$$

The integrated form of the equation describes the change in carbon content as a function of time.

$$(-([C]-[C_o]) - [Ceq]\ \ln)\ \frac{[Ceq] - [C]}{[Ceq] - [C_o]} = \frac{2k_1\ PCO_2\ t}{\delta} \tag{51}$$

δ = thickness of square Fe foil

$[C]_{eq}$ = final concentration of carbon[35]

$[C_o]$ = initial concentration of carbon

$[C]$ = carbon concentration in foil at any time t

A plot of the left hand side of equation (51) versus time gives a linear distribution with slope equal to $2k_1\ PCO_2/\delta$. Thus, the results are essentially in accord with those of Doehlemann[31] for thin foils.

2.8 Simultaneous Oxidation of Metal and Carbon in Binary Metal-Carbon Alloys

Wagner[32] et al have discussed the oxidation of metal-carbon alloys in a general qualitative way. Three distinct reaction sequences are suggested. These are: (1) diffusion of carbon to the metal/scale interface where it reacts with scale (2) ruputre of the scale caused by the equilibrium pressures of the carbon oxides generated in sequence (1),

and hence further decarburization and increased scaling rate - since the gas can now penetrate through cracks in the scale to the surface of the metal, and (3) diffusion of carbon through the scale which allows decarburization to take place without scale rupture. Sequences (1) and (2) may be described in the following way:

$$C_{M/O} + MO \rightarrow M + CO \quad (52)$$

$$C_{M/O} + 2MO \rightarrow 2M + CO_2 \quad (53)$$

No mechanism is given for the diffusion of carbon through the scale if scale rupture does not occur. Wagner's results for Mn and Ni - carbon alloys are in accord with sequences (1) and (2). Sequence (3) was proposed because Wagner found for Ni - 2.3%C, that the fast oxidation of carbon is not accompanied by the expected large increase in Ni scaling rate as would necessarily be the case if a real rupture of scale was occurring.

Engell[33] oxidized Fe - carbon alloys in air and carbon dioxide-carbon monoxide atmospheres over the temperature range 750° to 1050°C. He found that the specimens oxidized in air decarburized (as evidenced by Vickers hardness measurements and metallography) without a real rupture of the scale taking place. Iron oxidized according to a parabolic rate law, and, with normal cooling rates, virtually no scale spalled off on quenching. Chemical analysis of the scale showed that the solubility of carbon in the scale was so low that transport of carbon through the scale was not too likely. Moreover the concentration of carbon in the scale was found to be only slightly dependent on the concentration of carbon in the alloy.

For Fe - carbon alloys in $CO-CO_2$ mixtures, Engell assumed the results of Doehlemann[31] and made some inferences as to the influence of FeO on the decarburization rate. For experiments where the decomposition pressure of wüstite is exceeded in the atmosphere so that wüstite can form and be stable the following possibilities were ascribed to the influence of scaling on decarburization:

(1) The decarburization rate is not influenced by the $CO-CO_2$ ratio if the diffusion of carbon in the metal is rate determining and if the carbon concentration at the Fe - FeO interface is independant of oxygen pressure in the gaseous phase.

(2) The decarburization rate increases with increasing PCO_2 slightly, if diffusion of carbon in the metal is rate determining and the carbon concentration in the metal at the Fe - FeO interface decreases with increasing oxygen partial pressure in the gas phase.

(3) The growth of FeO on pure Fe[23, 25, 26, 27] follows a linear rate law above 900°C and the linear rate constants increases with $(PCO_2/PCO)^{2/3}$ under isothermal conditions.

From this one would expect decreasing decarburization rate with increasing PCO_2 if and when the diffusion of Carbon in the FeO layer determines the decarburization rate. The rate of diffusion of carbon in the metal to the Fe - FeO interface, if the process is rate determining, is proportional to $\sqrt{t}$. However, the thickening of FeO follows a linear rate law above 900°C and consequently it is possible to get decarburization which is independent of CO_2 content, or at least a slightly increasing decarburization rate could occur. For longer times, the decarburization rate should decrease with increasing CO_2 content of the gas phase.

The author then performed tests to elucidate the dependence of decarburization rate on CO_2 gas pressure for Fe - .97%C at 1050°C and for CO-CO_2 ratios of .4/1 to 4/1. From these tests formation of FeO was noted at CO/CO_2 = 2.6. Specimens were analyzed for carbon content and a wüstite containing 23.5% oxygen, as determined from the experiments with pure Fe in CO-CO_2 was assumed as the oxide which formed on the Fe-97%C alloy as well. The results showed that after one hour, employing CO-CO_2 atmospheres in which CO_2 content was more than 28% by volume, a slight increase in amount of carbon lost with increasing CO_2 was noted. After three hours, the decarburization was at a maximum for an atmosphere of CO-CO_2 in which CO_2 was only slightly greater than 28% by volume. After six hours, a decrease in decarburization rate was noted for atmospheres containing more than 28% CO_2 by volume.

The author notes that the results were not extensive enough for a quantitative statement to be made. However, the results were summarized as follows for the Fe - .97% carbon alloy at 1050°C: For short oxidation times the decarburization is dependent on the diffusion of carbon in the metal, and for longer times the transport of carbon through the scale layer, is rate determining for the decarburization process in atmospheres where CO_2 content exceeds 28% by volume.

Sachs and Brown[36], suggested on the basis of the results of Wagner et al [32] which were previously reviewed that the mechanism of scale rupture, might play an important part in the oxidation of steel in air. In particular, the case where carbon build-up may occur at the Fe/scale interface, is discussed with reference to works by Stout[37] and Eisenhuth et al [38]. Stout, found that for carbon steels heated in severely

oxidizing atmospheres, carbon build-up reached a maximum in the first hour of oxidation. After that time, the carbon content of the surface layer diminished and finally, when it became less than the original carbon content, decarburization began. Eisenhuth and co-workers, measured the thickness of the decarburized layer for steel oxidized in air at 900, 1000, and 1200°C for varying periods of time. Backward extrapolation indicated no decarburization had occurred in the first hour. In general, they showed that scale inhibits decarburization rather than forestalls it. Hence if decarburization is suppressed to a sufficient extent, carbon may build up at the Fe-scale interface. On the basis of these two works Sachs and Brown suggest that carbon build-up occurs quite frequently in the early stages of oxidation of a carbon steel, particularly if a compact oxide is forming. Hence decarburization can take place only after mechanical rupture of the scale has occurred. Further, the change in mechanism of oxidation resulting from scale rupture should be reflected in the kinetics of growth of iron oxide and decarburization. Now the atmosphere can gain direct access to the metal via cracks formed in the scale and oxidation of both Fe and carbon should be speeded up. Oxidation should thus proceed by a continuous cycle of rupture and healing of the scale and will eventually achieve an overall parabolic rate slightly higher than for pure Fe. In the meantime, carbon oxidizes in regular bursts, but eventaully diffusion of carbon through the decarburized layer will become rate controlling and decarburization also will follow a parabolic law.

Engell[39, 40] studied oxidation of various Fe-carbon alloys in CO-CO_2 and H_2-H_2O mixtures over the temperature range 750 to 950°C. A linear rate law was found to hold for the oxidation of carbon, until

noticeable decarburization of the surface had occurred. In addition, direct reaction of the carbon with the metal oxide was proposed.

The oxidation mechanism was proposed as occurring in three steps: transport of carbon in the metal, reaction of the carbon at the metal surface, and transport of the reaction products through the scale. The surface reaction is represented by:

$$C + FeO \rightarrow Fe + CO \tag{54}$$

and

$$CO + FeO \rightarrow Fe + CO_2 \tag{55}$$

Iron formed by these reactions diffuses through the scale if concurrent oxidation of metal can take place. If scale cannot form, then iron should precipitate at the metal/gas interface. Experiments with scaled specimens in vacuo, showed that the dissolved carbon might in fact react with FeO under scaling conditions. The dissolved carbon can also react with CO_2 according to

$$CO_2 + C \rightarrow 2CO \tag{56}$$

The reactions (54) to (56) pose the problem that the carbon oxides formed must pass through the scale. Himmel[41] et al have shown that ionic diffusion of O in FeO through the scale seems unlikely, for even oxygen has no measurable mobility in FeO. Diffusion of carbon through the scale with its ensuing oxidation at the oxide/gas interface was discounted since the solubility[42] of carbon in FeO is about .003%. Since in all the experiments, decarburization occurred without increase in scaling rate of iron, the scale rupturing mechanism[32, 36] was discounted. Instead, Engell proposed that pores were present in the scales on Fe-carbon alloys which enabled effusion of the carbon oxides. He further proposed that pore formation required some critical value of carbon at the

metal/oxide interface since oxidation of carbon in alloys of .17% C was very slow in the early stages of oxidation. He further assumed that the pores offer a constant resistance to gas flow at all times during oxidation, irrespective of scale thickness, such that oxygen could not be transported directly from the gas phase to the metal surface.

In general, oxidation of carbon was found to increase linearly at small CO_2 pressures with a slope independent of carbon concentration, in accord with the results of Doehlemann[31]. Higher rates of carbon oxidation were noted in the case of a scaled Fe - .82% carbon alloy at 850°C for $PCO/PCO_2 = 2$. This was attributed to direct reaction of carbon with metal oxide according to equation (54).

Merchant[43] studied the oxidation kinetics of cast iron in dry air at elevated temperatures and found that the true oxidation behaviour was obscured by simultaneous decarburization. Because of this masking effect, no quantitative conclusions could be drawn. Significant influence of the graphite and carbide morphology on oxidation and decarburization behaviour, was noted. The oxidized cast iron surface was characterized by abnormal scale growth in the form of blisters or rough surfaces. In the flake type cast irons blisters originated from the flakes and in some cases penetration of scale into the metal was noted.

Langer and Trenkler[45] oxidized Fe-carbon alloys in oxygen and some CO-CO_2 mixtures over the temperature range 920° to 1000°. Two possibilities are proposed for the interpretation of oxidation phenomena in oxygen. The first considers that carbon can react with Fe oxide to form CO and CO_2 and then the CO_2 formed can participate further in the decarburization process according to:

$$C + CO_2 = 2CO \qquad (57)$$

The second, is that carbon diffuses to the scale/gas interface and burns to form CO or CO_2. The experimental findings showed a dependence of decarburization rate on PO_2 and since scaling rates were not observed to change with changing PO_2, it was assumed that the second possibility might be valid. This dependence of decarburization rate was found to be proportional to $\sqrt{PO_2}$ which led the authors to believe that the dissociation of O_2 was the rate determining step. A comparison of the decomposition energy of O_2 with the experimentally determined activation energy for the tests demonstrated that the dissociation of O_2 was the slowest, and hence, rate determining step for decarburization.

For Fe in CO-CO_2 mixtures, the results seemed to show on the basis of CO_2 dissociation[31, 44] being rate controlling, that less Fe ions were reacting to form FeO (assuming a linear rate law)[23, 25, 26, 27] as PCO_2 was decreased. Thus for Fe-carbon alloys, where scales are formed, part of the available oxygen is used to form carbon oxides while the remainder combines with iron. Thus a decrease of scaling rate should occur. Carbon and iron oxidation are stated then as being dependent on PO_2 and total gas pressure. Hence for a small concentration of CO_2 the effect of carbon on the scaling rate of iron should be large. Since the carbon at the metal surface is used up very rapidly, the decarburization becomes diffusion controlled after long times.

Thus it appears that three mechanisms; scale rupture, scale porosity, and diffusion of carbon in wüstite, may play a role under different environmental conditions for different carbon alloys. Direct proof for a single mechanism under the varying conditions stated, has not been established.

CHAPTER 3

THEORETICAL CONSIDERATIONS

3.1 Introduction

From an examination of the experimental results, as will be shown in the next chapter, three distinct possibilities had to be examined in order to elucidate the type of process controlling the decarburization for the cases of non-scaling and scaling of the base metal iron. These possibilities were pure diffusion controlled decarburization, pure surface controlled decarburization, and a combination of diffusion and surface controlled decarburization. The nature of the scale with regard to transport of carbon or carbon oxides and the subsequent effect on decarburization rate had to be considered. The following sections in this chapter will deal with the theory behind two of the processes mentioned above, and the development of the theory of simultaneous decarburization and oxidation of iron for short experimental times will be presented.

3.2 Diffusion Controlled Decarburization

In this case, it is convenient to consider the non-steady state diffusion-controlled desorption of carbon from a plane sheet of infinite extent and finite width. If this process is rate controlling, it follows that the concentration of carbon at the metal surfaces must be maintained constant in keeping with the conditions for the desorption. This

Hence for a given experimental time v can be calculated from (61). Values of Mt/M_∞ can be found from McKay's tables for various values of v. Comparisons of calculated values of Mt/M_∞ can then be compared with experimental values of Mt/M_∞ by plotting the values versus time, to see if there is reasonable fit. Such comparisons are made in the next section and will not be shown here. In the present investigation it was found for samples of intermediate thickness, that earlier periods of oxidation were always characterized by linear decarburization corresponding to the Doehlemann reaction controlled model. However, at later periods, under reducing conditions, decarburization was more sluggish than expected for a surface controlled model and we suppose this to be due to the onset of partial diffusion control of decarburization. Figures 5-(33) to 5-(36) show typical structures of the decarburized alloy under conditions where iron is also oxidizing. Such microstructures are indicative of onset of partial diffusion control of decarburization. In the following section we develop a surface control model **ignoring** diffusion effects. We later discuss the effects of partial diffusion control on the predictions of this model.

3.3 Theory of Simultaneous Decarburization and Oxidation of Iron At Short Times

As will be shown in the experimental section, nucleation and growth of FeO has a pronounced effect on the decarburization rate of the metal and the following model has been induced from experiment in combination with previous [31] [44] theories of decarburization and

Model exhibiting reaction sites at the surface of a polycrystalline alloy.

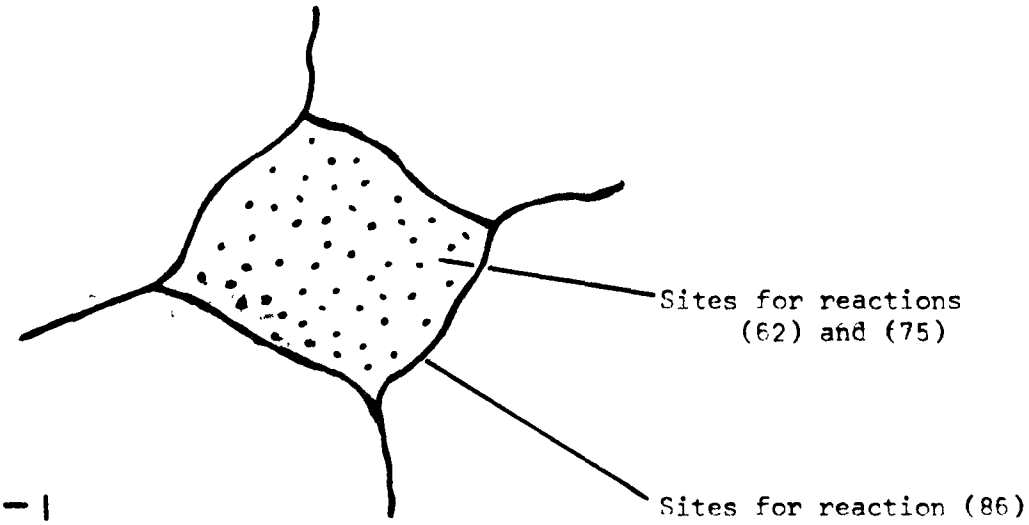

FIG. 3-1

Activated Reaction Rate Model For the reaction

$$CO_2 \underset{k_1'}{\overset{k_1}{\rightleftharpoons}} O^*_{ads} + CO \uparrow \text{(slow)} \quad (62)$$

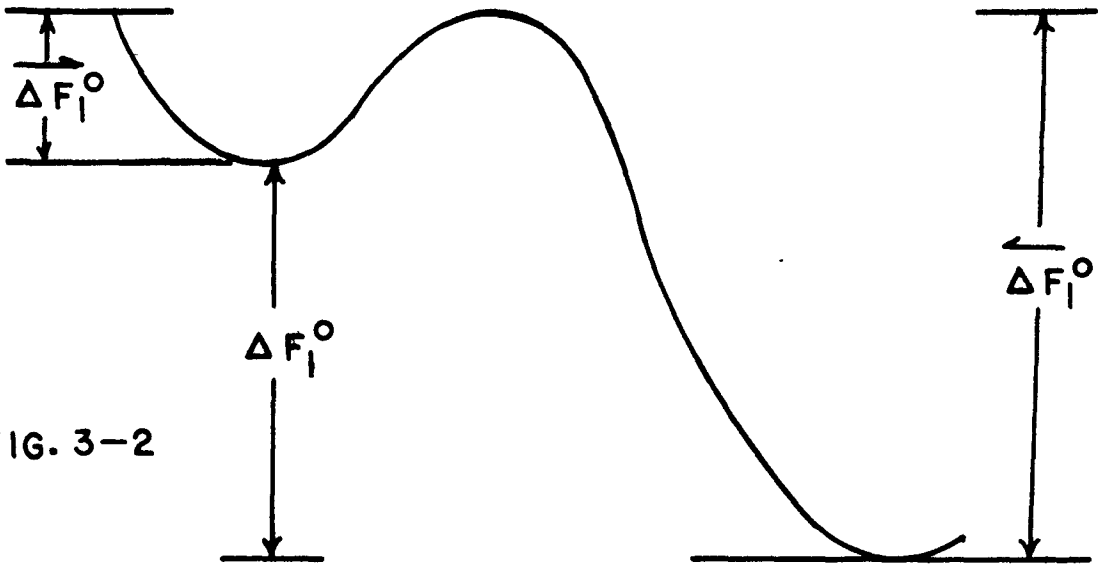

FIG. 3-2

$$\Delta F_1^\circ = \overrightarrow{\Delta F_1^\circ} - \overleftarrow{\Delta F_1^\circ}$$

classical nucleation theory[57].

Kirkaldy[48] has suggested a rephrasing of Doehlemann's theory in the absolute reaction rate formalism[28] for the case of simultaneous decarburization and oxidation of a metal whose microstructure appears as in Figure 3-(1). Such a microstructure contains grain (and sub-grain) boundaries which are active sites for the nucleation of oxides, and, kinks or ledges which are active sites for combination of carbon with adsorbed oxygen. The latter sites are assumed to have a high areal density, although direct evidence for their existence has not been obtained.

Continuing then, Doehlemann considers two parallel reaction chains which describe the transfer of oxygen from a CO-CO_2 mixture to react with carbon on an active site at the surface of iron and to produce CO gas, which is emitted.

In the first chain

$$CO_2 \underset{k_1'}{\overset{k_1}{\rightleftharpoons}} O^*_{ads} + CO\uparrow \quad \text{(slow)} \tag{62}$$

$$O^*_{ads} + \underline{C} = CO\uparrow \quad \text{(fast)} \tag{63}$$

O^*_{ads} refers to adsorbed oxygen transferring directly to sites where it can react instantly with dissolved carbon at the surface ($\underline{C}$). In this chain the first reaction is assumed to be controlling and the second to be substantially in equilibrium. The activated rate model for the controlling reaction is given in Figure 3-2.

We may therefore write the net forward rate as

$$R_1 = \vec{R}_1 - \overleftarrow{R}_1 = k_1' P_{CO_2} e^{-\frac{\vec{\Delta F}_1^{\circ}}{RT}} - k_1' P_{CO}\, a^*_{O ads.}\, e^{-\frac{\overleftarrow{\Delta F}_1^{\circ}}{RT}} \tag{64}$$

The equality of the rate constants being required by the vanishing of the rate at equilibrium. This reduces to:

$$R_1 = k_1' P_{CO_2} e^{-\frac{\overrightarrow{\Delta F_1}^o}{RT}} \left(1 - \frac{P_{CO}\, a^*_{O_{ads}}}{P_{CO_2}} e^{-\frac{\Delta F_1^o}{RT}}\right) \tag{65}$$

If we multiply the second term by

$$\frac{a^*_{O_{ads.\ eq.}}}{a^*_{O_{ads.\ eq.}}} = 1 \tag{66}$$

and note that the equilibrium constant

$$K_1 = \frac{P_{CO}\, a^*_{O_{ads,\ eq.}}}{P_{CO_2}} = e^{-\frac{\Delta F_1^o}{RT}} \tag{67}$$

then equation (64) simplifies to

$$R_1 = k_1 P_{CO_2} \left(1 - \frac{a^*_{O_{ads}}}{a^*_{O_{ads,\ eq.}}}\right) \tag{68}$$

where $$k_1 = k_1' e^{-\frac{\Delta F_1^o}{RT}} \tag{69}$$

Referring next to equation (63) which is in equilibrium with the CO in the atmosphere we have the equilibrium constant

$$K_2 = \frac{P_{CO}}{a^*_{O_{ads}}\, a_{\underline{c}}} \tag{70}$$

which for a reaction at fixed P_{CO} gives

$$a^*_{O_{ads}}\, a_{\underline{c}} = \text{constant} \tag{71}$$

This must include the special case where both reactions are in equilibrium, and the carbon has its equilibrium value in the metal, $a_{\underline{C}}$ eq. Thus

$$\frac{a^{*}_{O_{ads}}}{a^{*}_{O_{ads,\ eq.}}} = \frac{a_{\underline{C}\ eq.}}{a_{\underline{C}}} = \frac{C_{eq.}}{C} \tag{72}$$

where the C's are dilute concentrations of carbon in the iron. Finally

$$R_1 = k_1 P_{CO_2} \left(1 - \frac{C_{eq.}}{C}\right) \tag{73}$$

Doehlemann's second chain of reactions is

$$CO_2 = O_{ads} + CO\uparrow \quad \text{(fast)} \tag{74}$$

$$O_{ads} = O^{*}_{ads} \quad \text{(slow)} \tag{75}$$

$$O^{*}_{ads} + \underline{C} = CO\uparrow \quad \text{(fast)} \tag{63}$$

where O_{ads} refers to inactive adsorbed oxygen which is in equilibrium with the atmosphere and presumably freely occupies random surface sites. The controlling reaction (75) must therefore be a short surface diffusion step in which O_{ads} proceeds to active sites to form O^{*}_{ads}. By analogy with the above analysis the rate for equation (75) may be written as:

$$R_4 = k'_4 a_{O_{ads}} e^{-\frac{\Delta F_4^{\circ}}{RT}} \left(1 - \frac{a^{*}_{O_{ads}}}{a^{*}_{O_{ads,\ eq.}}}\right) \tag{76}$$

and from the equilibrium constants for (74) and (63) this reduces to

$$R_4 = k_4 \frac{P_{CO_2}}{P_{CO}} \left(1 - \frac{C_{eq.}}{C}\right) \tag{77}$$

The net reaction, in agreement with Doehlemann's result is therefore

$$R = \left(k_1 P_{CO_2} + k_4 \frac{P_{CO_2}}{P_{CO}}\right)\left(1 - \frac{C_{eq.}}{C}\right) \tag{78}$$

or $$R = k\left(1 - \frac{C_{eq.}}{C}\right) \quad \text{(moles/unit area/unit time)} \tag{79}$$

for a given atmosphere.

The differential equation for decarburization in the absence of oxidation is

$$\frac{dc}{dt} = -k \frac{A}{V}\left(1 - \frac{C_{eq.}}{C}\right) \tag{80}$$

The integral is

$$\int_{C_o}^{C} \frac{CdC}{C-C_{eq}} = -k \frac{A}{V} t \tag{81}$$

which has the solution (identical to the Grabke formalism):

$$C-C_o + C_{eq.} \ln \frac{C-C_{eq.}}{C_o-C_{eq.}} = -k \frac{A}{V} t \tag{82}$$

In the limit of short times we can see from the differential equation that

$$\frac{C-C_o}{C_o-C_{eq.}} = \frac{k}{C_o} \frac{A}{V} t = \frac{Mt}{M_\infty} \tag{83}$$

where kA/C_oV is the magnitude of the initial slope in time. A comparison of results obtained in the present study with the Doehlemann[31] theory fitted to the initial slope is shown in Figure 3-(3). A sample calculation for the case of simple diffusion controlled decarburization based upon data obtained by Mehl[58] et al, and Smith[35] is also shown. The resultant fit is rather poor for longer times, but in view of

FIG. 3—3 Effect of Onset of Partial Diffusion Control of decarburization Kinetics of Fe-1.065%C specimens of intermediate thickness in a 10/90 = CO_2/CO atmosphere at 950°C.

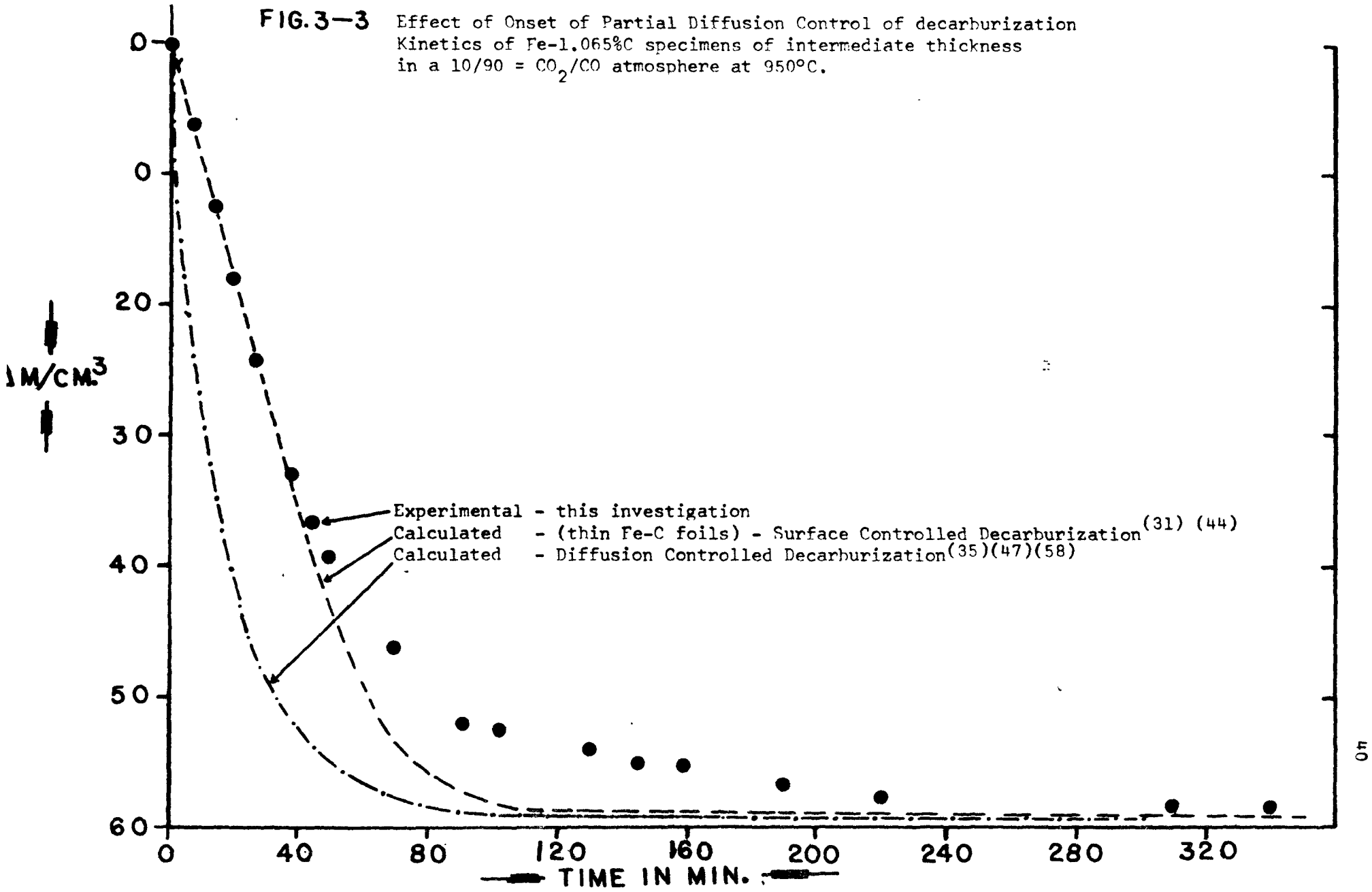

FIG. 3–4 Oxidation Kinetics over the range 10% to 100% CO_2 by volume

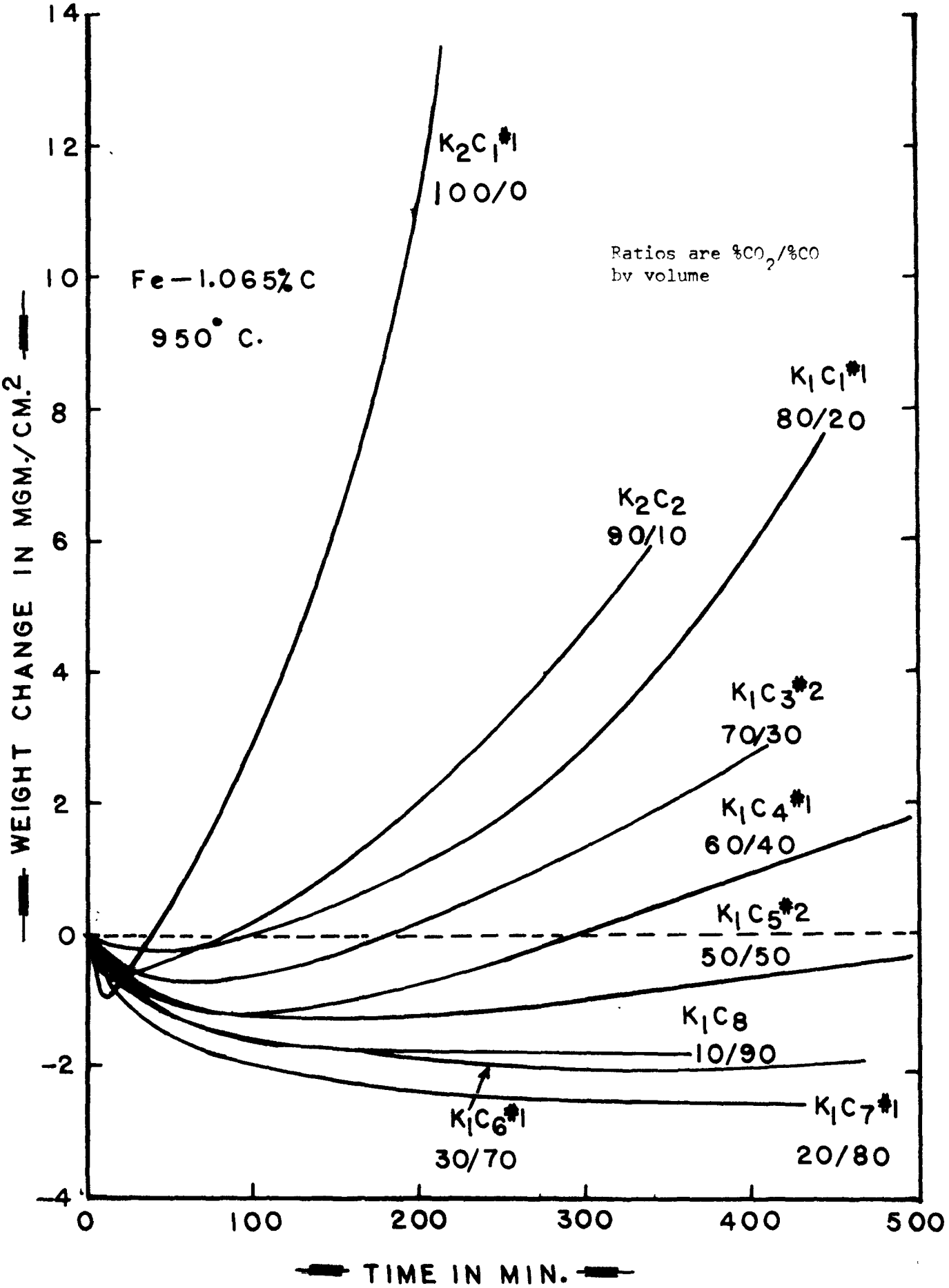

Grabke's [44] definitive experiments with thin foils, the long tail of the curve must be attributed to the onset of partial diffusion control at long times.

From the Doehlemann equation, the initial slopes for iron-carbon alloys oxidized in reducing atmospheres are very nearly proportional to the partial pressure of CO_2 up to the onset of iron oxidation. The results of this investigation are not inconsistent with this prediction.

Figure 3-(4) shows a typical set of curves for the entire gas composition range. Note particularly that all the curves are initially linear.

In Figure 3-(5), a plot of initial and final practical rate constants in mgm./cm.^{2}/min. versus PCO_2 (in atmospheres for PCO_2 + PCO = 1 atmosphere), abstracted from the curves given in chapter 5, Figure 5-(1) to 5-(11), is given. A detailed explanation of this plot will be given later in the discussion section of chapter 6. Suffice it to say that the results of the comparison of our results with those of Grabke[44] show the required linear relationship of decarburization rate with PCO_2 in the low PCO_2 range. Our agreement with Grabke's results tends to support our neglect of diffusion inhibition in the early stages of the surface controlled decarburization reaction even though our specimens were thicker.

The problem now is to explain why onset of oxidation has such a strong effect on the initial slopes and in particular why the initial portion of the loss curves remain linear (see Figure 3-4) at the onset of the nucleation and growth process of initial oxidation, and, decrease in

FIG. 3-5 Practical Initial and Final Rate constants abstracted from Figure 5-1 to 5-11 as a function of P_{CO_2} and comparison with values from the literature for oxidation in CO-CO_2 atmospheres at 950°C and $P_{CO} + P_{CO_2} = 1$ atm.

(The error bars shown are the upper and lower limits of the r. m. s. deviation.)

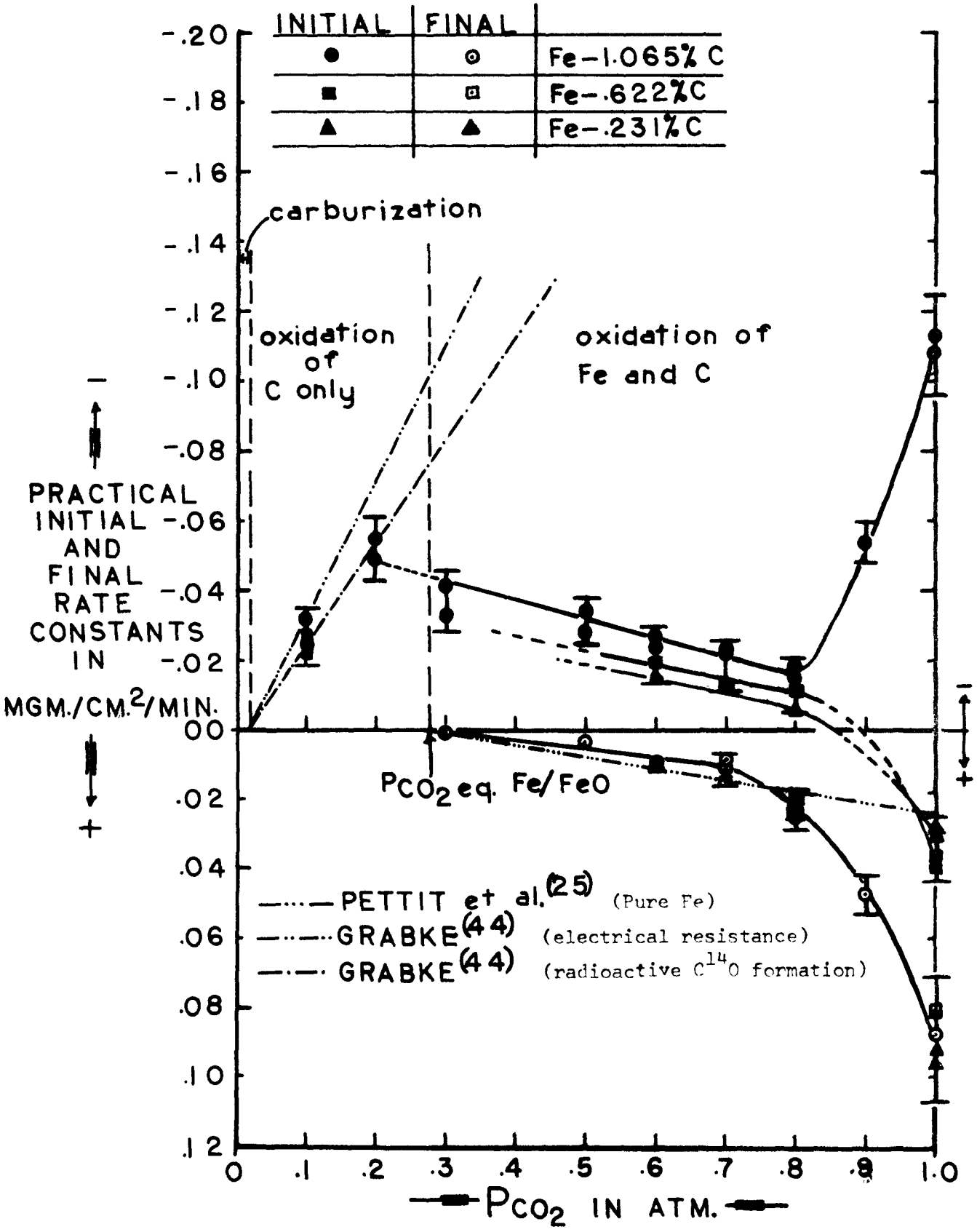

FIG. 3–6 Modes of Dissociation of CO_2, adsorption of O_2, and surface Diffusion of O_{ads}

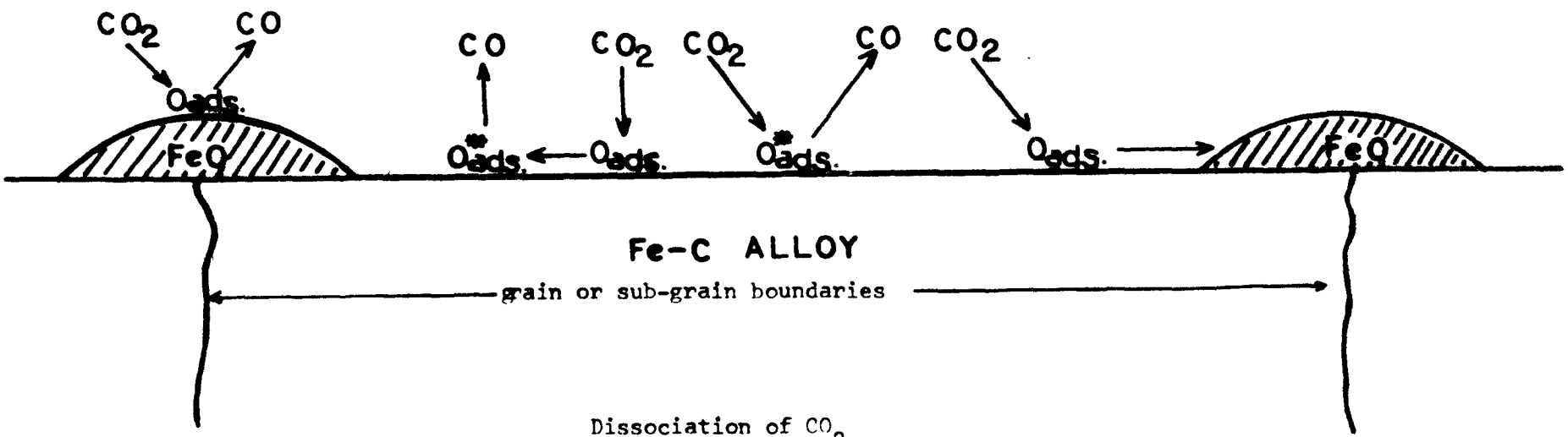

Dissociation of CO_2

Sequence I

$CO_2 = O_{ads} + CO$ (fast) (74)

Sequence II

$CO_2 = O^*_{ads} + CO$ (slow) (62)

Oxidation of Carbon

Surface Diffusion Step

$O_{ads} = O^*_{ads}$ (slow) (75)

then

Directly From - 62

$O^*_{ads} + C = CO$ (fast) (63)

In Atmospheres Where the Dissociation Pressure of FeO is Exceeded

$O_{ads} + Fe = FeO$ (86)

thus establishing a competition for O_{ads} between reactions (75) and (86)

value between 30 and 80% CO_2. A process of random nucleation and growth of oxide at point sites can contribute nothing to the weight gain initially since such transformation curves are typically sigmoidal. If the anomaly associated with Figure 3-(5) is to be associated with oxidation weight gain (and we can think of no other simple explanation) then we have to find an oxidation model which adsorbs oxygen at a steady rate from time zero (steady to assure constant initial overall kinetics, as observed). We are therefore forced to consider initially a grain boundary nucleated oxide of early boundary coverage which accumulates at a steady rate by reaction with inactive O_{ads} as indicated in the profile of Figure 3-(6). Of course, weight-gain by direct oxidation will also supply a component but this will follow a sigmoidal relation (see later) and so can be neglected for initial slopes.

The side-wise growth of oxide via oxygen adsorbed on Fe must be determined by a complicated process of surface diffusion and adsorption control which is difficult to describe analytically. It must, however, result in a quasi-steady O_{ads} concentration profile as indicated in Figure 3-(7) so as to provide a surface diffusion flux. Such a configuration requires that reaction (74) be increasingly out of equilibrium as the oxide is approached, with an increasing flux of O_{ads} from the gas phase. By analogy with the rate process treatment of equations (62) and (63) (replacing O^*_{ads} by O_{ads}) we obtain the rate equation for adsorption at each location of the profile

$$R_2 = k_2 P_{CO_2} \left(1 - \frac{a_{O_{ads}}}{a_{O_{ads.\ eq.}}}\right) = k_2 P_{CO_2} \left(1 - \frac{C_{O_{ads}}}{C_{O_{ads,\ eq.}}}\right) \quad (84)$$

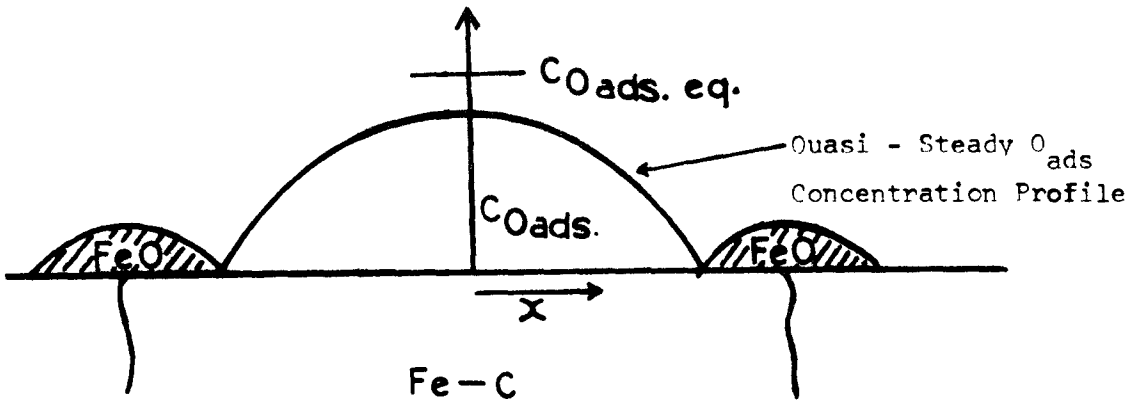

FIG. 3—7 Uni-Dimensional Model Exhibiting Concentration Profile of Adsorbate For side-wise growth of FeO Determined by a complex surface diffusion process and adsorption control such that a surface diffusion flux is provided.

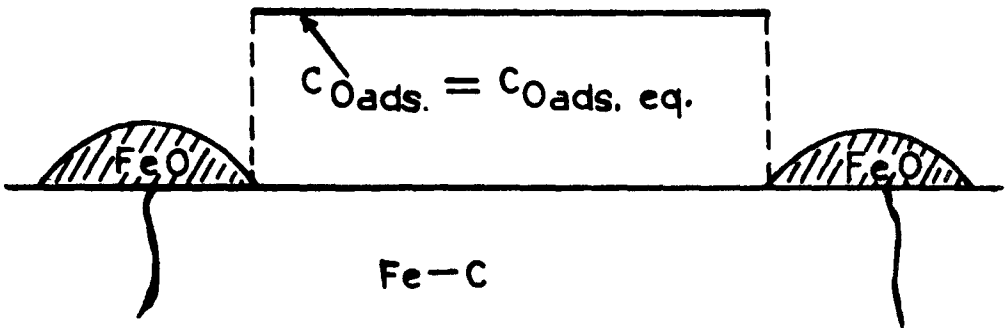

FIG. 3—8 Uni-Dimensional Model Exhibiting Concentration Profile of Adsorbate having replaced the surface diffusion step of Figure 3-(7) above by a simple surface process.

The differential equation will be

$$- \text{div } J = D \frac{\partial^2 C_{O_{ads}}}{\partial x^2} = - R_2 = - k_2 P_{CO_2} \left(1 - \frac{C_{O_{ads}}}{C_{O_{ads,\ eq.}}}\right) \quad (85)$$

If the diffusion step were very fast, and was controlling, then $C_{O_{ads}} << C_{O_{ads,\ eq.}}$ and the curvature $(\frac{\partial^2 C}{\partial x^2})$ would be constant, ie. the diffusion solution would be a low-lying arc of a circle. Furthermore the rate would be proportional to P_{CO_2}. However, the above limiting case is in contradiction to our assumption of surface diffusion rate control in equation (75). In this limit, $C_{O_{ads}} \cong C_{O_{ads,\ eq.}}$ everywhere except close to the oxide. We can therefore replace the surface diffusion step by a simple surface process corresponding to the profile of Figure 3-(8).

The appropriate reaction is

$$O_{ads} + Fe = FeO \quad (86)$$

which has a rate of the form

$$R_5 = k_5 \left(\frac{P_{CO_2}}{P_{CO}} - \frac{P_{CO_2}}{P_{CO\ \text{eq., oxide}}} \right) \quad (87)$$

Insofar as equation (74) remains in equilibrium, reactions (62), (75) and (86) tend to ∞ as $P_{CO_2}/P_{CO} \to \infty$ which is impossible; thus at high ratio, equation (74) must tend to become limiting. This means that reactions (75) and (86) enter a competition for O_{ads} coming from reaction (74). Since (75) is proceeding via much shorter diffusion paths (see Figure 3-1) than (86) we might expect it to win the competition and the overall weight change kinetics swing in favour of equation (75).

We are now in a position to understand the initial kinetics as a

Representative curves corrected for saturation of reaction (74) at high rates with partition between reactions (75) and (86) to the advantage of (86) with appropriate choices of rate constants and a correction for high rates, the previous Figure 3-5 can thus be generated.

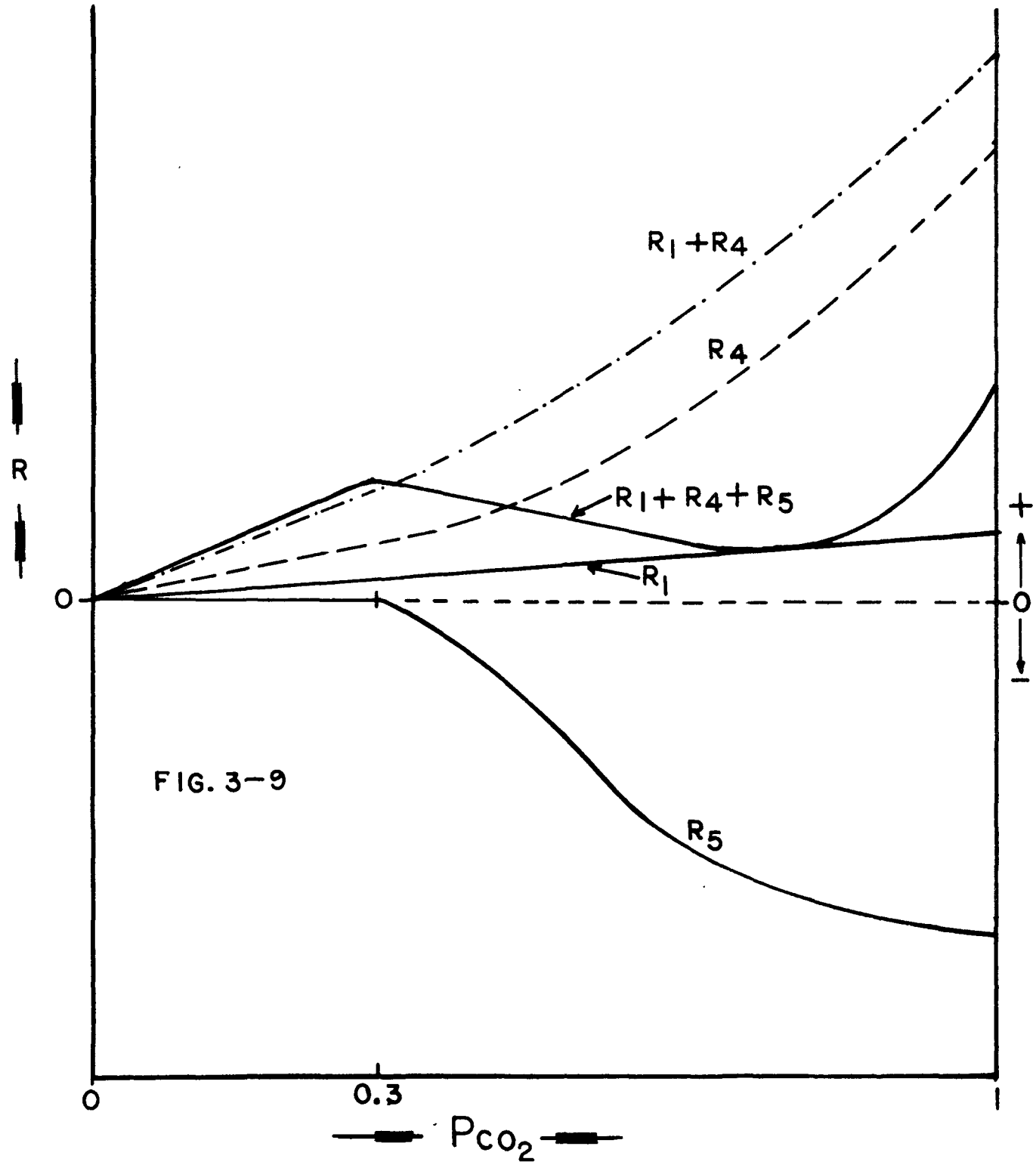

FIG. 3-9

function of P_{CO_2} ($P_{CO_2} + P_{CO} = 1$) given in Figure 3-(5). Since the initial slopes are proportional to the rates (R) we designate the decarburization rates as positive loss rates and oxidation rates as negative loss rates. We assume that both decarburization reactions are occurring at about the same rates at low P_{CO_2} (ie. $k_1 \cong k_4$) Figure 3-(9) shows some representative curves corrected for saturation of (74) at high rates with partition between (75) and (86) to the advantage of (86). With appropriate choices of rate constants and a correction for high rates, it is obvious that we can generate Figure 3-(5). The metallography is reasonably consistent with this model in regard to morphology of oxide coverage and the weight partition between the competing reactions.

Further evidence in support of this interpretation is obtained from the theory for later times.

3.4 Description of Late Time Kinetics

The decarburization reaction rate will decrease in proportion to the area coverage by oxide. We must therefore develop an oxidation model which generates this area change and which simultaneously predicts the oxide weight gain kinetics. Let us approximate the grain in Figure 3-(1) by a circle of radius r_o as shown in Figure 3-(10). We assume that the annular ring of oxide grows inward at a steady rate by reaction (86) and that the ring thickens by a linear (reaction controlled) surface mechanism. The rate of ring thickening, dr/dt, will therefore be

$$\frac{dr}{dt} = - B_1 \qquad (88)$$

FIG. 3—10 Oxidation model generating surface area change due to area coverage by FeO

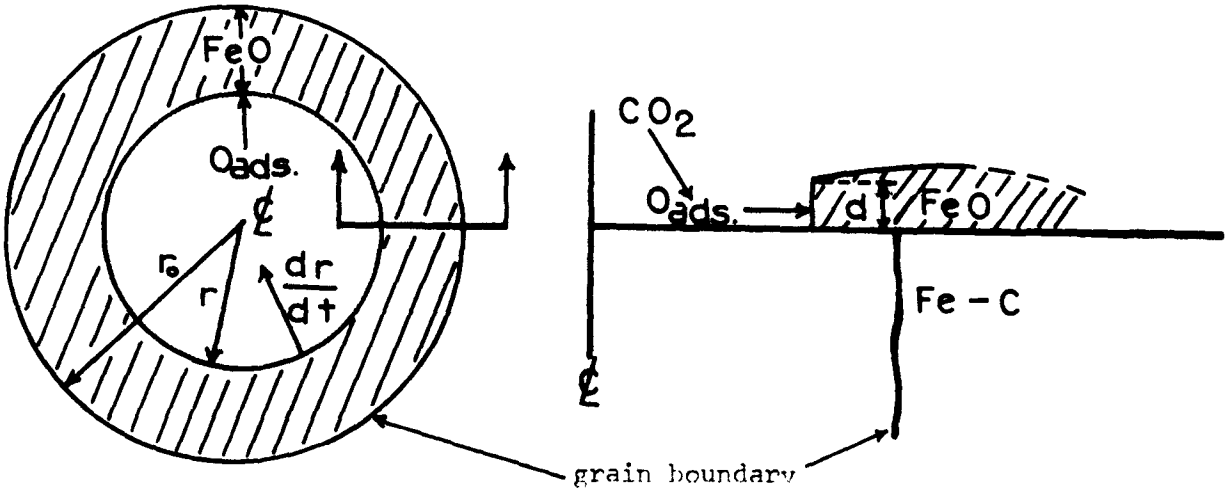

FIG. 3—11 Typical Shape of Kinetic Curves for Concurrent Oxidation of Carbon and Iron Predicted From the Theory

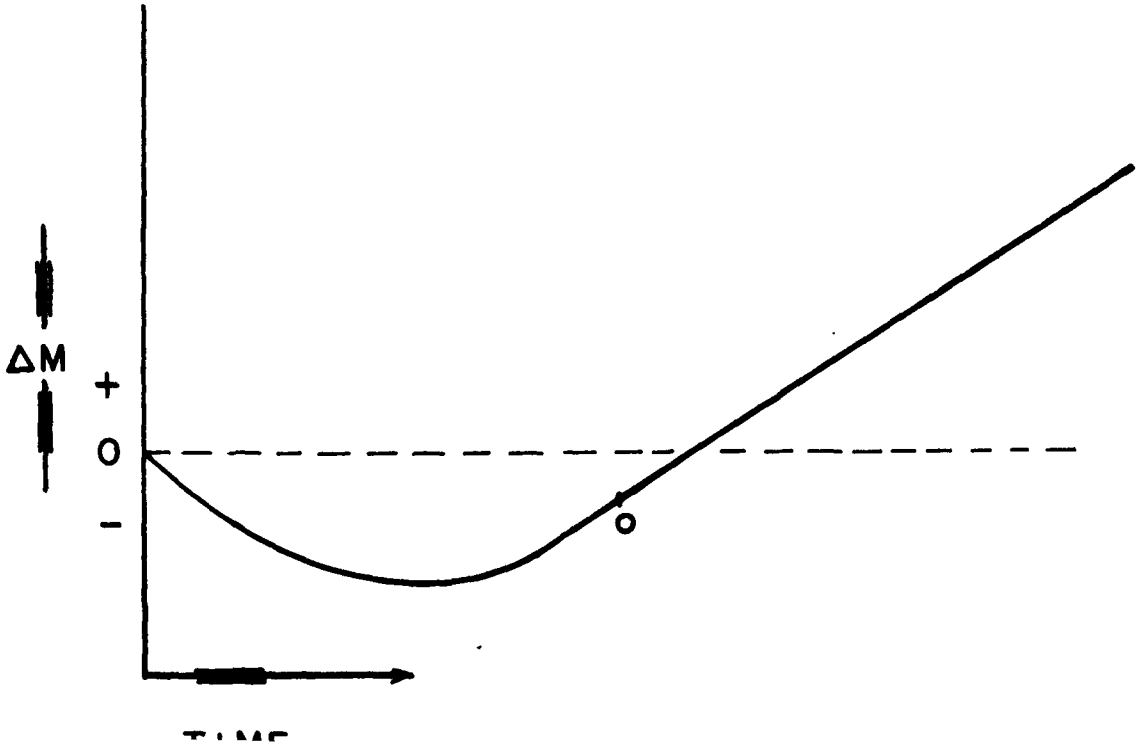

where B_1 is a constant including k_5, the volume of oxide per mole of $O_{ads.}$ transferred and the effective thickness, d, of oxide which is sustained by this reaction. This integrates to

$$r = r_o - B_1 t \tag{89}$$

The differential area increase (ie. area covered by oxide) is given by:

$$dA = -2\pi\, r dr = -2\pi r \frac{dr}{dt} dt \tag{90}$$

$$dA = 2\pi\, B_1 \left(r_o - \frac{B_1 t^2}{2}\right) \tag{91}$$

and the instantaneous area is

$$A = 2\pi\, B_1 \left(r_o t - \frac{B_1 t^2}{2}\right) \tag{92}$$

This reaches its maximum value at time $t = r_o/B_1$ where its value is $A^o = \pi\, r_o^2$.

The weight gain as a function of time due to growth of the ring will go as $B_2\, An_A$ where n_A is the number of grains per unit area, while the weight gain due to thickening will go as $K_L \int A/A_o dt$. The decarburization kinetics will follow $-\Delta m\, A/A_o$ where Δm is the decarburization mass loss per unit area according to Doehlemann's theory. For strong oxidation Δm will be proportional to t right up to the time of complete coverage. We may therefore represent this term by $-B_3 \int dt\, (A_o - A)/A_o$. The overall kinetics will therefore follow

$$\Delta M = -B_3 t \left[1 - \frac{\pi B_1 r_o}{A_o}\left(t - \frac{B_1 t^2}{3r_o}\right)\right] + 2\pi B_1 B_2 n_A r_o \left(t - \frac{B_1 t^2}{2r_o}\right) + \frac{\pi K_L B_1 r_o}{A_o}\, t \left(t - \frac{B_1 t^2}{3r_o}\right) \tag{93}$$

It is to be noted that the first term must become constant at $t = r_o/B_1$ and remain constant thereafter; the second takes the value $\pi r_o^2 B_2 n_A$ and remains constant thereafter and the third term takes the value $K_L t$ and continues thusly indefinitely. We see that the effect of oxidation is to change the initial slope from $-B_3$ to

$$-B_3 + 2\pi B_1 B_2 n_A r_o \tag{94}$$

Empirically, the second term is always negative so B_3 is the largest in magnitude. There are three quadratic terms whose co-efficients total

$$\frac{\pi B_1 B_3 r_o}{3A_o} - \pi B_1^2 B_2 n_A + \frac{\pi K_L B_1 r_o}{A_o} \tag{95}$$

From the previous sentence the first term must be always greater than the second so the sum is positive. The co-efficients of the cubic terms total

$$-\frac{\pi B_1^2 B_3}{3A_o} - \frac{\pi K_L B_1^2}{3A_o} \tag{96}$$

which is always negative. For long times $\Delta M \to K_L t$ which represents a continuing mass increase. We see therefore that provided the initial slope remains negative (as observed) the curves must always have the shape of Figure 3-(11). It is clear that this simple model nicely reproduces the qualitative character of all features of the reaction. However, it does not take account of long time leakage and the known change of oxidation kinetics to parabolic kinetics at very long times which prevents its quantitative use. One further qualitative point of agreement may be found by examining the quadratic co-efficient which goes roughly as

$$\frac{\pi r_o}{A_o} B_1(B_3 + K_L) \qquad \text{(from combination of the 1st and 3rd quadratic terms on previous page)} \qquad (97)$$

Noting that all three rate co-efficients contain terms in P_{CO_2}/P_{CO}, we expect this to blow up as $P_{CO_2} \to 1$. It is the quadratic term which determines the location of the minimum of the curve, the larger is the co-efficient, the shorter is t min, ie., they should be inversely proportional. We have plotted 1/t min versus P_{CO_2} in Figure 3-(12)and we indeed see the predicted tendency very clearly.

There would, however, be little point in fitting curves since there are too many adjustable parameters and the model is quite inadequate in detail.

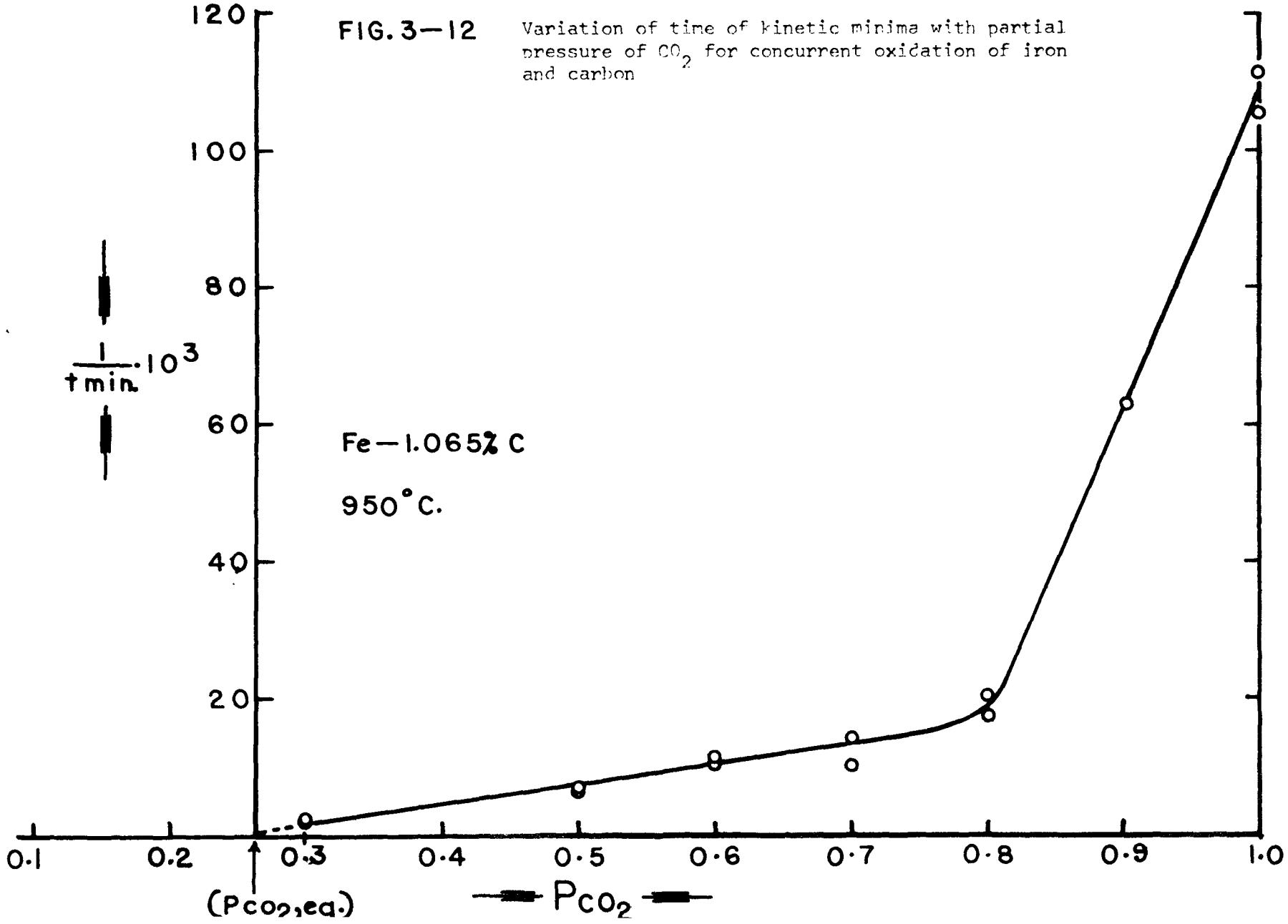

FIG. 3—12 Variation of time of kinetic minima with partial pressure of CO_2 for concurrent oxidation of iron and carbon

CHAPTER 4

EXPERIMENTAL TECHNIQUE

4.1 Introduction

This section will deal with specimen preparation, the details of the experimental apparatus and the equipment and technique used to study the metal and oxide properties.

4.2 Experimental Specimens

The iron-carbon alloys used in this study were obtained from Dr. G. R. Purdy, McMaster University, as bars of the homogenized alloys at various carbon compositions. As received, the bars had a square cross section of 2.5 in. These bars were then machined down to a cross section of approximately 1 in. in diameter. Disks 1/4 in. thick were then cut from the rods. For the test specimens of lower carbon content, the disks were cold rolled directly to sheet of the appropriate thickness. The disks of higher carbon content, however, could not be cold reduced at all. These disks had to be soaked at 1000°C in dry argon and then hot rolled to give sheet of the required thickness. The sheets were rolled to a thickness of approximately .07 cm. Experimental specimens were then prepared by shearing the prepared sheets into rectangular platelets 1 cm. x 1.5 cm.

It was decided that specimens of intermediate thickness would be employed since these would best match the sensitivity of the kinetic

apparatus to be employed and since enough carbon would be available to detect the competition between the decarburization and oxidation processes. Furthermore, such tests would be more realistic from the technological point of view than the earlier works on thin foils.[31, 44]

Inspection of the specimens was carried out to eliminate cracked and pitted specimens. Holes were then drilled in the specimens to facilitate inclusion in the kinetic apparatus. A drill bit was selected such that the area removed from the specimen was equal to the area introduced. The specimens were then cleaned by abrasion with silicon carbide paper and again visually examined. Next, the specimens were batch annealed in dry argon for three hours at the temperature at which oxidation was to be observed to eliminate short range segregation and to assure that an equilibrium grain size for the temperature of oxidation would be attained.

After annealing, the specimens were mounted in bakelite. The mounted specimens were then polished on a 320 grit silicon carbide power wheel using a stream of water as a lubricant. Following this, the specimens were polished through 400 and 600 grit silicon carbide on stationary paper again using water as a lubricant. Final polishing was carried out on selvyt cloth power wheels impregnated with 1 micron diamond abrasive with kerosene lubricant. The specimens were then stored in dry reagent grade kerosene. Prior to an experiment the specimen was removed, rinsed with petroleum ether, dried in a stream of air, then rinsed with acetone and again air dried. Nylon gloves were used to handle the specimen from this point onward. The specimens were then weighed on a Mettler balance to ±2 micrograms. The specimen dimensions were measured with the

Table A

Chemical Analysis of Alloys Used

Element	Wt.%
P	.005
S	.005
Mn	.020
Si	.010
Cu	.002
Cr	.002
V	.002
Ni	.033
Mo	.015
Al	.002
Ti	.002
B	.001
Cb	.005

Alloy	Wt.% Carbon
KA	0.231
KB	0.622
KC	1.065

aid of a micrometer thus enabling the surface area of the specimen to be computed. The chemical composition of the test material is given in table A.

4.3.1 Apparatus - General

The standard vacuum system consisted of a 1 in. oil diffusion pump backed by a two stage belt-driven pump. A vacuum of 5×10^{-6} mm. of mercury could be realized in the reaction tube. Liquid air traps were employed to remove contaminants such as mercury and diffusion pump oil.

The oxidation experiments were carried out in flowing CO-CO_2 atmospheres with 100, 90, 80, 70, 60, 50, 30, 20, and 10% CO_2. The ratios of the two gases were controlled by metering the gases with simple capillary flowmeters. Darken and Gurry[52] have demonstrated that linear flow rates should exceed 0.6 cm./sec. in order to eliminate the undesirable effects of thermal segregation. Morris[53], who designed this apparatus, kept the above fact in mind when the capillary diameters were calculated. In the present investigation, the flow meters were re-calibrated by measuring the rate of displacement of a soap film up a graduated cylinder. The curves obtained from the re-calibration are shown in Figure 4-1. The gases used in all the experiments contained less than 0.05% impurity in CO_2 and less than 0.5% impurity in CO. Typical analysis of the two gases are given in table B. The carbon dioxide was passed through columns containing magnesium perchlorate, reduced copper oxide at 400°C and activated alumina. The carbon monoxide was passed through columns containing magnesium perchlorate and ascarite. The gases were then mixed in a 1 litre bulb packed with glass wool and directed by glass tubing

FIG. 4-1 FLOW METER RECALIBRATION

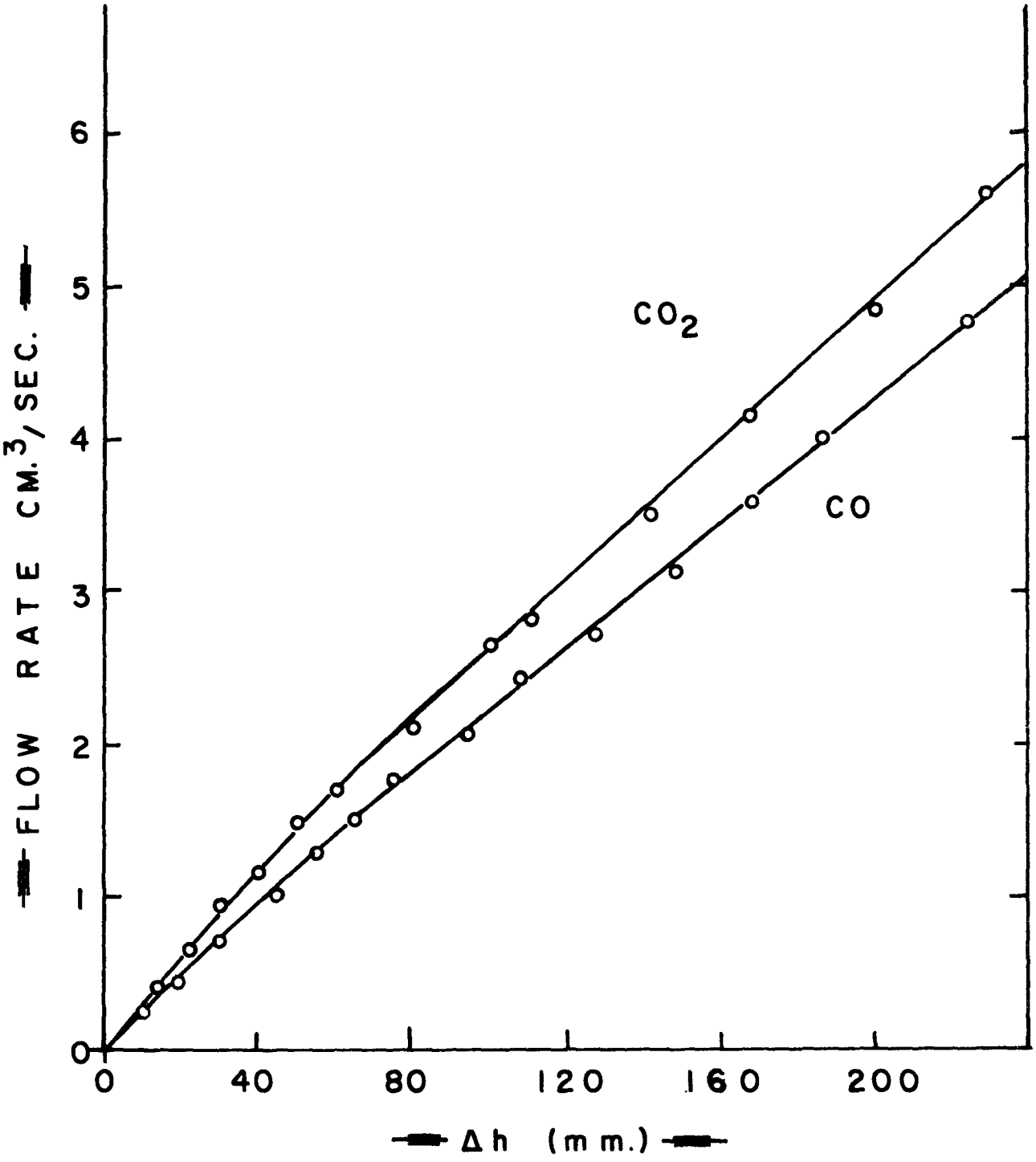

Table B

Typical Gas Analysis

Carbon Monoxide	Carbon Dioxide	
C.P. grade 99.5% CO	Bone Dry Grade 99 .95% CO_2	Grade
200	---	CO_2 ppm.
20	500	O_2 ppm.
75	500	N_2 ppm.
-60°F	-30°F	Dew point

Figure 4-2 Experimental Apparatus

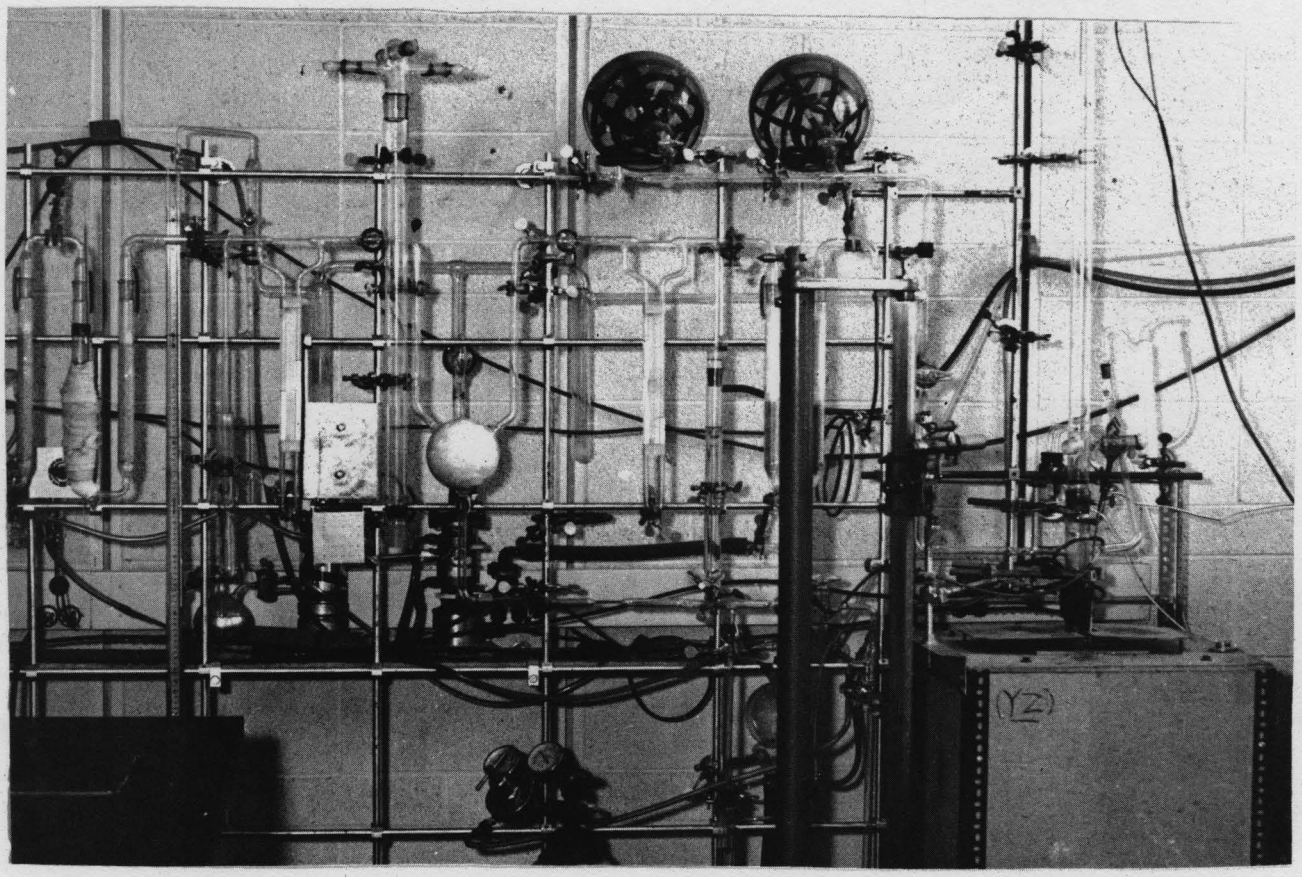

to the bottom of the reaction tube. The furnace assembly consisted of a 20 in. Kanthal element surrounding a 1-1/4 in. diameter mullite tube. The temperature was controlled to ± 2°C by a controller and a chromel-alunel thermocouple which activated a mercury relay in the supply circuit. The control thermocouple was located between the reaction tube and the heating element, and a measuring thermocouple was placed in the same position at the sample level. By this arrangement, a 6°C temperature difference was found to exist between the specimen and thermocouple, and this was compensated for in the temperature setting. The temperature variation over the 4 in. hot zone was 1°C over a distance of 1 in. on either side of the centre. It was experimentally verified that experimental flow rates did not affect the specimen temperature to any significant degree. A general view of the apparatus is given in Figure 4-2.

4.3.2 Kinetic Assembly

The kinetic cell consisted of a calibrated Ni-Span-C spring suspended from a glass winch by a nylon filament. A stationary reference target was suspended from the nylon filament also and extended down the axis of the spring. A schematic diagram of the assembly due to Morris[53] is given in Figure 4-3. The entire suspension was centered by means of two glass forks protruding from the sides of the pyrex envelope. Also, the entire assembly could be raised or lowered in order to position the specimen in the hot zone. Weight losses or gains were recorded by observing the extension or compression of the spring relative to the stationary reference marker, with a vernier cathetometer.

The spring was constructed by Morris from 5 mil Ni-Span-C wire by coiling it about a 1/2 in. rod and securely fastening the ends. The

SCHEMATIC OF KINETIC ASSEMBLY FIG. 4-3

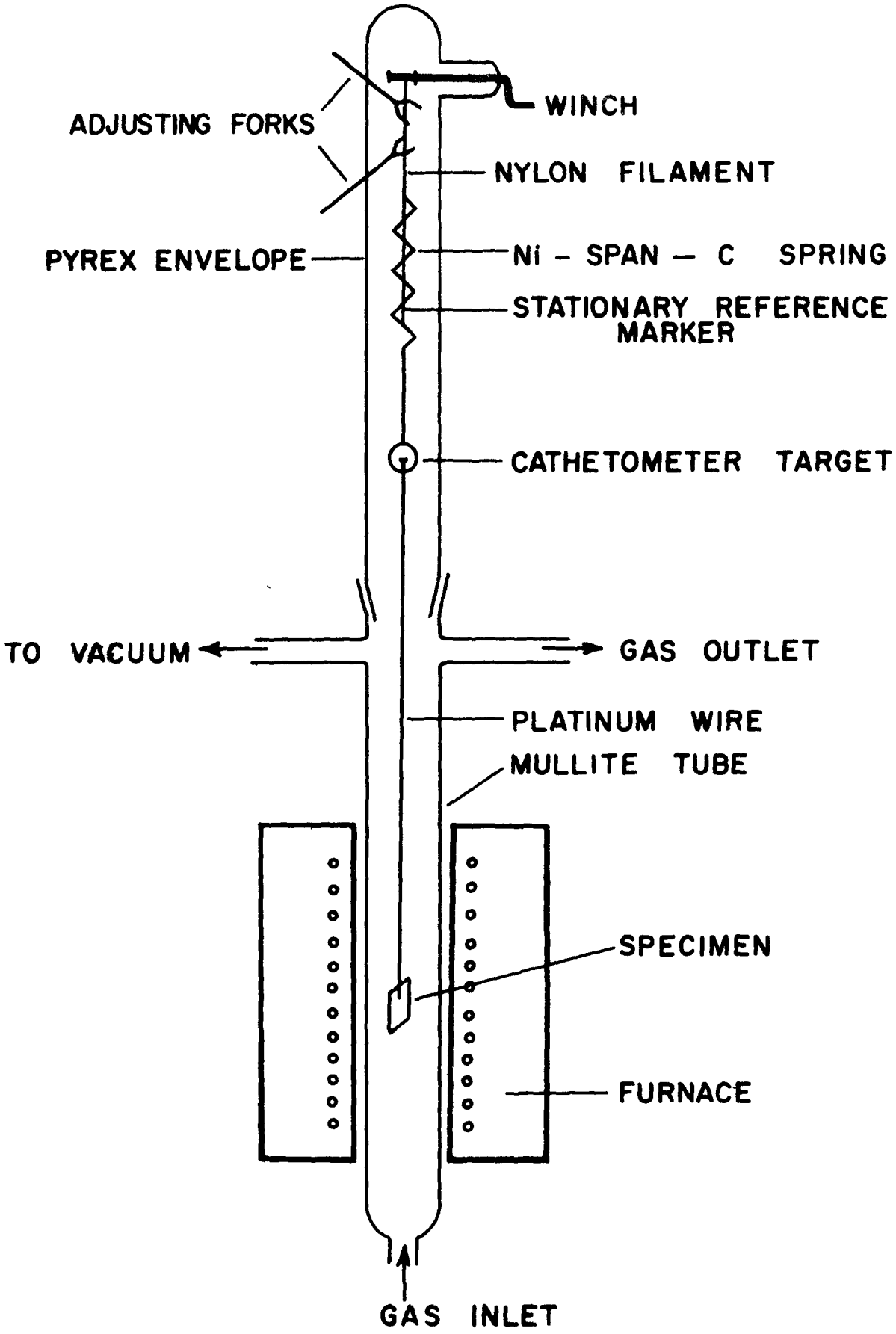

properties of Ni-Span-C are given in table C. After a suitable heat treatment, as indicated in the table, a spring with maximum mechanical properties and a zero co-efficient of expansion which remains constant over the temperature range 50 - 150°F was obtained, thus eliminating the need for a constant temperature controlling device in the spring compartment to compensate for fluctuations in room temperature. The spring was re-calibrated at the beginning of the experimental program and was found to yield the same force constant as Morris had found. The sensitivity of the spring was 36 mg./cm. and this value remained constant throughout the whole series of experiments.

4.4 General Procedure

A finished specimen was suspended from the spring and the assembly was coupled to the reaction tube by means of a ground glass joint. The apparatus was then evacuated with the mechanical pump at the reaction temperature. After about one hour the system was flushed with surgical grade nitrogen. The reaction gas mixture was then allowed to flow through the assembly for at least an hour. The specimen was then lowered into the hot zone and weight gains or losses were measured at intervals from 2 - 15 min. throughout the experiment. At the end of the experiment the specimen was raised as rapidly as possible to the cooler portion of the tube (about 9 sec.) and allowed to cool to room temperature in the flowing gas. The specimen was then removed and the oxide surface was examined. Subsequently, the specimen was mounted in epoxy resin so that the cross section might be observed after polishing. The polishing sequence was essentially the same as for the surface

Table C

Properties of Ni-Span-C spring

General Composition	Cr, Ti, Ni, Fe
thickness	5 mil.
hardening	age hardenable
elastic limit in hardened condition	quite high
heat treatment	Ar anneal for 4.5 hr. at 1350°F
co-efficient of expansion	zero over the temperature range 50 - 150°F

FIG. 4-4 SPRING RECALIBRATION

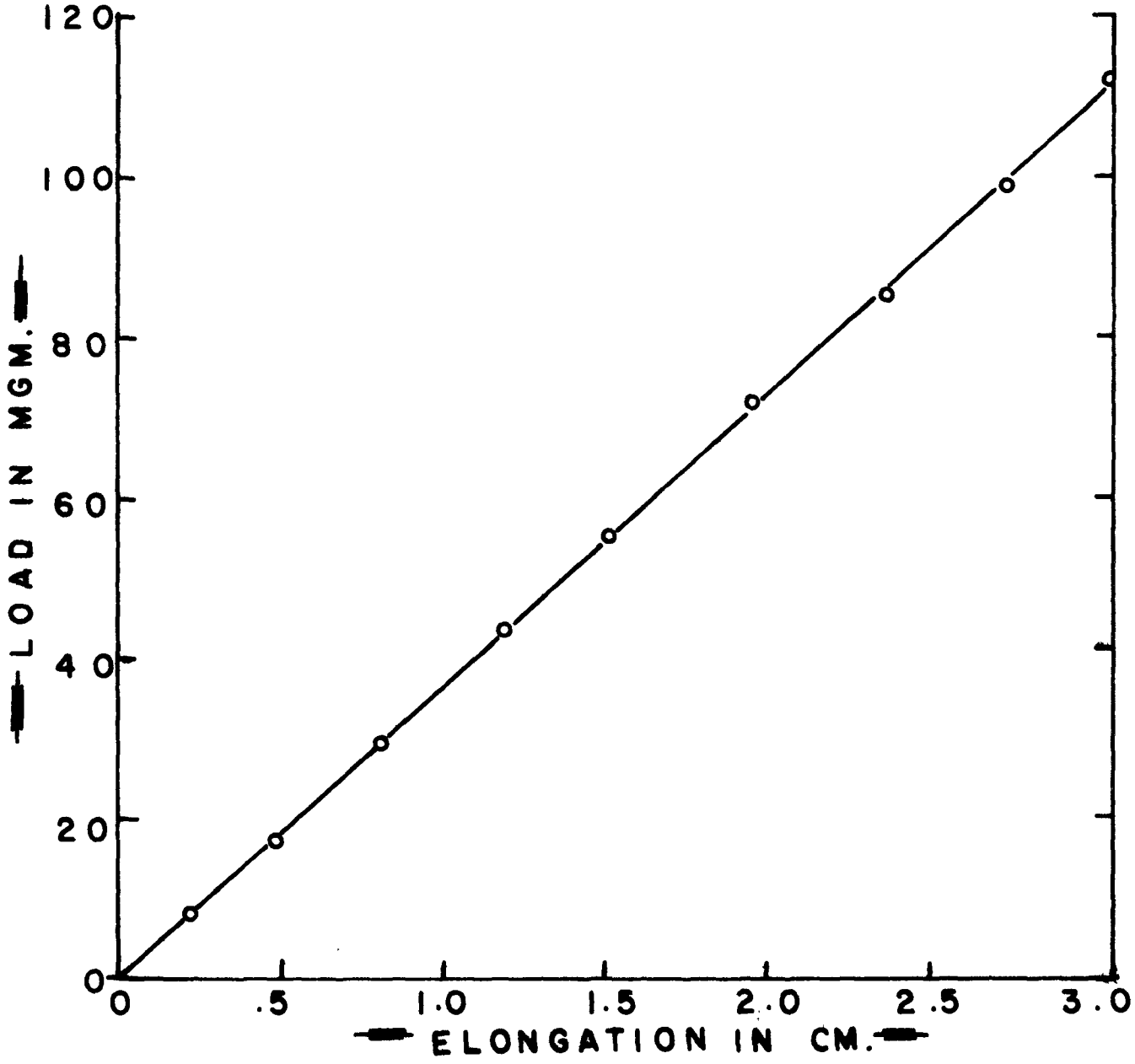

preparation except that the cross section was polished in only one direction with the silicon carbide papers.

4.5 Microscopy

Specimens prepared in the manner described previously, were oxidized for varying time intervals in flowing CO-CO_2 mixtures of constant CO/CO_2 ratio, quenched in the gas stream and removed for observation. The initial and final weights of these specimens were recorded and specimens were then sectioned and cold mounted so that the metal oxide interface could be observed; also the surface topography of the specimens was observed. In a few cases, specimens of oxide were prepared for examination via transmission electron microscopy; however, the specimens so prepared were found to be so thick that they could not be penetrated by the electron beam, even for relatively short oxidation times. Thus, most of the metallographic study employed the standard techniques of light microscopy.

4.6 Oxide Morphology

For the conditions of the tests only one oxide phase was found to be present, namely wüstite. In addition to topographical and interfacial examination, certain aspects of the scale were emphasized by chemical complexing techniques which gave characteristic diagnostic colours. Hence colour photomicrographs were taken in some cases. Due to the nucleation and growth characteristics of the scale, both the scale/gas interface and metal/scale interface were extremely rugged. Hence, rates of scale growth obtained from optical methods were of very limited value, particularly for short oxidation periods when microscopic

holes in the scale were observed to penetrate right down to the metallic phase.

CHAPTER 5

EXPERIMENTAL RESULTS

5.1 Introduction

The raw data obtained for the oxidation of iron - .231, .622 and 1.065 weight percent carbon in flowing $CO-CO_2$ gas atmospheres will now be presented, along with a preliminary discussion of the results. Since most of the experiments were carried out at 950°C, the discussion will be concerned mainly with oxidation at this temperature.

5.2 Experimental Data

Kinetic data are recorded as decrease or increase in specimen weight as a function of time. Graphic illustrations of the kinetic curves are given in Figure 5-(1) to Figure 5-(11) for the three alloys investigated. In all cases, weight losses or gains are expressed in $mgm./cm.^2$ with time in minutes. Alloy concentrations are in weight percent unless otherwise stated. Gas atmosphere compositions are expressed in volume percent CO_2/volume percent CO. Identification of experimental runs for purposes of comparing experimental curves with calculated curves is carried out in the following way: The experimental curves will be designated as K_aA_b, K_aB_b, and K_aC_b. The letter K represents a kinetic experiment, the symbols A, B, and C represent carbon concentrations of .231, .622 and 1.065 weight percent respectively,

and the subscripts a, and b are numbers representing the experimental series and the particular run in the series, respectively. For example, K_1C_3 refers to the third run in the first series of a kinetic experiment for Fe-1.065% carbon. A small "c" in brackets after the experimental designation, for example $K_1C_3(c)$, refers to a curve calculated from the theory, this enables the experimental curve to be located quickly for comparison purposes.

5.3 Experimental Reproducibility

The curves given in Fig. 5-7 will be used to estimate the experimental reproducibility. The sum of values of the limiting slopes for these curves taken as A, B, C, ... result in the arithmetic mean

$$X = \frac{A + B + C + ...}{n} \tag{98}$$

where n is the number of experiments. The differences, (A-X), (B-X), ..., regardless of sign, may be denoted by a, b, c, ... The standard diviation is then defined by:

$$d = \left(\frac{a^2 + b^2 + c^2 + ...}{n-1}\right) \tag{99}$$

The final result is written X ± d.

The experiment carried out with Fe-1.065%C, in the 30/70 atmosphere, as illustrated in Figure 5-(7), exhibited the poorest reproducibility and hence the extreme case for calculation of the experimental reproducibility. This calculation yields ± 17% r.m.s. deviation from the mean giving a precision of ± 11%. All other curves have a better reproducibility. This value is in good agreement with Morris[53] who

FIG.5-1 Experimentally Observed Kinetics

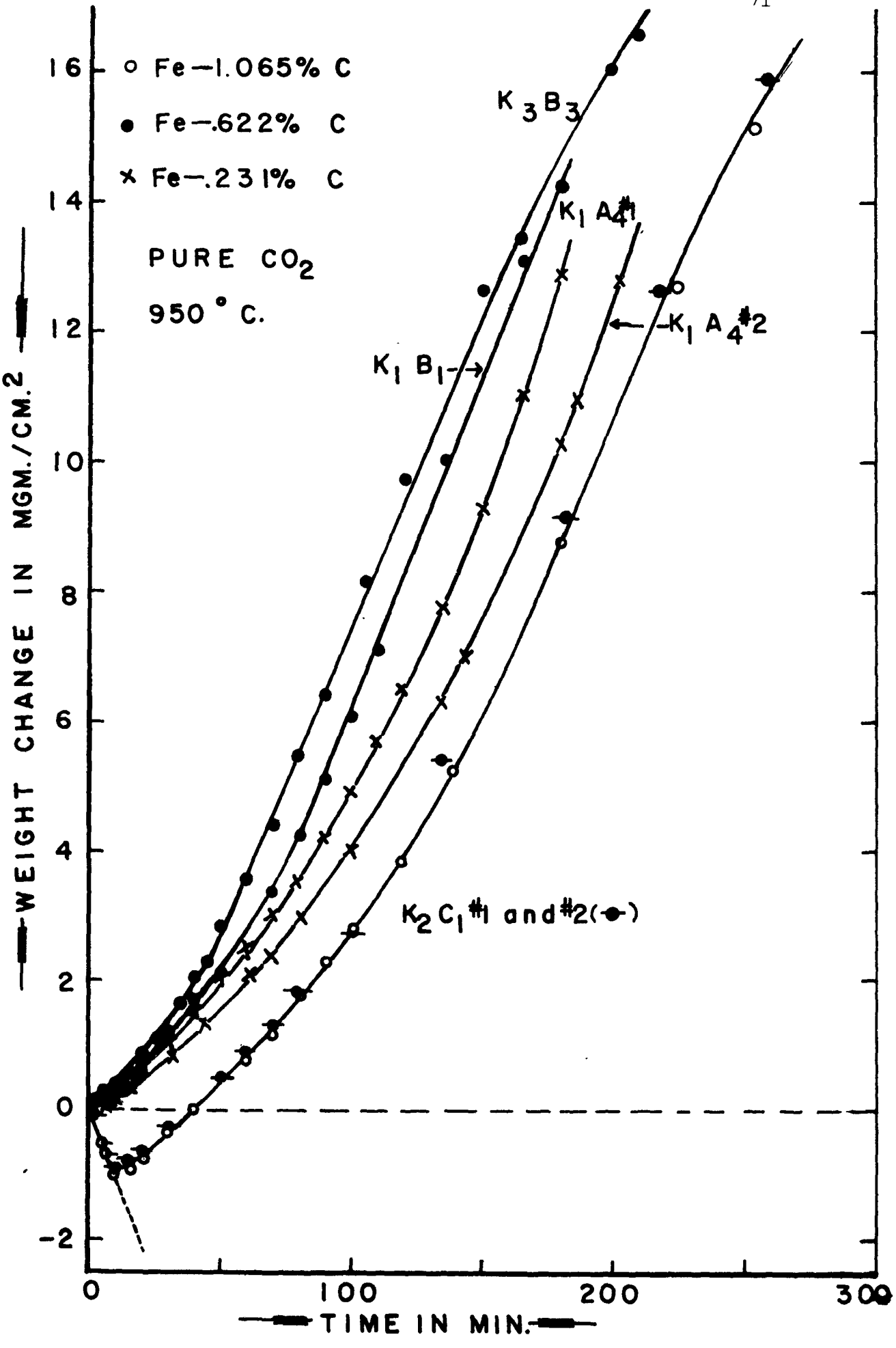

FIG. 5–2 Kinetic Curves continued

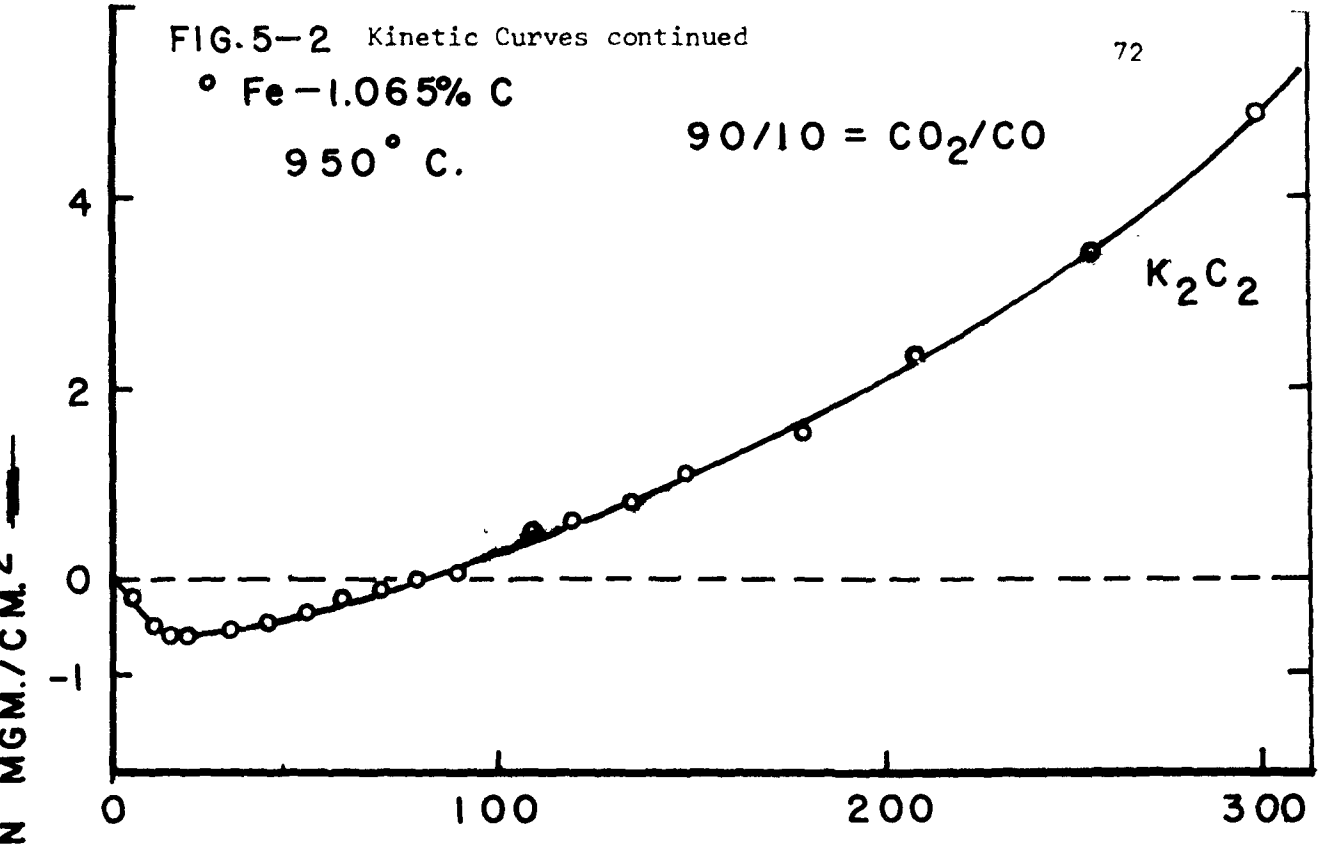

FIG. 5–3

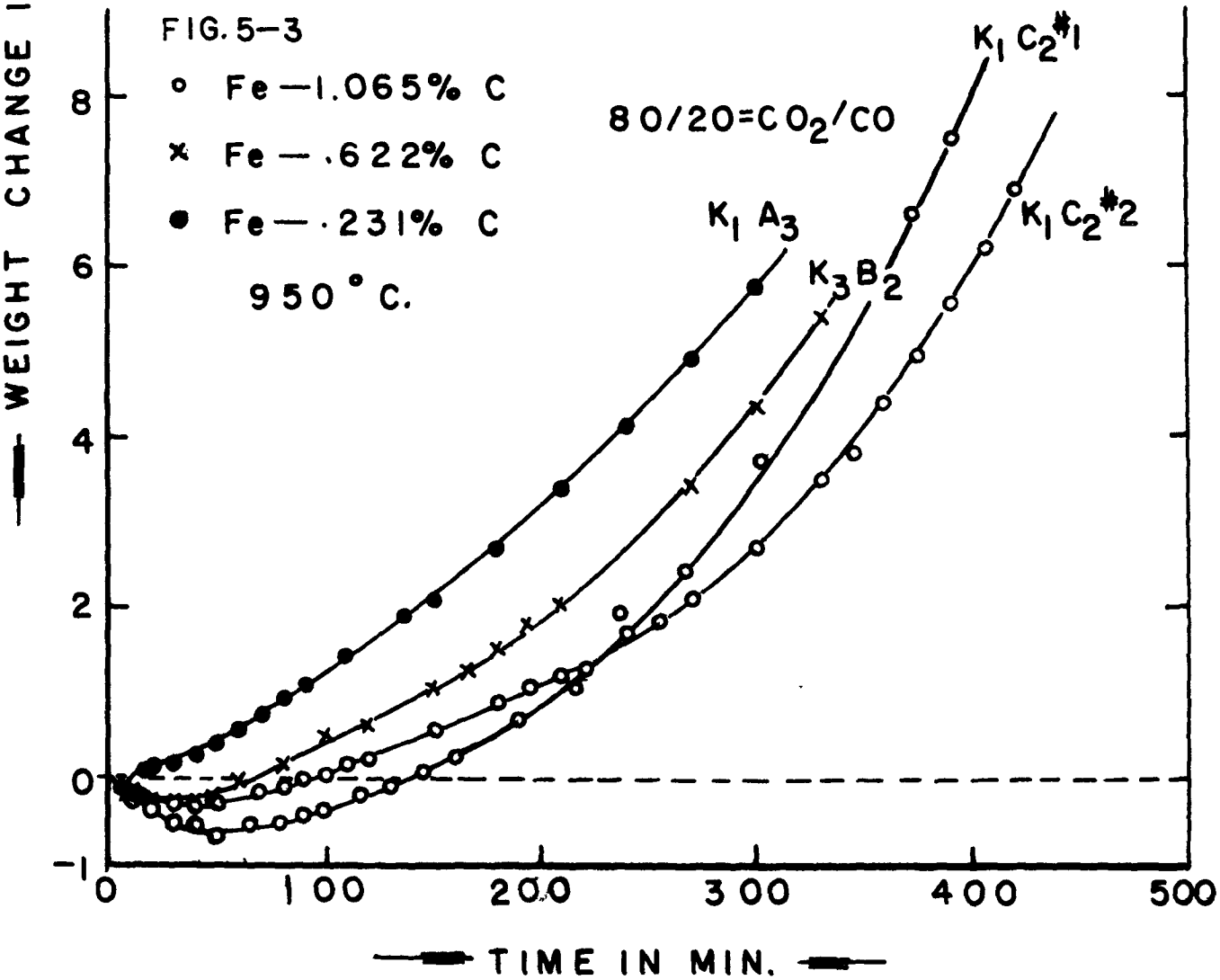

WEIGHT CHANGE IN MGM./CM.^{2}

TIME IN MIN.

FIG. 5—4 Kinetic Curves continued

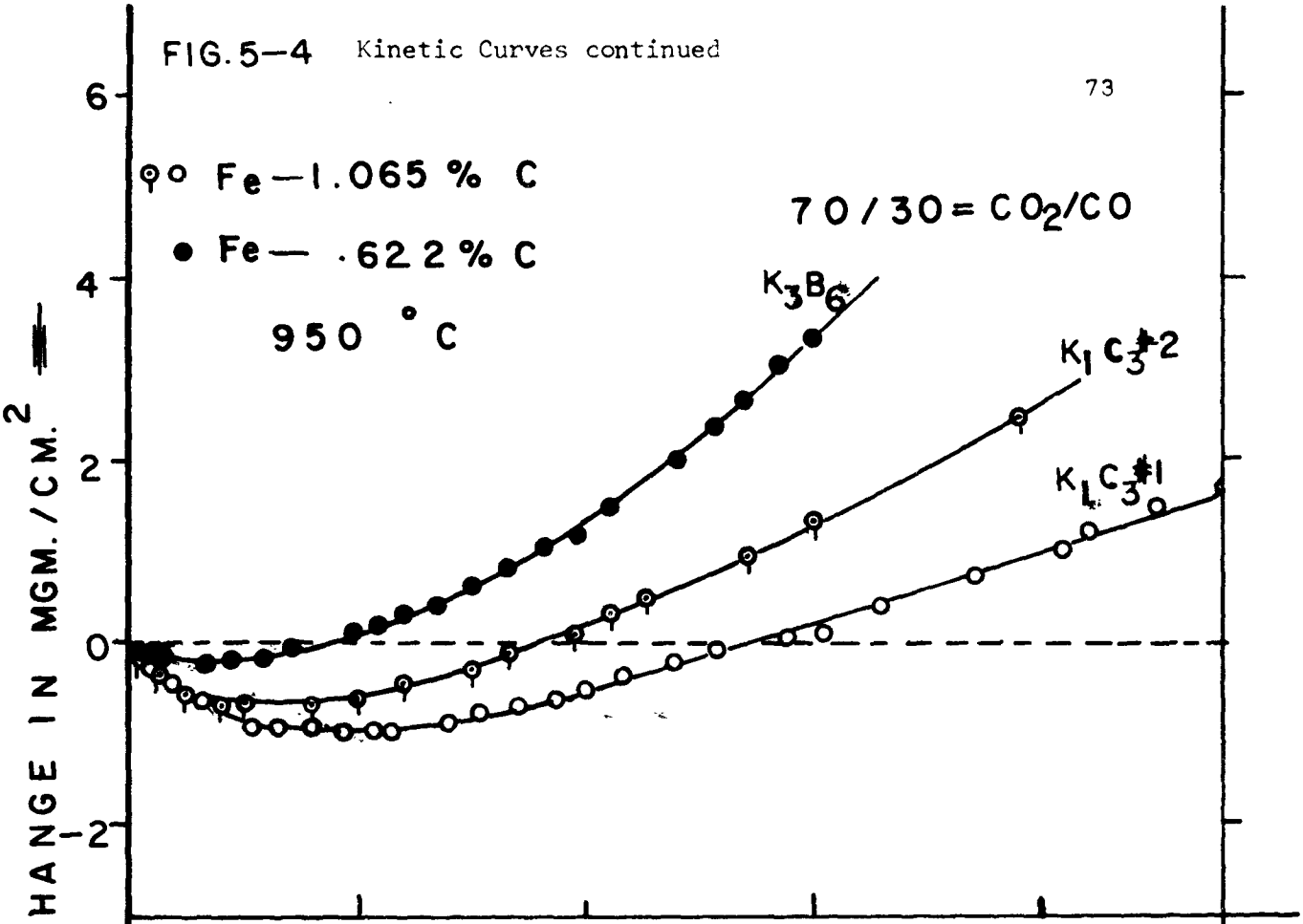

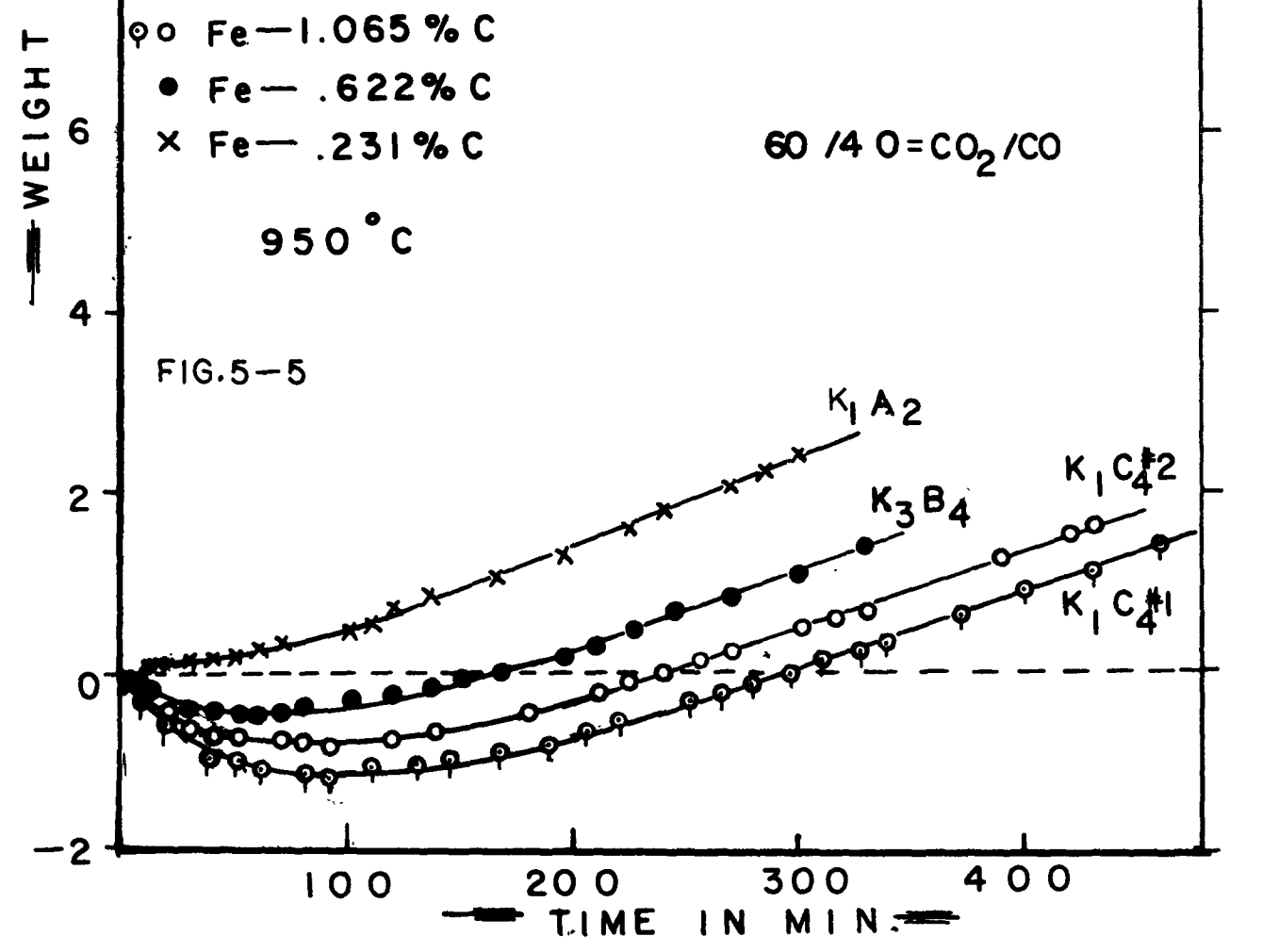

FIG. 5—5

FIG. 5—6 Kinetic Curves continued
[(eq*) denotes nominal equilibrium Carbon Content]

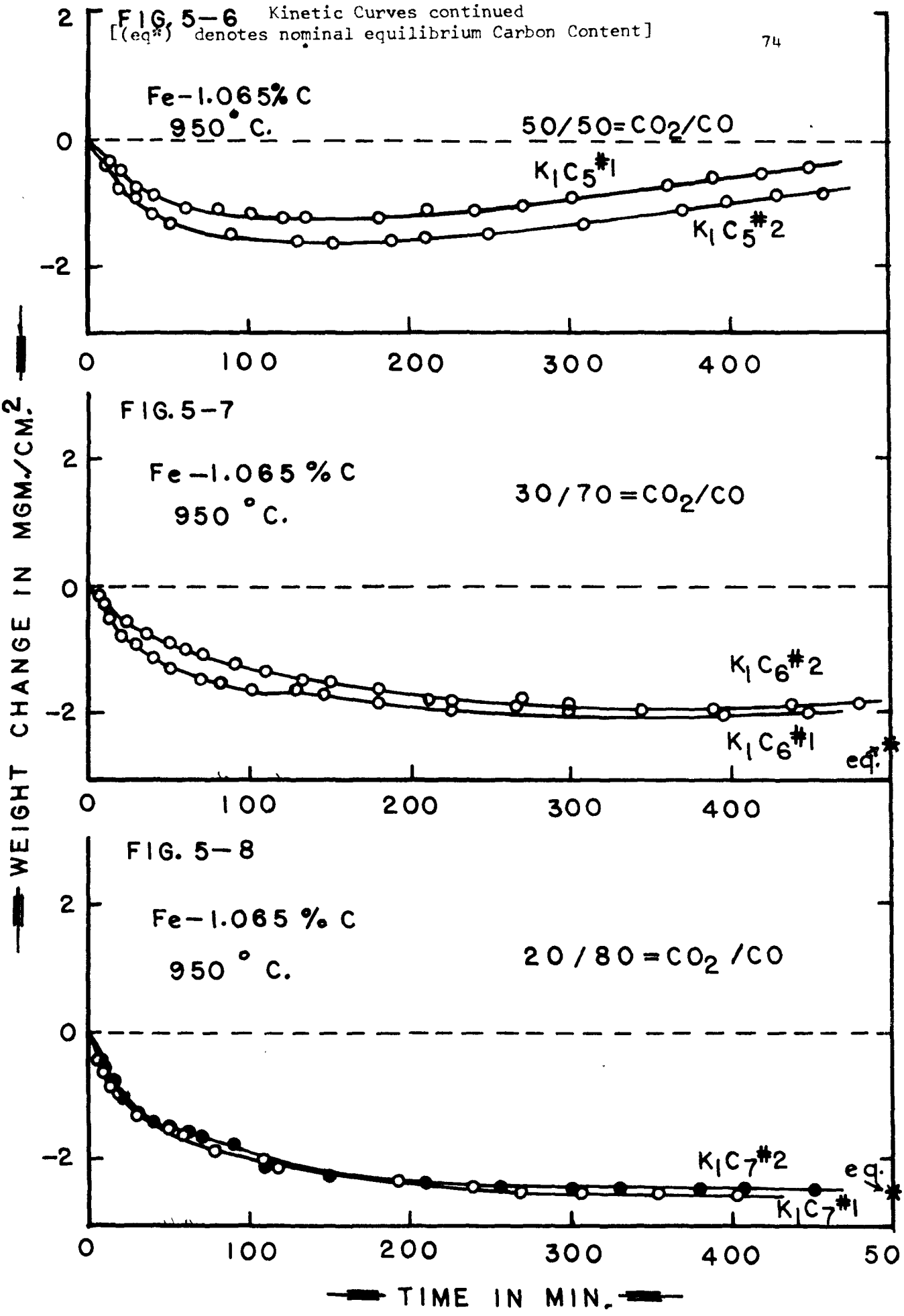

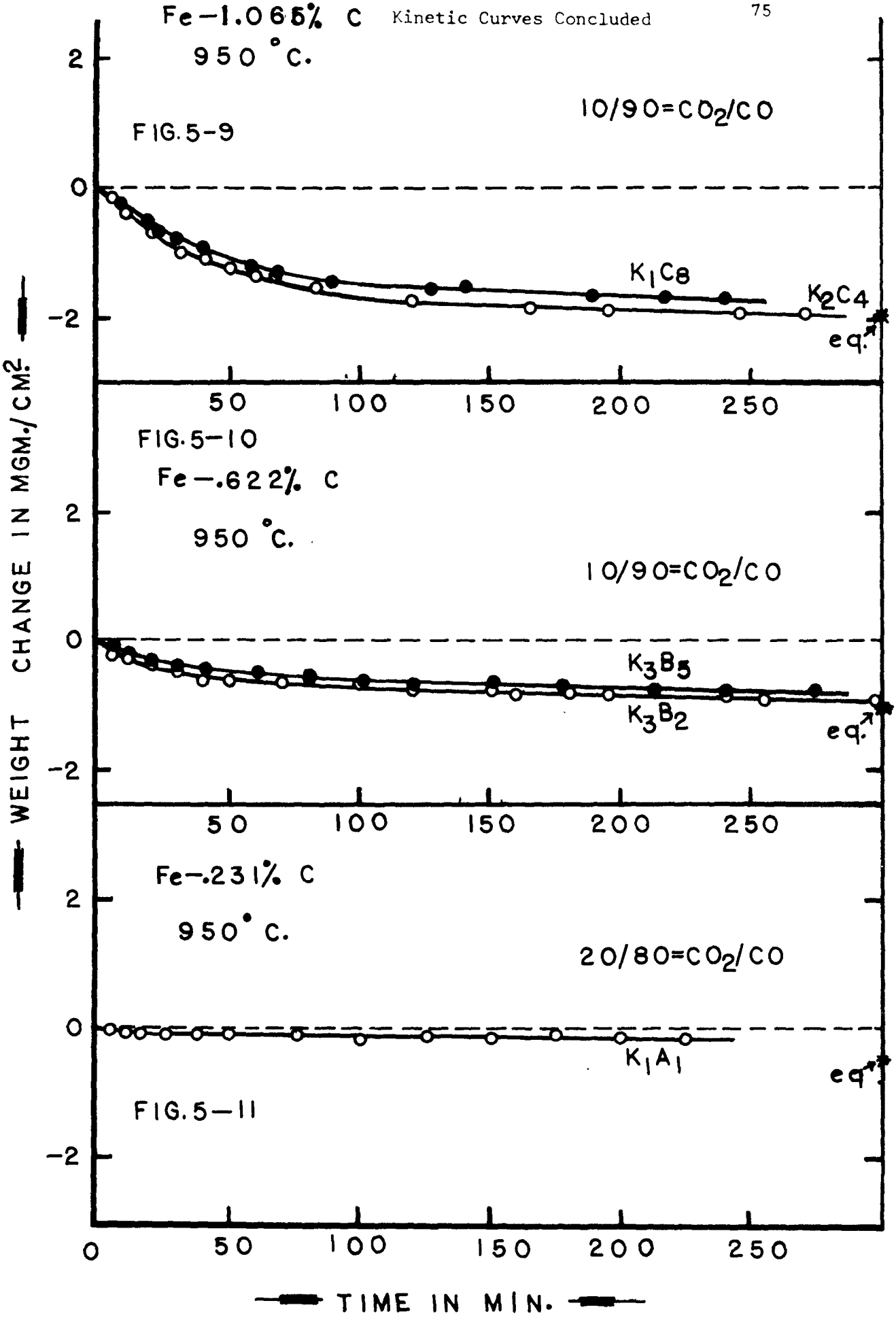
Fe—1.065% C
950 °C.
10/90=CO2/CO
FIG.5-9
K1C8
K2C4
eq.
FIG.5—10
Fe—.622% C
950 °C.
10/90=CO2/CO
K3B5
K3B2
eq.
Fe—.231% C
950° C.
20/80=CO2/CO
K1A1
eq.
FIG.5—11
WEIGHT CHANGE IN MGM./CM.2
TIME IN MIN.
2
0
-2
50
100
150
200
250

TABLE D

Initial and Final Practical Oxidation Rates at 950°C Abstracted From the curves of Fig. 5-1 to 5-11 for oxidation of the three Fe-C alloys - comparisons with values from the literature.

Specimen	PCO_2 (atm.)	Initial Slope mgm/cm^2/min	Final Slope mgm/cm^2/min	*Grabke Fe-C	**Grabke Fe-C	***Pettit Pure Fe
K_2C_1#1	1	-.113±.012	.0875±0096	† .23	† .32	.025
K_2C_1#2	"	-.108±.012	' —	"	"	"
K_1B_1	"	+0356±.0039	.0800±0088	"	"	"
K_3B_4	"	+0392±.0043	.0807±0089	"	"	"
K_1A_4#1	"	+0365±.0040	.0961±011	"	"	"
K_1A_4#2	"	+0280±.0031	.0921±010	"	"	"
K_2C_2	.9	-.0535±0058	0475±0052	—	—	.022
K_1C_1#1	.8	-.0182±002	0255±0028	—	—	.018
K_1C_1#2	"	-.0154±0017	0197±0022	—	—	"
K_1B_2	"	-.0125±0014	0245±0027	—	—	"
K_1A_3	"	-.00606±00067	0199±0022	—	—	"
K_1C_3#1	.7	-.0234±0026	00851±00094	—	—	.015
K_1C_3#2	"	-.0222±0024	0113±0012	—	—	"
K_3B_6	"	-.0131±0014	0143±0016	—	—	"
K_1C_4#1	.6	-.0268±0030	00874±00096	—	—	.011
K_1C_4#2	"	-.0235±0026		—	—	"
K_3B_4	"	-.0201±0022	00876±00096	—	—	"
K_1A_2	"	-.0155±0017	0100±0011	—	—	"
K_1C_5#1	.5	-.0341±0038	00313±00034	—	—	.0074
K_1C_5#2	"	-.0277±0031		—	—	"
K_1C_6#1	.3	-.0410±0045	$1.57\times10^{-4}\pm1.7\times10^{-5}$	† .085	† .12	2.6×10^{-4}
K_1C_6#2	"	-.0324±0036	$3.31\times10^{-4}\pm3.6\times10^{-5}$	"	"	"
K_1C_7#1	.2	-.0545±0060	—	.055	.076	—
K_1C_7#2	"	-.0484±0053	—	"	"	—
K_1A_1	"	-.0187±0021	—	"	"	—
K_1C_8	.1	-.0250±0028	—	.023	.032	—
K_2C_4	"	-.0316±0035	—	"	"	—
K_3B_2	"	-.0278±0031	—	"	"	—
K_3B_5	"	-.0214±0024	—	"	"	—

* ref.[44] from measurements of $C^{14}O$ formation at 800°C

** ref.[44] from electrical resistance measurements at 800°C

*** ref.[25] from oxidation of pure Fe in $CO-CO_2$ atmospheres at 967°C

† value calculated considering no Fe oxidizes

All values calculated from[44] and [25] have been corrected to 950°C and are all in $mgm/cm^2/min$.

obtained a precision of ± 12% for experiments with the same apparatus. In the appendix at the end of the last section of this thesis, curves associated with experiments carried out at various other temperatures are seen as a further test of the precision.

5.4 Shape of Curves

The kinetic curves have been replotted in Figure 3-4, (see Chapter 3), 5-12 and 5-13, for the purpose of convenient comparison. It is seen from these curves, that they all exhibit a linear weight loss initially followed by a levelling-off period. Then, for atmospheres where the dissociation pressure of FeO is exceeded, the slope again becomes positive; under reducing conditions in the atmosphere, the curves appear to tail off almost exponentially and(also initial periods of linear weight loss tail off sooner as $[C_o]$ decreases). From the experiments it was found that iron oxidized in the atmospheres containing 30% CO_2 or more. From the kinetic curves for decarburization alone, for the 1.065% carbon alloy, a linear weight loss is noted for all curves, in the time interval $0<t<$ 20 minutes (max.). In Figure 3-(4), for the 1.065% carbon alloy, the limiting slope of the curves was a maximum for the test carried out in pure CO_2; the limiting slope then decreased for the test in 80/20 = CO_2/CO; then, increased again, until a maximum was reached for the 20/80 = CO_2/CO test. In Figure 5-(12) for the .622% carbon alloy, no weight loss due to decarburization was noted for the test in pure CO_2; the rest of the tests gave curves of similar shape to those for the 1.065% carbon alloy. In Figure 5-13,

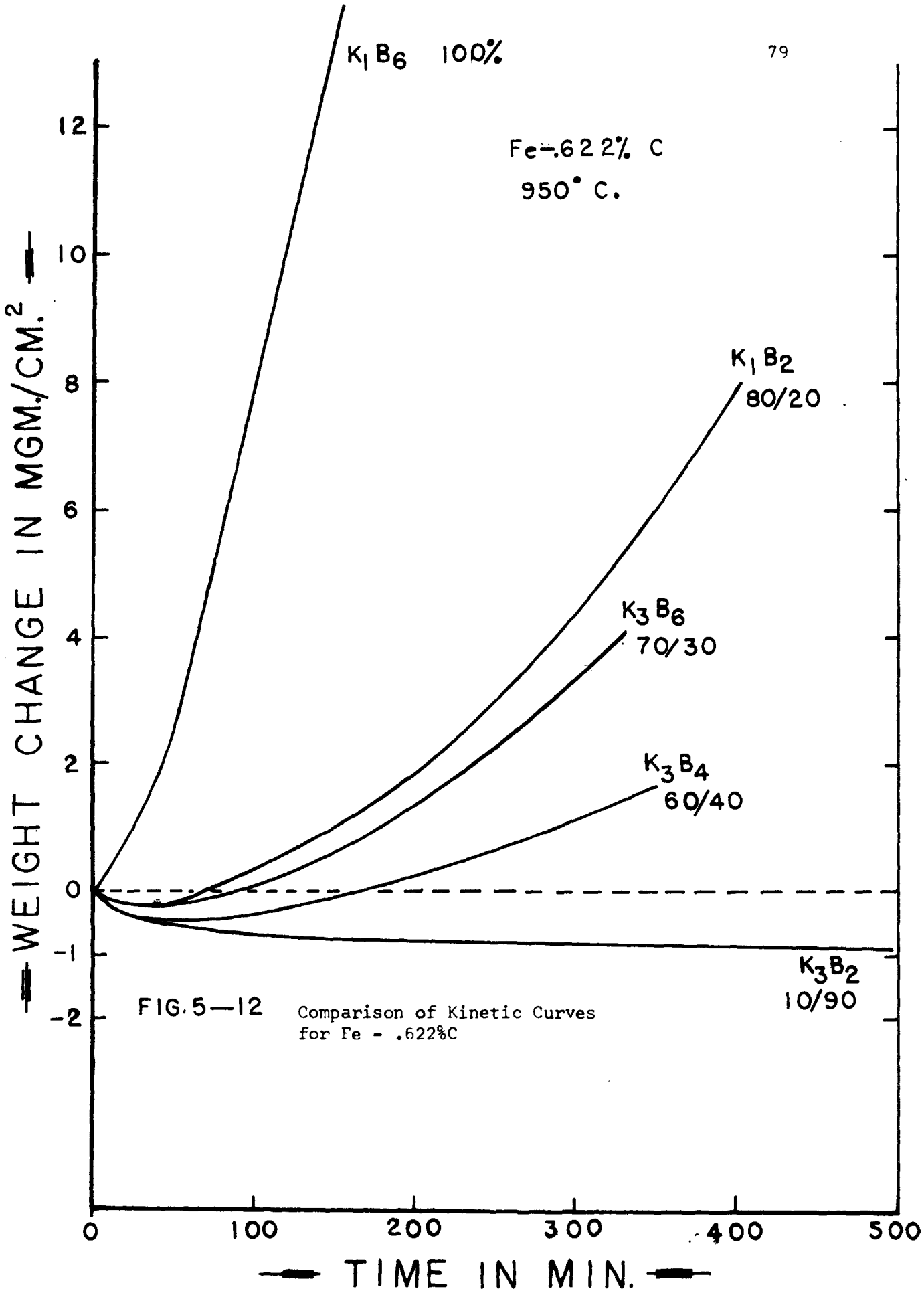

FIG. 5—12 Comparison of Kinetic Curves for Fe - .622%C

FIG. 5-13 Comparison of Kinetic Curves for Fe - .231%C

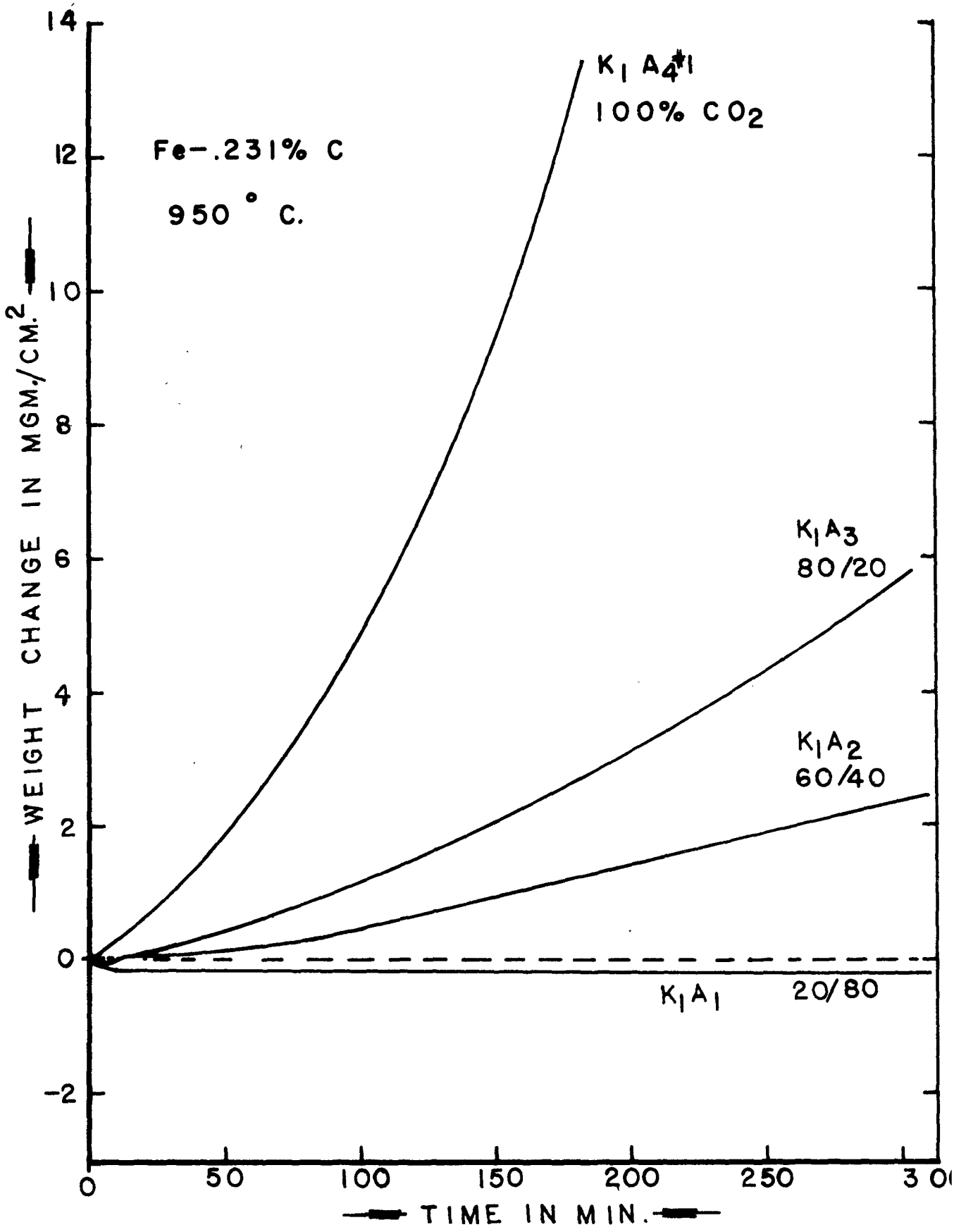

the .231% carbon alloy showed no measurable weight loss due to decarburization, while short periods of weight loss were noted for tests in 80/20 and 60/40 CO_2/CO; decarburization only occurred for the test in the 20/80 = CO_2/CO atmosphere.

For the three alloys, in atmospheres where iron could oxidize, the periods of weight loss, and levelling-off were followed by periods of weight gain, as stated previously. These portions of the kinetic curves were generally concave upwards except in cases where iron was oxidizing slowly, and linear weight gain with time was noted. With the exception of the tests carried out in pure CO_2 (Figure 5-1), the slope of the portion of the kinetic curves exhibiting weight gain increased slightly with decreasing initial carbon content of the specimens. In the pure CO_2 atmosphere the slopes decreased in the order .622 > .231 > 1.065% C carbon. A comparison of these linear portions of the curves obtained for the three alloys with the curve obtained by Pettit et al[25] for a 60/40 = CO_2/CO atmosphere at 950°C is given in Figure 5-(14). It is seen that the slope for the Fe-.231%C alloy is slightly higher than, and the slopes for Fe-.622%C and Fe-1.065%C are slightly lower, than that for pure iron. However, all the slopes are within the experimental precision of this investigation. Hence it may be concluded that the linear portions of the curves give oxidation kinetics as for pure iron. The important conclusion to be drawn from this is that carbon oxidation does not appear to affect the linear oxidation of iron; rather, the oxidation of iron affects the carbon oxidation.

* See Fig. 3-(5) Chapter 3, pg. 43

FIG. 5-14 Comparison of final linear oxidation rates for Fe-C alloys with the oxidation rate of pure Fe in a 60/40 = CO_2/CO atmosphere at 950°C

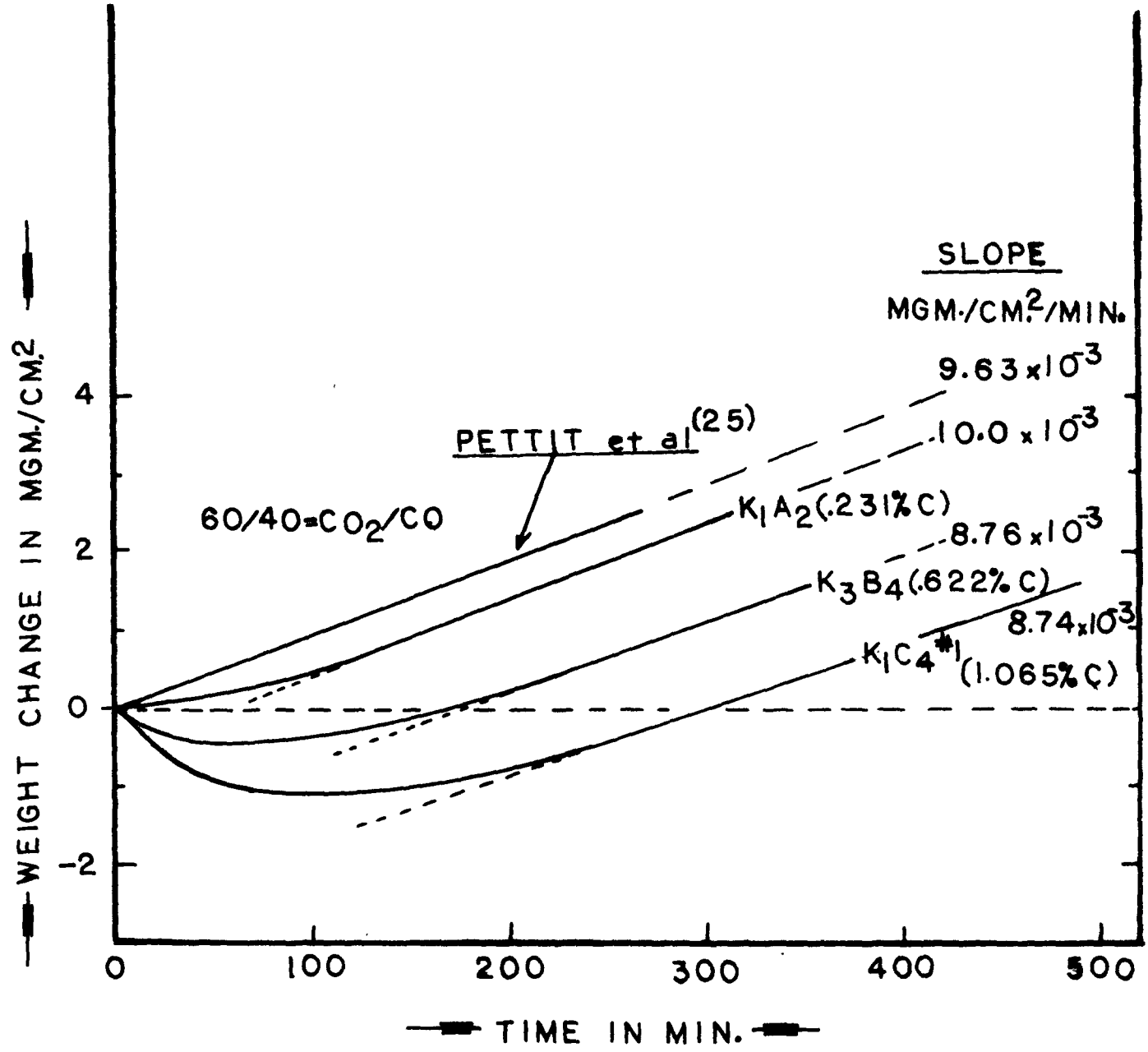

5.5 Oxide Morphology

5.5.1 Introduction

For the three alloys at 950°C only one oxide phase, wüstite, was present in the microstructure. The oxide showed good adherence and good mechanical properties under all the conditions of the experiments. The small number of cracks which appeared in the oxide were attributed to the normal cooling conditions employed. In all cases, the oxide appeared to nucleate at grain boundaries and then grow laterally from the boundaries. However, soon after, random growth centres appeared which seemed to be growing vertically more than laterally, as time proceeded. These centres coalesced rapidly leaving less and less metal exposed, until finally only oxide crystallites were visible.

The crystallites themselves were characterized by very rugged surfaces consisting of macroscopic ledges. Thus it was thought that upon impingement of rugged surfaces consisting of such ledges, rather tortuous porous paths which might allow continued transport of carbon, or carbon oxides, might be formed. However, the presence of such pores could not be found for long experimental times since the scale thickened so rapidly. For short experimental times sites where carbon or carbon oxide could be removed, were found.

Tests were carried out using a solution of potassium (.5%) ferricyanide and sodium chloride (6%) in anhydrous methanol. Colour changes were noted due to reaction of iron with the ferricyanide for

short experimental times and intermediate reaction times. For intermediate reaction times specimens treated with the ferricyanide solution became coated with complexed iron. This was thought to be due to the effusion of ferricyanide through the pores to the metal. Upon reaching the metal the complex would form and gradually fill up the pore or fissure and would be visible using standard metallographical techniques. Unfortunately, the test was inconclusive for intermediate experimental times since a few cooling cracks would cause formation of sufficient complex to give the appearances of porosity. The test therefore, was only of value for short experimental times where the crystallite growth centres were coalescing and virtually no cooling cracks were noted in the areas studied.

5.5.2 Oxide Nucleation and Growth

Since the nucleation and growth processes were observed to be relatively similar for the three alloys studied, the oxide topographies observed will be discussed with reference to the 1.065%C alloy. Photomicrographs presented in Figure 5-(15) to Figure 5-(24) show the mode of growth of the oxide. The tests in a 60/40 = CO_2/CO atmosphere were studied since oxidation and decarburization were of such magnitude as to be observed conveniently. In Figure 5-(15) the oxide after 5 minutes has already become quite thick, nuclei are growing laterally, and large macroscopic areas of metal are visible. After 10 minutes as shown in Figure 5-(16), lateral oxide coverage is only slightly more

Figure 5-(15) Fe - 1.065%C X357 5 min. in $\frac{60}{40} = \frac{CO_2}{CO}$

Topography of oxidized specimen

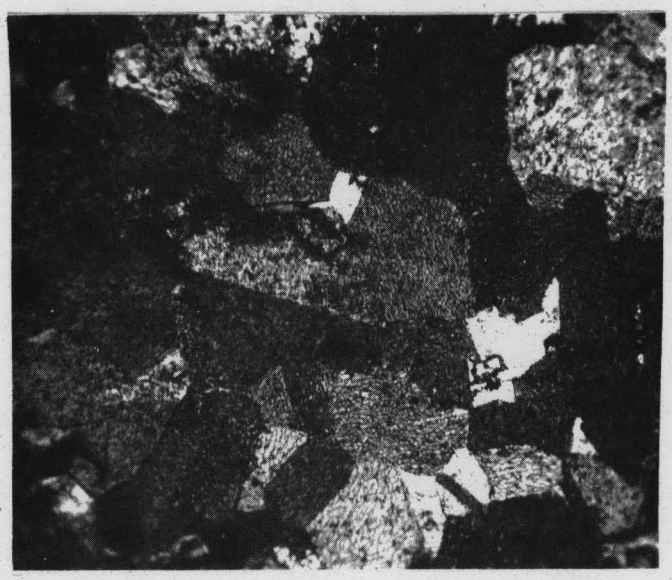

Figure 5-(16) Fe - 1.065%C X540 10 min. in $\frac{60}{40} = \frac{CO_2}{CO}$

Topography of oxidized specimen

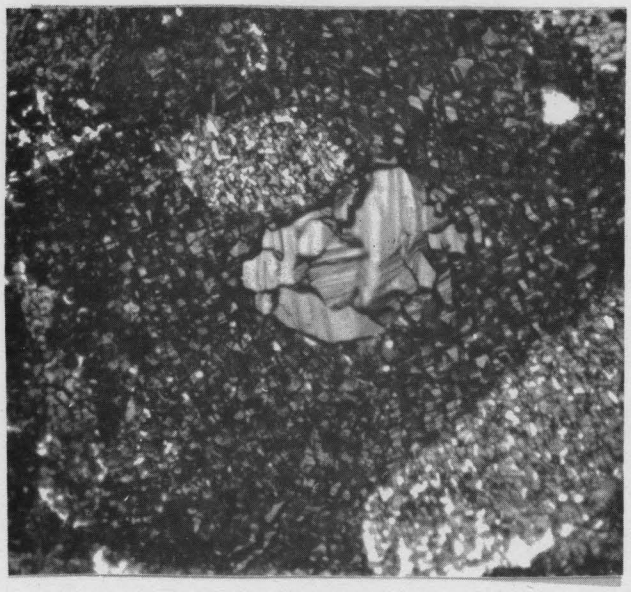

Figure 5-(17) Fe - 1.065%C X590 25 min. in $\frac{60}{40} = \frac{CO_2}{CO}$

Oxide Growth Centre (centre of micrograph)
Note metal visible between smaller crystallites and ledges on crystallites in the growth centre.
Note approximate roundness of centre

Figure 5-(18) Fe - 1.065%C X590 25 min. in $\frac{60}{40} = \frac{CO_2}{CO}$

Large Growth Centre of Oxide
Same specimen as above - Again note metal (white areas) visible between crystallites.

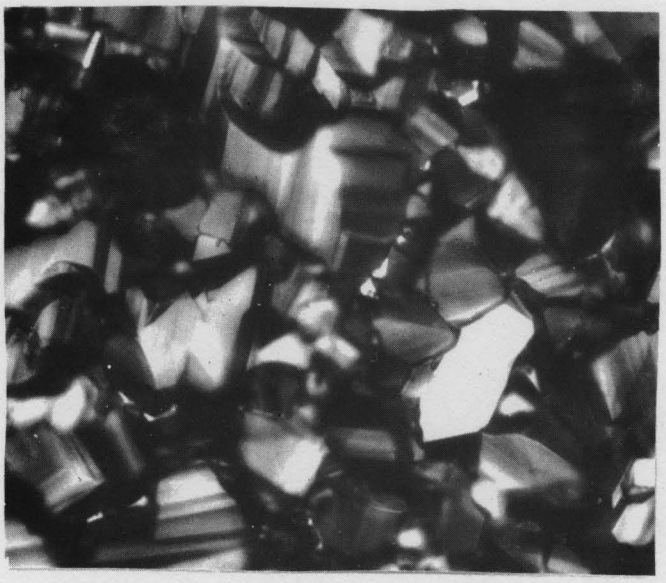

Figure 5-(19) Fe - 1.065%C X700 20 min. in $\frac{60}{40} = \frac{CO_2}{CO}$

Impingement of crystallite boundaries

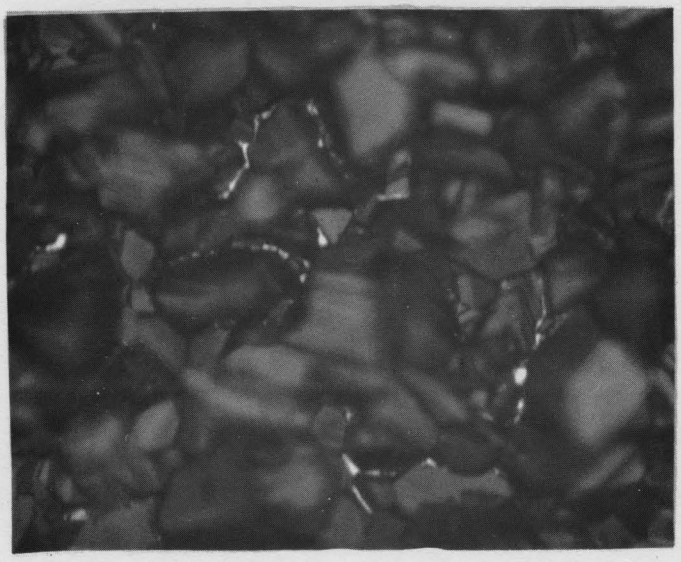

Figure 5-(20) Fe - 1.065%C X350 70 min. in $\frac{60}{40} = \frac{CO_2}{CO}$

Impingement of crystallite boundaries

Figure 5-(21) Fe - 1.065%C X1100 90 min. in $\frac{60}{40} = \frac{CO_2}{CO}$

Impingement of two oxide crystallites

Figure 5-(22) Fe - 1.065%C X1100 110 min. in $\frac{60}{40} = \frac{CO_2}{CO}$

Impingement of three oxide crystallites

Figure 5-(23) Fe - 1.065%C X1100 130 min. in $\frac{60}{40} = \frac{CO_2}{CO}$

Impingement of crystallite boundaries

Figure 5-(24) Fe - 1.065%C X200 180 min. in $\frac{60}{40} = \frac{CO_2}{CO}$

Typical Topography of specimen showing extensive coverage by oxide

extensive and large areas of metal are still visible. Growth centres of various size next appeared as shown in Figure 5-(17) and Figure 5-(18); macroscopic ledges were associated with the crystallites in these centres and macroscopic areas of metal surface were still quite prevalent, particularly in and around the larger growth centres (Figure 5-18). These growth centres appeared to be growing vertically more than laterally.

Paths through the scale would appear to be associated with two features of the scale. The first is that macroscopic areas of metal surface are available for easy removal of carbon or carbon oxides, as mentioned above for short experimental times. The second is semi-microporosity associated with crystallite boundaries due to impingement of rugged crystallite boundaries frought with macroscopic ledges, as shown in Figure 5-(19) to Figure 5-(23). Thus the evidence for macro-porosity, and semi-microporosity might account for transport of carbon or its oxides through the scale for a period of about 130 minutes in the 60/40 atmosphere. However, if carbon is still being removed after that period, ie. in the case of thick specimens, no direct evidence was found for the presence of micropores as shown by Figure 5-(24).

Observation of the metal/oxide interface showed that this interface was very rugged, as evidenced by Figure 5-(25) - 5-(28). The oxide/gas interface was also found to be so rugged as to make optical thickness measurements of only very limited value. The previous figures show that the impingment of oxide crystallite boundaries was often associated with small spires of iron protruding through the

oxide at the impingment site; these range from sharp pointed (Figure 5-25) to round-topped (Figure 5-26) spires. This suggests the lateral growth of the oxide.

One would expect[25] that if the amount of CO_2 in the atmospheres is increased, the rate of nucleation and growth of oxide should increase also. All observations in the experiments showed that this was so. For example in pure CO_2, Figure 5-(29) shows that growth centres appeared after only 5 minutes reaction time, coalesced rapidly (Figure 5-30) and that coverage of the surface by the oxide was nearly complete Figure 5-(31) after only thirty minutes.

For specimens decarburized under conditions where no scale could form, topographical examination yields only evidence of thermal etching (Figure 5-32). Examination of the metallic phases gave results in accord with the microstructures observed by Engell[33]. The decarburized structure consisted of Widmanstätten ferrite plates with amounts of pearlite at the plate boundaries characteristic of the reaction time (Figures 5-33 - 5-35). The Widmanstätten plates spiked very irregularly into the unaffected metal which consisted of pearlitic grains with Fe_3C nucleated at the grain boundaries. These structures point to the probability that the surface concentration of carbon is at a low value and that carbon segregates rapidly to the grain boundaries during a typical experiment under reducing conditions.

5.5.3 Ferricyanide Tests

Coloured photomicrographs were employed to show some of the effects of chemical complexing tests done on specimens oxidized for

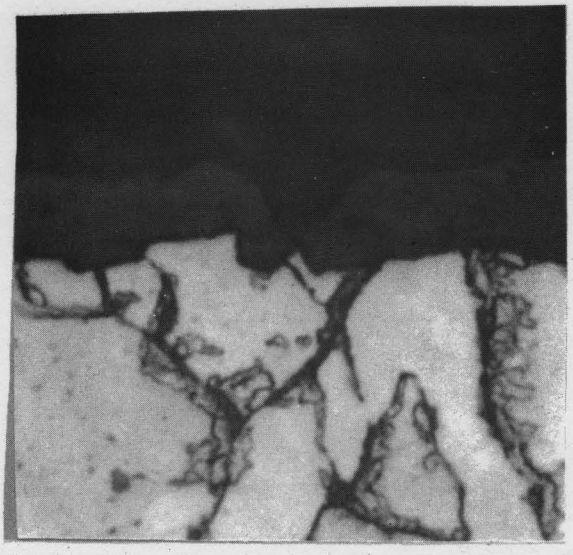

Figure 5-(25) Fe - 1.065%C X1300 20 min. in $\frac{60}{40} = \frac{CO_2}{CO}$

Cross Section of oxidized specimen showing impingement of crystallites to form a macropore

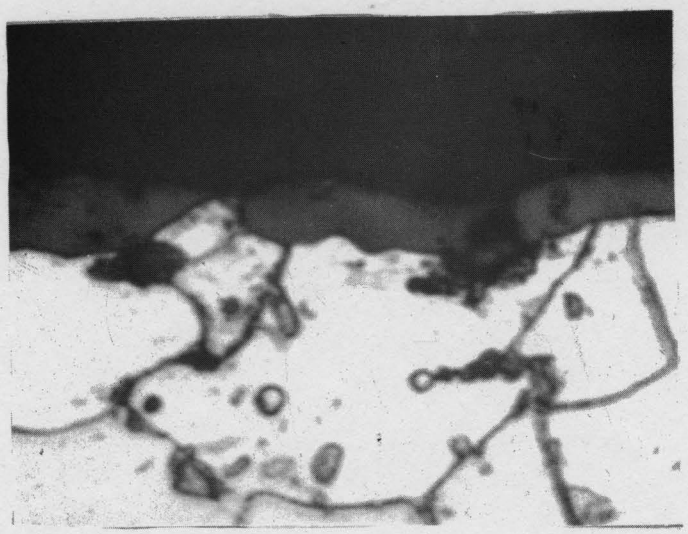

Figure 5-(26) Fe - 1.065%C X1300 10 min. in $\frac{60}{40} = \frac{CO_2}{CO}$

Cross Section of specimen showing Iron "Spire" at point of impingement of oxide crystallites

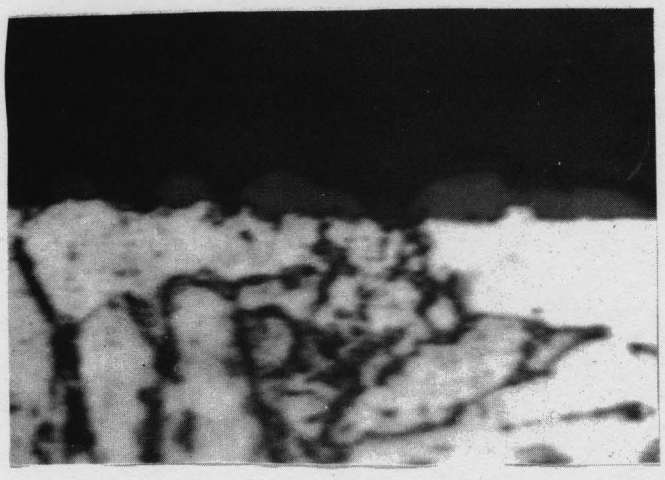

Figure 5-(27) Fe - 1.065%C X1300 20 min. in $\frac{60}{40} = \frac{CO_2}{CO}$

Specimen Cross Section showing General mode of Oxide Growth

Figure 5-(28) Fe - 1.065%C X1300 20 min. in $\frac{60}{40} = \frac{CO_2}{CO}$

Mode of Oxide Growth

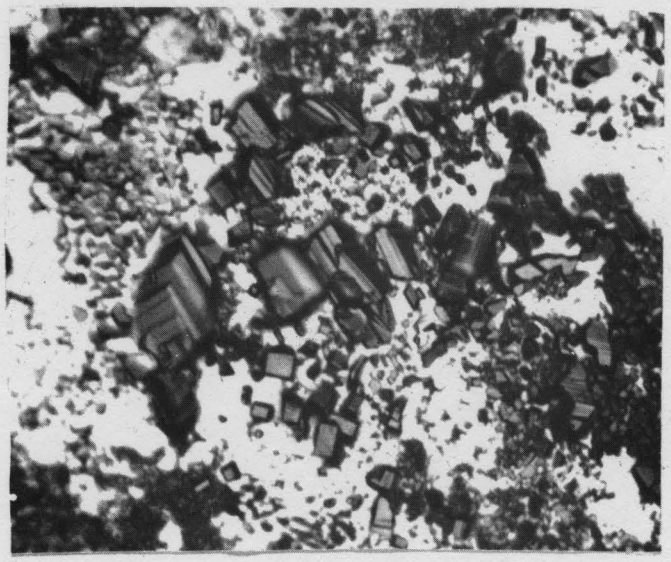

X530

Figure 5-(29) Fe - 1.065%C 5 min. in pure CO_2
Topography of Specimen showing Oxide Growth Centres (square or rectangular)

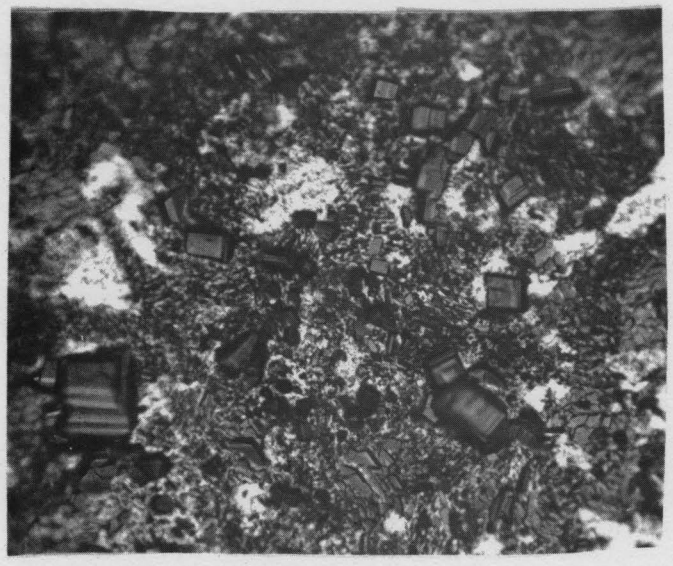

X530

Figure 5-(30) Fe - 1.065%C 10 min. in pure CO_2
Topography of Specimen showing Oxide Growth Centres and Oxide Coverage

Figure 5-(31) Fe - 1.065%C X530 30 min. in pure CO_2
Surface Oxide Coverage

Figure 5-(32) Fe - 1.065%C X150 11 hrs. in $\frac{20}{80} = \frac{CO_2}{CO}$
Topography of Specimen exhibiting Thermal etching

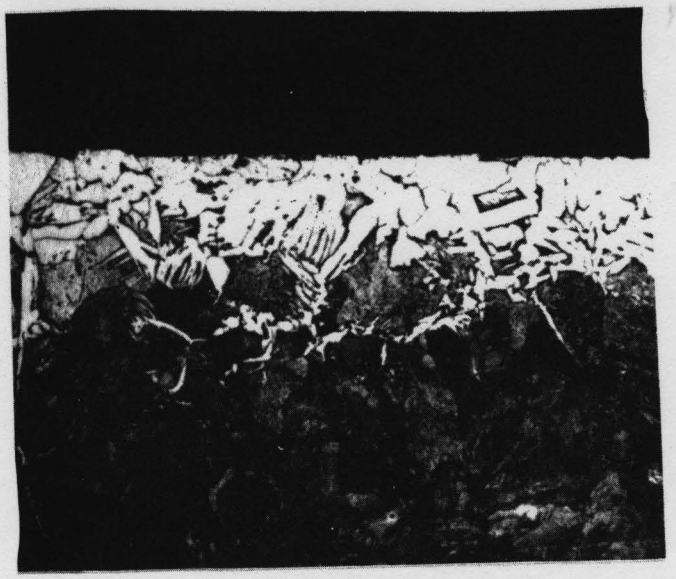

Figure 5-(33) Fe - 1.065%C X250 25 min. in $\frac{60}{40} = \frac{CO_2}{CO}$

Structure of Decarburized Alloy exhibiting evidence for onset of diffusion controlled decarburization

Figure 5-(34) Fe - 1.065%C X250 50 min. in $\frac{60}{40} = \frac{CO_2}{CO}$

Structure of decarburized Alloy

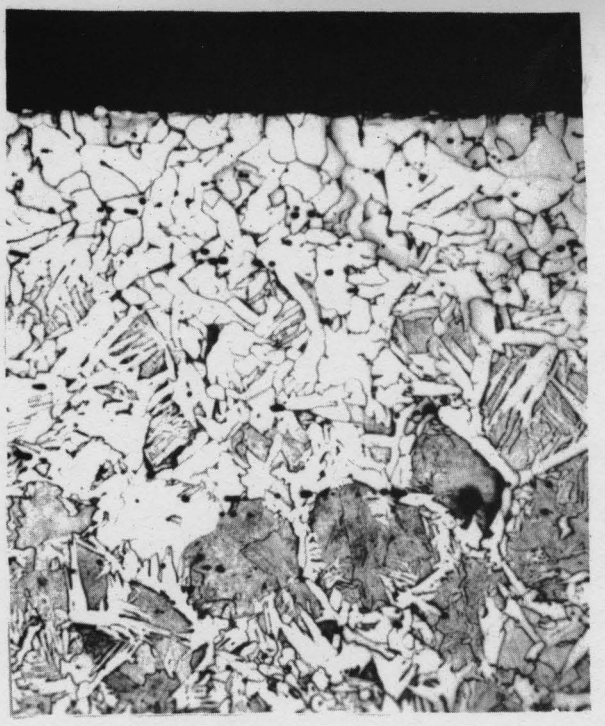

Figure 5-(35) Fe - 1.065%C X250 75 min. in $\frac{60}{40} = \frac{CO_2}{CO}$

Structure of Decarburized Alloy

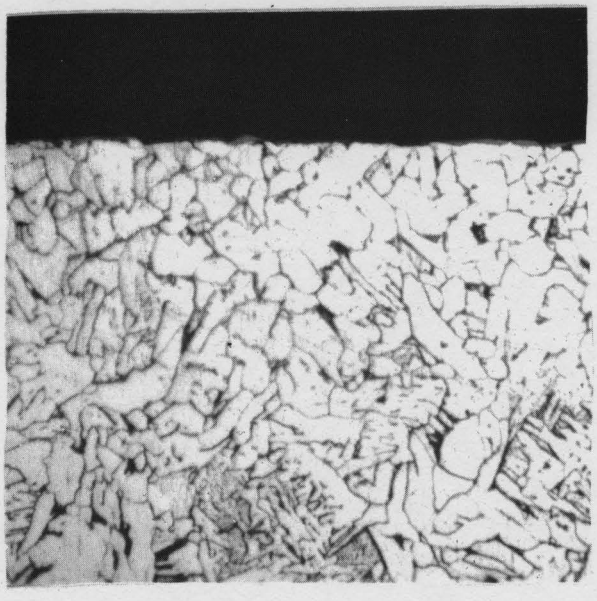

Figure 5-(36) Fe - 1.065%C X250 100 min. in $\frac{60}{40} = \frac{CO_2}{CO}$

Structure of Decarburized Alloy

Note scale clearly visible

varying periods of time in a given atmosphere. None of the micrographs are shown because these tests served only to heighten the suspicion of the presence of the two types of porosity mentioned previously in 5.5.2. The tests do not prove the existence of micropores, but do not discount the possibility that they are present.

5.6 Residual Carbon Analyses

In order to ascertain how the loss of carbon during oxidation of Fe-C alloys compared with the kinetics observed for the simultaneous oxidation of iron and carbon, the following experiments were carried out. Specimens oxidized in a given atmosphere were quenched after varying periods of time and then analysed for residual carbon content. Some of these results may be seen in Figure 5-(37). The significant factor here is that for the atmospheres of 100 and 60% CO_2, the nominal equilibrium carbon concentration is zero and for the atmosphere of 30% CO_2 the nominal equilibrium value (denoted by an asterisk) is .053 weight percent (=-2.56 mgm./cm.^{2} for the specimen shown). The carbon analyses show that the nucleation and growth of oxide stifles the decarburization reaction so much so that the full decarburizing power of the atmosphere is never realized and the carbon content of the specimen proceeds only very slowly to the equilibrium value. For example, in the atmosphere containing 100% CO_2, the decarburizing power is infinite ie. the decarburization curve would fall theoretically along (very close to) the weight change axis. However, as can be seen in Figure 5-(37) the curve showing the carbon loss via analysis exhibits an initial slope indicative of an atmosphere of decarburizing power

FIG. 5-37

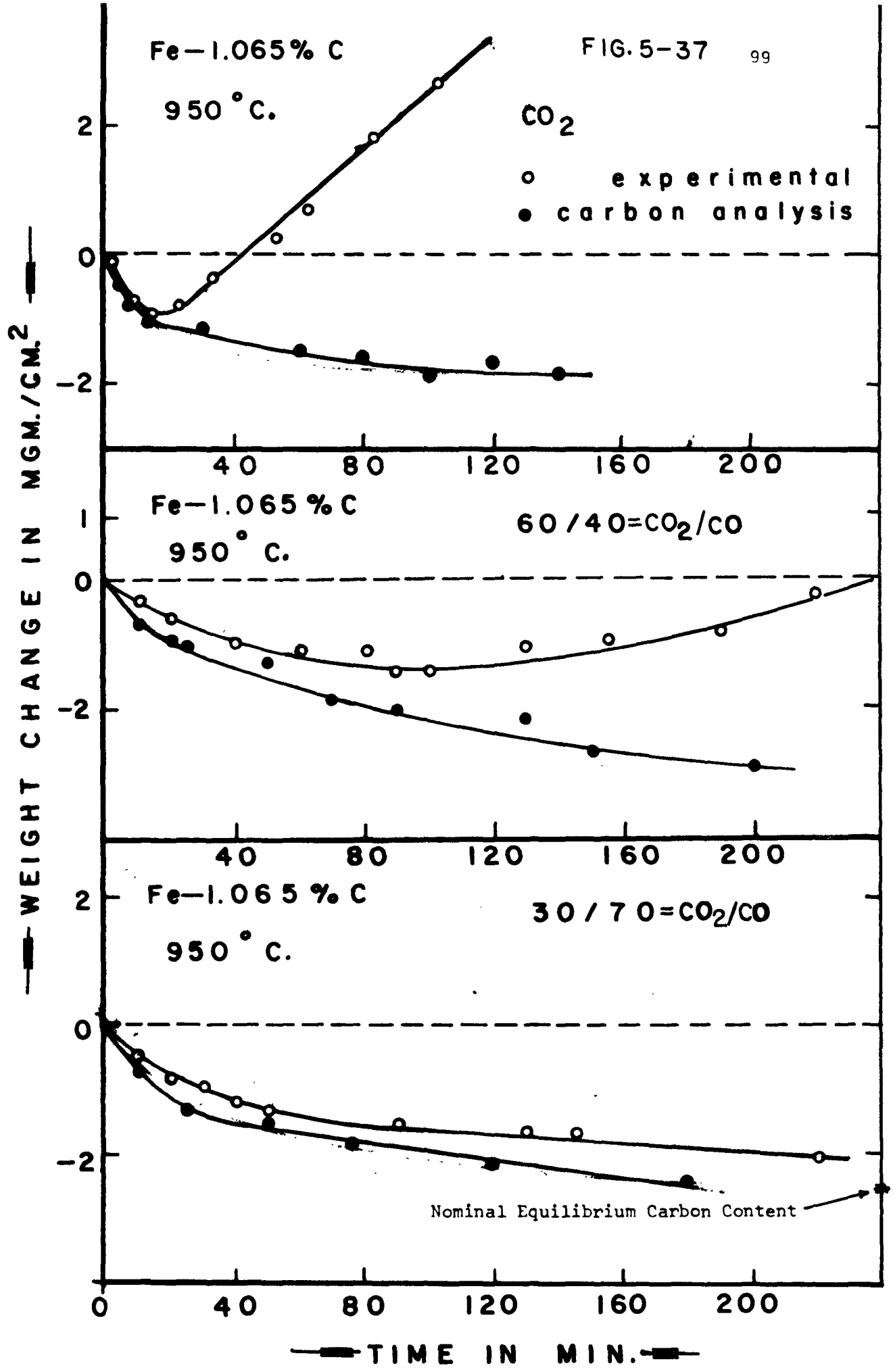
Fe—1.065% C
950°C.
CO_2
o experimental
● carbon analysis
Fe—1.065% C
950° C.
60/40=CO_2/CO
Fe—1.065% C
950° C.
30/70=CO_2/CO
Nominal Equilibrium Carbon Content
WEIGHT CHANGE IN MGM./CM.^{2}
TIME IN MIN.
2
0
-2
1
40
80
120
160
200

about 40% less than it should be in 100% CO_2. These results also show that masking of the true weight loss kinetics for carbon oxidation by oxidation of iron increases as the volume % CO_2 increases in the atmosphere as evidenced by the experimental curves given in Figure 5-(37). Also, the stifling of decarburization by scale growth masks any evidence of the onset of partial diffusion control of decarburization because the tail-off of decarburization weight loss is probably a combination of the stifling effect on decarburization of scale growth and onset of partial diffusion control of decarburization. Figure 5-(33) to 5-(36) support the fact that onset of partial diffusion control of decarburization still occurs despite stifling of decarburization by scale formation (Figure 5-36).

CHAPTER 6

DISCUSSION

6.1 Introduction

Because of the conditions of the experiments previously mentioned, wüstite, the iron oxide of lowest oxygen content was the only solid oxide phase present on Fe-C specimens oxidized in $CO-CO_2$ atmospheres in the temperature range 800° to 950°C. Results discussed in this chapter are those mainly associated with experiments at 950°C.

Kinetics observed in atmospheres where selective oxidation of carbon occurred yielded a linear relationship between decarburization rate and partial pressure of CO_2 for short experimental times. These results are in agreement with the basic postulates of the reaction-controlled decarburization model of Doehlemann[31] and the definitive experiments of Grabke[44]. After longer periods of time, the decarburization rates were lower than predicted from the above model. It was shown that this behaviour was due to the onset of partial diffusion control of decarburization.

In atmospheres of higher oxygen potential where iron and carbon were oxidized, a gradual decrease of the initial (negative) practical rate constant for all alloys observed in the range PCO_2 = .3 atmos. to PCO_2 = .8 atmos. at 950°C (Figure 3-5). However, this rate for the Fe-1.065%C alloy, became more negative above PCO_2 = 0.8 atmos. A different behaviour was exhibited by the Fe-.622 and -.231%C alloys. For these alloys the initial practical rate constant eventually became positive.

Accordingly, the oxidation of carbon was severely complicated by a competition between iron and carbon for adsorbed oxygen.

It has also been possible from the results of this investigation to bracket a certain critical initial carbon concentration for Fe-C alloys which, when exceeded, caused the practical rate constants to suddenly become more negative by enhanced oxidation of carbon. If the initial carbon content of the alloy lies below this critical value, the decarburization kinetics are suppressed giving a corresponding decrease of the oxidation rate for PCO_2 greater than .8 atm. An account must be made of the variations in oxygen consumption from the atmospheres by the two species carbon and iron, as the competition proceeds, keeping in mind that for a process controlled by a chemisorption reaction, the total uptake of oxygen must be directly proportional to time. Before proceeding to this specific topic, several general considerations will be discussed which have been shown to apply to linear oxidation kinetics of metals.

6.2 General Considerations

Observation of initially linear practical rate constants might be explained by rate-controlling steady state diffusion through a resisting layer of uniform thickness, either in the solid or gas phase. For short times, however, a solid phase of constant layer thickness was not found on any of the Fe-C alloys. Diffusion of CO_2 through a stagnant gas film adjacent to the oxide surface is another possibility. However, the activation energy[44] of 47.5±1 k cal. for the decarburization kinetics of the alloys is much larger than would be expected for the gaseous diffusion

process. Hence, the rate determining step must be a chemical reaction. The plots (Figure 3-5) of decarburization rate versus PCO_2 were linear over the whole range of CO_2 pressures and this is taken as verification of the statement in Chapter 3 that a chemisorption reaction is rate controlling.

As outlined previously in the review section, Wagner[32] has advanced an oxidation model based upon a scale cracking mechanism to account for simultaneous decarburization and oxidation of alloys containing carbon. In our investigation, evidence was not found for cracking of the wüstite scale at the temperature of reaction. Since, moreover, evidence of carbon build-up at the metal-oxide interface was not observed, carbon was oxidized from the alloy without the necessity of a cracking mechanism. To overcome this conceptual problem Engell[39] proposed that porosity of the scale is responsible for the transport of carbon or carbon oxides to the gaseous environment. In our investigation, direct evidence was not found for scale porosity. Rather, the formation of an irregular defective scale by the nature of the nucleation and growth processes appeared to be a prime factor at short experimental times.

Langer and Trenkler[45] found that the rate of iron oxidation decreased as the pressure of CO_2 in the atmosphere was decreased. This was attributed to a proportioning out of available oxygen to carbon, the remainder reacting with iron. Our study has shown that such a competition for available adsorbed oxygen does occur, but we refer to a decrease not in scaling rate, but of the initial practical rate governing both decarburization and oxidation of iron. It is imperative to consider both of the aspects of the reaction because the results of chemical analyses for

bulk carbon (Figure 5-37) illustrated that the decarburization rate was affected by a combination of (a) onset of partial diffusion control of decarburization and (b) stifling of the decarburization reaction by scale formation. Furthermore, final practical rates are generally found to be either only approximately equal (Figure 5-14), or larger than for pure Fe (Figure 5-14) indicating that scaling rate is not generally decreasing (Figure 3-5) over the entire range of PCO_2 in the atmospheres.

6.3 Kinetics of Decarburization in CO-CO_2 Atmospheres

A concise representation of the initial decarburization rates is shown in Figure 3-5. In atmospheres where decarburization only occurred, in the range PCO_2 = .02 atm. to PCO_2 = .28 atm. at 950°C. and 760 Torr. decarburization rate exhibited a linear dependence on PCO_2. Its magnitude was independent of initial alloy carbon content for the investigated range 0.231 to 1.065%C. The kinetics are thus indicative of oxidation rate control by a chemisorption reaction in agreement with the work of previous authors[31, 39, 44].

An absolute decarburization rate of $k_1 = 1.91 \times 10^{-6}$ mol C/Cm^2-sec. atmos. was obtained from the results of this investigation at 950°C. The constant k_1 is defined by the relation

$$k_1 = K_{practical} / PCO_2 \left[1 - \frac{C_{eq}}{C_o}\right] \qquad \text{from (50)}$$

as previously derived by Grabke[44] (see chapter 2.7) and confirmed via rate theory[48] in Chapter 3 of this thesis. The results thus demonstrated that our determination of the absolute decarburization rate constant at 950°C was in excellent agreement with the value obtained from the Arrhenius extrapolation of results reported by Grabke[44].

6.4 Model For Simultaneous Oxidation of Iron and Carbon In $CO-CO_2$ Atmospheres

In agreement with predictions from thermodynamic data, simultaneous oxidation of iron and carbon was found to occur in the range PCO_2 = .3 atm. to PCO_2 = 1 atmos. at 950°C. and 760 Torr. For a detailed picture of the findings of this investigation the reader is urged to consult the theoretical section (Chapter 3) of this thesis in conjunction with Chapter 5.

The experimental results show that the nucleation and growth of wüstite on γ-Fe has a definite effect on the decarburization of carbon steels. Accordingly, a rephrasing of the Doehlemann[31] theory, (in the light of the definitive experiments of Grabke[44]) in the absolute reaction rate formalism, coupled with the basic concepts of classical nucleation theory[57] has formed the basis of our treatment of the problem. A basic postulate of the model advanced for simultaneous oxidation and decarburization was that initially, oxide nucleates and grows laterally at grain and sub-grain boundaries of the metal by reaction of iron ions with adsorbed oxygen (reaction 86). Metallographic examination of specimens oxidized for varying times (Figure 5-15 to 5-36) demonstrated the validity of this consideration. Decarburization takes place concurrently in the central portion of the grains (Figure 3-1) at active sites for combination of carbon with adsorbed oxygen according to reactions (62) and (75). Direct evidence for the presence of the latter type of sites was not obtained.

Since the practical initial oxidation rates remained relatively linear over the whole range of CO_2 pressures, the idea of simultaneous

oxidation of iron and carbon controlled by a chemisorption reaction was induced, neglecting diffusion inhibition of decarburization (Figure 3-3). The oxidation model describes oxygen consumption from the atmosphere at a steady rate (Figure 3-7). The model was then simplified by assuming in the light of our neglect of reaction control of decarburization by diffusion that the concentration of adsorbed oxygen was at its equilibrium value everywhere except close to the boundaries of the oxide nuclei (Figure 3-8). The essence of this model is that as the ratio of PCO_2/PCO becomes increasingly larger the reaction of iron ions with inactive $O_{ads.}$ (reaction 86) and the surface diffusion of inactive $O_{ads.}$ (reaction 75) to active sites, enter into a competition for inactive $O_{ads.}$ produced by dissociation of CO_2 according to reaction (74).

It is appropriate to briefly recapitulate the predictions of the oxidation - decarburization model for long exposures before presenting a detailed resume of the diverse reaction phenomena. Since the variation of decarburization rate depended, in our experiments, on the surface coverage by oxide, an oxidation model generating this area change was outlined in Figure 3-10.

At long times the growth of oxide is more vertical than lateral (Figure 5-17 and 5-18). This is in accord with Irving[61] who induced from the results of Wood[59] and Le Claire[60] that for nucleation and growth of an oxide thickening by cation diffusion, the effect of oxide growing toward the centre of the grains from more than one boundary will be to reduce the tendency for cations to diffuse laterally. In addition Irving reasoned that this effect would increase as grain size was reduced. This model predicted the observed weight gain kinetics and reproduced all

the qualitative features of the reaction sequence without taking account of long range leakage in the scale or any rate law other than a linear oxidation law for iron. The tendency of the minima of the kinetic curves as PCO_2 tends to unity was predicted for the Fe-1.065%C alloy in good agreement with the experimentally observed minima (Figure 3-12). Stifling of the decarburization rates by growth of the oxide film was demonstrated by the results of the residual carbon analysis of the alloys (Figure 5-37).

6.5 Oxidation of Iron-Carbon Alloys in the Carbon Steel Range in $CO-CO_2$ Atmospheres

From Figure 3-5- it is evident that the practical initial rate constant decreases linearly in the range PCO_2 = .3 atm. to .8 atm. at 950°C. As confirmed by microscopy, the oxide appeared to be growing laterally from grain boundaries at first, and then thickening later in a conventional manner[23, 24, 25, 26, 27] by diffusion of iron ions through the oxide to react with the adsorbate. We have dotted in the extension of the linear curve of the initial reaction rates obtained for the 1.065%C alloy into the zone of selective oxidation of carbon because the flowmeters could not be read sufficiently accurate to reveal the reaction rate dependence on CO_2 pressure. The rate changed from the possible upper limit of .08 mgm./cm.^{2}/min. for PCO_2 slightly less than .28 atm., to about .04 mgm./cm.^{2}/min. at PCO = .3 atm. Similarly, a smooth curve was drawn in the range PCO_2 = .8 atm. to .9 atm., for the 1.065%C alloy and dotted curves drawn for the .622 and .231%C alloys because more accurate determinations are needed in this range of high

variation of rates. On account of this, we limited our theoretical description of Figure 3-9 to qualitatively explain this particular variation of reaction kinetics.

It is evident from Figure 3-5 that the rate decrease in the range PCO_2 = .28 to .30 atm. was increasingly larger for specimens of decreasing carbon content. In fact, it is possible that the curve defining decarburization and oxidation undergoes a discontinuity. Conversely, the rate decrease due to onset of iron oxidation should become increasingly less for alloys of increasingly higher carbon content, the upper limit of the practical rate constant being the theoretical decarburization rate. This behaviour is in accord with the results of Merchant[43] for the oxidation properties of cast iron. The carbon content in these alloys is so large that the decarburization kinetics almost entirely mask the effects of concurrent iron oxidation. Obviously, more work must be done in the range PCO_2 = .25 atm. to .3 atmos. with an apparatus which enables very accurate monitoring of CO_2/CO ratios.

Since the initial practical rate constant decreases for all alloys in the range PCO_2 = 0.3 to 0.8 atm. (Figure 3-5), the surface reaction step involving chemisorbed oxygen for formation of wüstite (reaction 86) played an effective role. On the basis of the reaction control model, this behaviour would be accounted for by the lengthening of the surface diffusion paths for reaction of chemisorbed oxygen with carbon (reaction 75) leading to a shift in the competition for oxygen in favor of reaction 86. This shift of reaction mechanism was most pronounced for the alloys of low carbon contents since the initial practical rate constants decreased markedly in the high CO_2 pressure range above PCO - 0.8 atm. On the other

hand, the initial practical rate constant for the 1.065%C alloy increased above PCO = 0.8 atm. which suggests that reaction(75)involving the surface diffusion step for reaction of oxygen with carbon was increasingly significant. According to the reaction model this behaviour implies a corresponding shortening of oxygen diffusion paths above the previously mentioned critical initial carbon alloy content under conditions of large surface coverage of adsorbed oxygen.

This influence of more or less than a certain critical alloy carbon concentration at high values of the atmospheric CO_2/CO ratio on a process whereby scaling and decarburization rates are determined by the availability of adsorbate from a surface chemisorption step seems reasonable in the light of the competitive nature of the two reactions. For example, in the case of the 1.065%C alloy for $PCO_2 > .8$ atm., the critical value is exceeded causing the concentration of carbon at the surface for the particular high oxidizing potential to be of such magnitude that the mean surface diffusion path is shortened thus causing decarburization to become increasingly significant. Conversely, in the case of the .622 and .231%C alloy at $PCO_2 > .8$ atmos., the initial carbon content is less than the critical value. Thus, the concentration of surface carbon for the particular high oxidizing potential is of such magnitude that lengthening the mean surface diffusion path is facilitated to the advantage of wüstite formation. The morphologies observed (compare Figures 5-15 and 5-16 with 5-29 and 5-30) are consistent with this explanation since the photomicrographs illustrate that lateral growth of the oxide transforms to vertical growth. These characteristics are to be expected when carbon oxidation becomes increasingly predominant at

high values of CO_2 pressure. However, in the light of the morphological observations another more favourable explanation could be advanced. Assuming that at the start of oxidation an initial thin oxide layer was present and that the oxidizing potential of the gas was high enough, surface carbon might react with oxygen in this thin oxide layer during a short induction period to partially reduce this layer. A patchy vertical thickening of oxide might then occur which (Figure 5-29) (a) in the case where more than the critical amount of carbon present, allows more area for contact of carbon with adsorbate and (b) in the case of less than a critical amount of carbon allows more iron to oxidize giving even higher rates than for pure iron. As evidenced by the comparison (FIgure 3-5) of final practical rates with those for pure iron oxidation, the latter explanation is quite reasonable. Both explanations are alike in that surface diffusion paths of adosrbate are affected and that specific reaction rates of (75) and (86) must be non-constant. However, the former explanation considers that the morphological growth is a consequence of increase of surface carbon activity while the latter explanation generates the morphological growth observed and is also consistent with observations that scaling affects decarburization.

The above interpretation of the decarburization and oxidation kinetics by the surface reaction control model, involving the absolute reaction rate formalism, coupled with the basic concepts of classical nucleation theory, may be only tentatively accepted until elucidation of all the diverse phenomena is realized by additional measurement methods. The interpretation may require modification to account for an initial distribution of available oxide growth centres. These sites would result from partial reduction of the air formed film on the metallographically

polished specimens by carbon from the alloy in oxidizing $CO-CO_2$ atmospheres. This partial reduction of the air formed film, approximately $25\mathring{A}$ thick[62, 63], would occur upon insertion of a specimen into the reaction zone of the apparatus. The resulting lateral morphological growth of the wüstite nuclei in atmospheres of low-oxidizing potential, coupled with decarburization through the partially-reduced film, would lead to the observed stifling of the decarburization reaction. On the other hand, predominantly vertical growth of wüstite on areas of the oxide film ineffectively reduced by reaction with carbon at higher oxidizing potentials, combined with increased decarburization of the alloy at these potentials and at high surface carbon concentrations, would be expected. These considerations would lead to a more complex interpretation of the reaction kinetics. To obtain a more complete understanding of the reaction parameters we must therefore overcome problems of measurements of diverse phenomena, the most notable being measurements of kinetics and oxide morphological developments at exceedingly short exposure times.

In Figure 3-5, a comparision is presented of final practical rate constants obtained for the oxidation of iron-carbon alloys with those for pure iron at 950°C. In the low PCO_2 range, up to PCO_2 = .8 atm., the final rate measured for iron-carbon alloys is equal to or slightly lower than for pure iron. At higher values of PCO_2 the final reaction rate of the iron-carbon alloys is much higher than for iron. The only possible explanation that we can presently advance for this behaviour is associated with morphological development of the scale. In the early stages of the reaction in atmospheres of high oxidizing potential, irregular crystallite growth, (Figure 5-29) were formed. Subsequent growth of such crystallites

could conceivably lead to a defective scale of pronounced surface irregularity. An additional supply of chemisorbed oxygen due to the increased surface area of oxide would lead to the observed enhanced final oxidation rate. In addition, CO_2 could rapidly migrate through non-blocking micropores in the defective scale to react at the metal-oxide interface which would further enhance oxidation. This interpretation is, of course, open to question since measurement of surface area increase were not obtained and evidence of microporosity was not directly observed by the standard methods of electron and light microscopy.

CHAPTER 7

CONCLUSIONS

1. Selective oxidation of carbon from iron-carbon alloy sheet specimens for short experimental times at 950°C in $CO-CO_2$ atmospheres, exhibited linear kinetics consistent with the recently published results of Grahke[44] for alloy foils. It was shown that these findings were consistent with the theory for control of decarburization by a surface reaction of carbon with adsorbed oxygen produced by dissociation of carbon dioxide. For longer periods of time, the onset of partial diffusion controlled decarburization was observed.

2. A model describing a qualitative theory of simultaneous oxidation of iron and carbon was induced from the experimental results. This model served to correlate all the qualitative aspects of the reaction kinetics.

3. A critical initial carbon alloy content, in the range 0.6 to 1.0 wt.% which profoundly influenced the competition between iron and carbon for chemisorbed oxygen particularly at high values of the CO_2-CO ratio, was bracketed.

4. In $CO-CO_2$ atmospheres the formation of defective wüstite scale influenced the decarburization kinetics of the 1.065%C alloy very markedly for $PCO_2 > .8$ atm. at 950°C. For alloys of lower carbon content this effect was not observed, the effect of defective scale growth being less pronounced. These statements proved consistent with the results

of the metallographic study on scale morphologies.

5. Specific rate constants for the surfac diffusion step of chemisorbed oxygen to react with carbon and the reaction of chemisorbed oxygen with iron appeared to vary with initial carbon content of the alloys and CO_2 pressure in the range PCO_2 = 0.8 to PCO_2 = 1.0 atm., for the 1.065%C alloy at 950°C. The extent of the variation is not known.

6. It was not possible to define the exact magnitude of the effect of oxide nucleation on decarburization kinetics at CO-CO_2 ratios in the atmosphere approaching values for equilibration of wüstite with iron. Additional kinetic data must be collected in the range PCO_2 = .25 to .30 atm. at 950°C. with flowmeters designed to control atmospheric compositions to a higher degree of precision than could be obtained in the present investigation.

APPENDIX

The following curves are a further test of the precision of the experiments. All tests were carried out in pure CO_2.

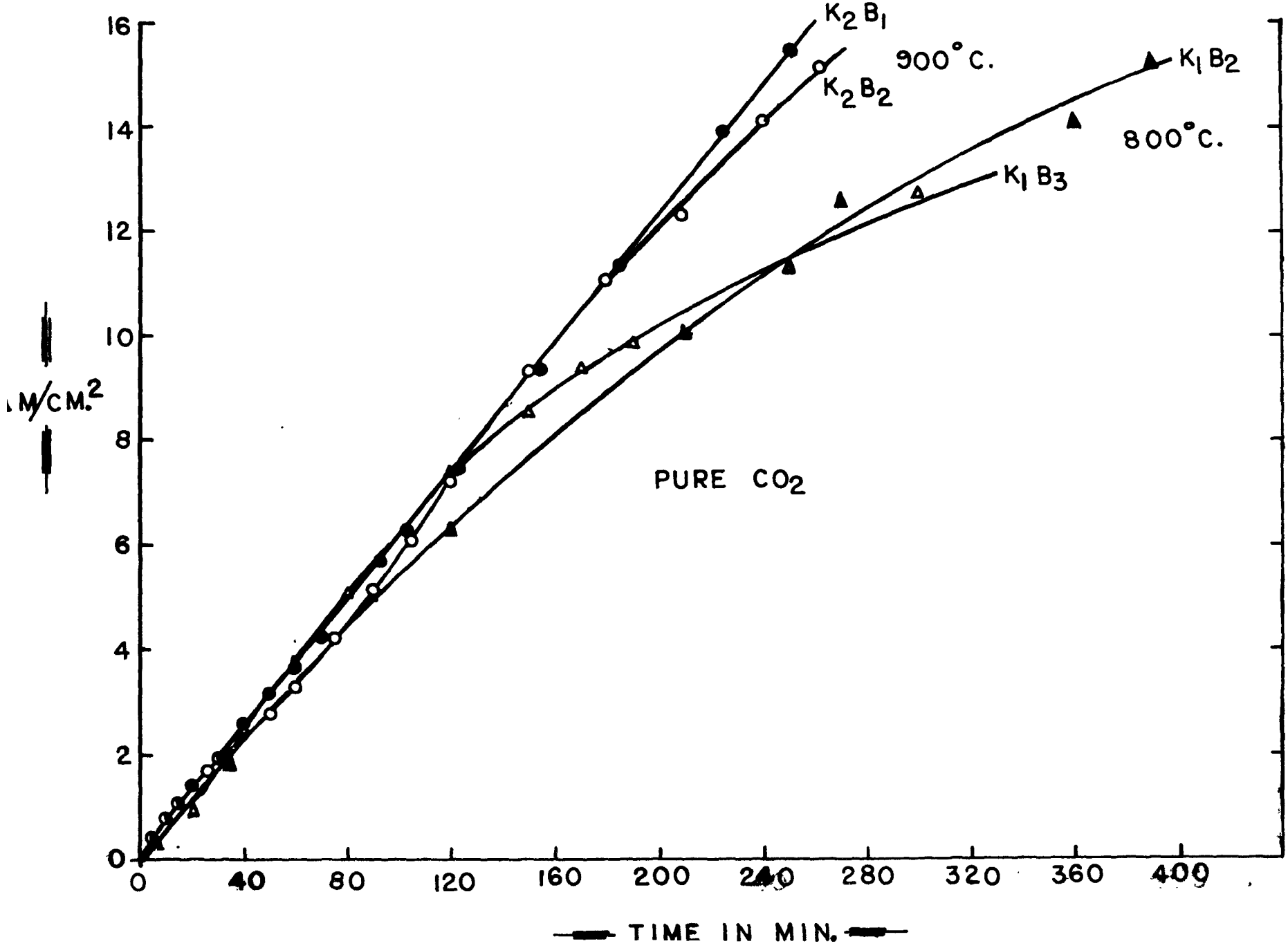
16
14
12
10
8
6
4
2
0
M/CM.²
0
40
80
120
160
200
240
280
320
360
400
TIME IN MIN.
K₂ B₁
900° C.
K₂ B₂
K₁ B₂
800° C.
K₁ B₃
PURE CO₂

BIBLIOGRAPHY

1. Seybolt, A., Oxidation of Metals, Report No. 62-RL 3151M, G. E. labs, Schenectady, N. Y.
2. Evans, U., The Corrosion and Oxidation of Metals, St. Martin's Press, N. Y., 1960 pg.836
3. Wagner, C., and Gruenewald, K., Zeit. Phys. Chem., B40, 455 (1938).
4. Pilling, M. and Bedworth, R., J. Inst. Metals 29, 529 (1923).
5. Vermilyea, D., Acta Met. 5, 492 (1957).
6. Smeltzer, W., Hoering, R., and Kirkaldy, J., Acta Met. 9, 880 (1961).
7. Wagner, C., Zeit. Phys. Chem., B21, 25 (1933).
8. Wagner, C., Atom Movements, Cleveland A. S. M., 153 (1951).
9. Wagner, C., and Ziemens, K., Acta Chem. Scand., 1, 547 (1947).
10. Gensch, C., and Hauffe, K., Zeit. Phys. Chem. 196, 427 (1951).
11. Grace, R., and Seybolt, A., J. Electrochem Soc., 108, 300 (1961).
12. Price, L., and Thomas, G., J. Inst. Metals, 63, 21 (1938).
13. Fueki, K., Ishibashi, H., J. Electrochem Soc. 108 306 (1961).
14. Gulbransen, E., and Andrew, K., J. Electrochem Soc. 106, 294 (1959).
15. Wagner, C., Zeit Electrochem Soc., 63 772 (1959).
16. Wagner, C., J. Electrochem Soc., 103, 627 (1956).
17. Wagner, C., J. Electrochem Soc., 103, 571 (1956).
18. Wagner, C., J. Electrochem Soc., 99, 369 (1952).
19. Paidassi, J., J. Trans. AIME, 197, 1570 (1953).
20. Davies, W., Simnad, M., and Bircherall, C., Trans AIME, 191, 889 (1951).
21. Kubaschewski, O., and Brasher, D., Trans. Far. Soc. 55 1200 (1959).

22. Davies, W., Simnad, M., and Birchenall C., J. Metals, 5, 1250 (1953).

23. Hauffe, K., and Pfieffer, H., Z. Metallkunde, 44, 27 (1953).

24. Pfieffer, H., and Laubmeyer, C., Zeit. Elektrochem, 59, 579 (1958).

25. Pettit, E., Yinger, R. and Wagner, J., Acta. Met., 8 617 (1960).

26. Smeltzer, W., Trans AIME, 218, 674 (1960).

27. Turkdogan, E., McKewan, W., and Zwell, L. J. Phys. Chem., 69, 327 (1965).

28. Eyring, H., J. Chem. Phys. 3, 107 (1934).

29. Hedden, K., Kopper, H., and Schulze, V., Zeit. Phys. Chem., Neue Folge, B22 23 (1959).

30. Suhrmann, R., and Wedler, G., Zeit. Elektochem., Ber. Busenges Physik Chem. 63 (1959).

31. Doehlemann, E., Zeit. Elektrochem., 42, 561 (1936).

32. Webb, W., Norton, J., and Wagner C., J. Electro Chem. Soc., 103 112 (1956).

33. Engell, H., Zeit. Elektrochem 63 842 (1959).

34. Wagner, C., Zeit. Anory. Allgem. Chemie, 197 321 (1931).

35. Smith, R., J. Am. Chem. Soc. 68 1163 (1946).

36. Sachs, K., and Brown, J., J. I. S. I., October (1958).

37. Stout, R., and Aho, T., A. S. M. Cleveland Symposium, p. 159 (1942).

38. Eisenhuth, C., et al Stahl und Eisen, 77 357 (1957).

39. Engell, H. and Bohnenkamp, K., Arch. Eisenhutt., 33 359 (1962).

40. Engell, H., and Bohnenkamp, K., J. Metallic Corr., p 215 (1962).

41. Himmel, L., Birchenall, C., and Mehl, R., J. Metals (N. Y.) 5 827 (1953).

42. Peters, F., Thesis, Technische Hockschule, Aachen (1958).

43. Merchant, H., Report, Owens-Illinois Tech. Centre, Toledo Ohio, (1964).

44. Grabke, H., Proc. 3rd Int. Congress on Catalysis, Amsterdam, July, (1964).

45. Langer, K., and Trenkler, H., Berg-und Hüttenmänn. Monatshefte 110 291 (1965).

46. Crank, J., The Mathematics of Diffusion, Univ. Press, Oxford (U.K.) p. 45 (1956).

47. McKay, A., Proc. Phys. Soc., 42, 547 (1930).

48. Kirkaldy, J., private communication

49. Crank, J., ibid (46) p. 56

50. Jaeger, J., and Carslaw, H., Conduction of Heat in Solids, Oxford 1947, p. 377.

51. Newman, A., Trans. Am. Inst. Chem. Engrs. 27, 203 (1931).

52. Darken, L., and Curry, R., J. Am. Chem. Soc., 67, 1398 (1945).

53. Morris, L., Ph.D. Thesis, McMaster Univ. Hamilton, Ont., Canada (1965).

54. Pettit, F., and Wagner, J., Acta Met. 12, 35 (1964).

55. Rickert, H., and Wagner, C., Z. Phys. Chem., N. F. 31, 32 (1962).

56. Himmel, L., Mehl, R., and Birchenall, C., TAIME, 197, 827 (1953).

57. Johnson, W., Mehl, R., TAIME, 135, 416 (1939).

58. Mehl, R., Wells, C., TAIME, 140, 279 (1940).

59. Wood, V., et al, J. App. Phys., 33, 3574, (1962).

60. Le Claire, A., Brit. J. App. Phys., 14, 351, (1963).

61. Irving, B., Nature, 204, No. 4963, 1082, (1964).

62. Kubaschewski, O., and Hopkins, B. E., Oxidation of Metals and Alloys, p. 38, 1962, Butterworths.

63. Cohen, M. et al, J. Electrochem Soc., 108, # 10, 933 (1961).